NASA CR-140201
ERIM 190100-27-T

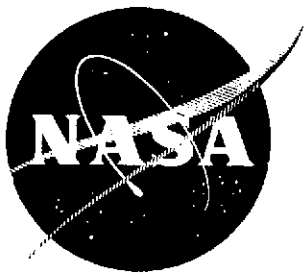

ANALYSIS OF MULTISPECTRAL SIGNATURES AND INVESTIGATION OF MULTI-ASPECT REMOTE SENSING TECHNIQUES

by

W. A. Malila
R. H. Hieber
J. E. Sarno

Infrared and Optics Division

ENVIRONMENTAL
RESEARCH INSTITUTE
OF MICHIGAN
FORMERLY WILLOW RUN LABORATORIES,
THE UNIVERSITY OF MICHIGAN

JULY 1974

prepared for
NATIONAL AERONAUTICS AND SPACE ADMINISTRATION

Johnson Space Center, Houston, Texas 77058
Earth Observations Division
Contract NAS 9-9784, Task VI

NOTICES

Sponsorship. The work reported herein was conducted by the Environmental Research Institute of Michigan for the National Aeronautics and Space Administration, Johnson Space Center, Houston, Texas 77058, under Contract NAS 9-9784, Task VI. Dr. Andrew Potter/TF3 is Technical Monitor. Contracts and grants to the Institute for the support of sponsored research are administered through the Office of Contracts Administration.

Availability Notice. Requests for copies of this report should be referred to:

National Aeronautics and Space Administration
Scientific and Technical Information Facility
P.O. Box 33
College Park, Maryland 20740

TECHNICAL REPORT STANDARD TITLE PAGE

1. Report No. NASA CR-ERIM 190100-27-T	2. Government Accession No.	3. Recipient's Catalog No.
4. Title and Subtitle ANALYSIS OF MULTISPECTRAL SIGNATURES AND INVESTIGATION OF MULTI-ASPECT REMOTE SENSING TECHNIQUES		5. Report Date July 1974 6. Performing Organization Code
7. Author(s) W. A. Malila, R. H. Hieber, J. E. Sarno		8. Performing Organization Report No. ERIM 190100-27-T
9. Performing Organization Name and Address Environmental Research Institute of Michigan Infrared and Optics Division P.O. Box 618 Ann Arbor, MI 48107		10. Work Unit No. Task VI 11. Contract or Grant No. NAS 9-9784
12. Sponsoring Agency Name and Address National Aeronautics and Space Administration Johnson Space Center Earth Observations Division Houston, Texas 77058		13. Type of Report and Period Covered Technical Report, 1 February through 31 October 1973 14. Sponsoring Agency Code

15. Supplementary Notes

Dr. Andrew Potter/TF3 is Technical Monitor for NASA.

16. Abstract

Two major aspects of remote sensing with multispectral scanners (MSS) are investigated. The first, multispectral signature analysis, includes the effects on classification performance of systematic variations found in the average signals received from various ground covers as well as the prediction of these variations with theoretical models of physical processes. The foremost effects studied are those associated with the time of day airborne MSS data are collected. Six data collection runs made over the same flight line in a period of five hours are analyzed; it is found that the time span significantly affects classification performance. Variations associated with scan angle also are studied.

The second major topic of discussion is multi-aspect remote sensing, a new concept in remote sensing with scanners. Here, data are collected on multiple passes by a scanner that can be tilted to scan forward of the aircraft at different angles on different passes. The use of such spatially registered data to achieve improved classification of agricultural scenes is investigated and found promising. Also considered are the possibilities of extracting from multi-aspect data, information on the condition of corn canopies and the stand characteristics of forests.

17. Key Words	18. Distribution Statement
Multi-aspect remote sensing Temporal characteristics of signatures Multispectral classification Multispectral signature analysis Remote sensing techniques Multispectral scanners	Initial distribution is listed at the end of this document.

19. Security Classif. (of this report)	20. Security Classif. (of this page)	21. No. of Pages	22. Price
UNCLASSIFIED	UNCLASSIFIED	112	

PREFACE

This report describes part of a comprehensive and continuing program of research in multispectral remote sensing of the environment from aircraft and satellites. The research is being carried out for NASA's Lyndon B. Johnson Space Center, Houston, Texas, by the Environmental Research Institute of Michigan (ERIM)—formerly the Willow Run Laboratories of The University of Michigan's Institute of Science and Technology. The overall objective of this program is to develop remote sensing as a practical tool for obtaining extensive environmental information quickly and economically.

Usually, remote sensing has been used to extract information only over limited areas and during times involving essentially similar conditions; it also has been restricted to a few selected types of terrain, most commonly agricultural areas. Yet, the need to economically extract information from ever-widening areas requires accurate recognition using remote sensing data, which, of necessity, will be collected at differing times. Examples of applications requiring wide-area collection of information include agricultural census taking, crop yield, detection of diseased plants, surveys and studies of air and water pollution, forest management, and general assessment of land-use patterns to permit land-use planning on a large scale. Further, many envisioned applications require more detailed information than is now available from customary multispectral data, whether collected by aircraft or satellites.

The work described in this report first deals with the problems of multispectral remote sensing under varying conditions and then those of improving discrimination by adding supplementary geometrical information from multiple viewing angles, or "aspects."

Variations induced in multispectral signals by different times of day, by dissimilar scan angles, and by atmospheric and bidirectional reflectance contributions are studied in detail and compared with the predictions of theoretical models to determine to what extent these models can predict the effects of changing conditions. Tests are made on the degradation of classification performance because of changing conditions.

Secondly, the use of a multi-aspect scanner is introduced. Data collected over both agricultural and forestry areas are analyzed to determine how much the addi-

tional geometrical information thus provided can improve both discrimination and extraction of other information.

The research covered in this report was performed under Contract NAS 9-9784, Task VI, and covers the period from 1 February through 31 October 1973. Dr. Andrew Potter served as Technical Monitor. The program was directed by R. R. Legault, a Vice-President of ERIM, by J. D. Erickson, Principal Investigator and Head of the Information Systems and Analysis Department, and R. F. Nalepka, Head of the Multispectral Analysis Section. The authors acknowledge the contribution of Tim Gregg in preparing Appendix B. The ERIM number of this report is 190100-27-T.

CONTENTS

FIGURES

TABLES

ANALYSIS OF MULTISPECTRAL SIGNATURES AND INVESTIGATION OF MULTI-ASPECT REMOTE SENSING TECHNIQUES

1 SUMMARY AND INTRODUCTION

Visible and infrared radiation reaching multispectral scanners contains spectral, spatial, and temporal information by which computers can recognize the surface materials present in individual spatial resolution elements and extract other types of scene information. The first of two major sections in this report describes investigation of some limiting factors of special importance in the machine processing of remotely sensed data from airborne multispectral scanners. The major factor is time-of-day change in average signals from each class caused by changes in overall irradiance and solar angles. Another important factor is scan-angle-related variation that depends on both the amount of haze present in the atmosphere and the viewing and illumination geometries. The second major section introduces multi-aspect remote sensing, a new concept in remote sensing with scanners, and explores its use for improved classification accuracy and information extraction.

The first major section, entitled "Multispectral Signature Analysis," considers systematic variations in multispectral scanner signatures (a signature, in this context, is a statistical description of scanner signals from a crop or some other ground cover). Variations associated with time of day and scan angle were studied both empirically and theoretically. Such variations present problems for many types of multispectral-data-processing techniques and procedures. Our empirical analysis was of a uniquely suited data set providing repeated data throughout the day (6 August 1971) over an agricultural area in Michigan. Six of 14 passes flown over the same flight line from 9:33 AM to 2:50 PM Local Solar Time were analyzed for time-of-day and scan-angle effects. Theoretical signal predictions obtained with a radiative transfer model for Lambertian (perfectly diffuse) surface reflectors were compared with the empirical data; some limited comparisons also were made with a different model developed at ERIM that predicts bidirectional surface reflectances. The multispectral scanner channels analyzed extend from 0.46μm (the visible blue) to 12.0μm (the thermal infrared). In discussing the theoretical radiative transfer model calculations, reference will be made to both "shorter" wavelengths (i.e., $\lambda < 0.6\mu$m) and "longer" wavelengths ($0.6 < \lambda < 1.0\mu$m), which together comprise a major portion of the reflective spectral region.

Major conclusions of the signature analysis investigation are as follows.

(1) Time-of-day effects in airborne scanner data are appreciable and cannot be ignored in the processing of large-area survey data, according to tests made to quantify the amount of degradation they produce in classification results.

(2) A theoretical radiative transfer model for Lambertian surfaces is capable of predicting time-of-day trends in reflective signals, as well as scan angle effects for the shorter wavelengths at which the atmosphere is a large contributor to scan-angle-dependent variations.

(3) Surface bidirectional effects at the longer wavelengths are thought to be the reason empirical data depart from the model predictions; calculations with a separate bidirectional reflectance model indicated the approximately correct curve shape, even though the parameters used did not closely match those of the empirical data.

The second major section of the present report is more specific in its focus. It explores for the first time a new data collection procedure, namely, multi-aspect data collection, as well as the use of data so collected for improved information extraction. The M-7 multispectral scanner installation in the ERIM C-47 aircraft was modified so the scanner could be tilted to view the ground ahead of the aircraft on repeated passes over a flight line. Multi-aspect data collected over an agricultural area on a standard (no-tilt) pass and on a subsequent 45^{o}-tilt pass over the same area were registered spatially and subjected to classification procedures. Related theoretical parametric studies were undertaken with a bidirectional reflectance model for crop canopys in order to explore the effects of plant density, plant vigor, tassels, and soil color on the multi-aspect reflectances of corn canopies. Finally, the canopy reflectance model was used to examine the relationships between the physical characteristics of a leafless deciduous forest (with snow covered ground) and the reflectances that would be observed during multi-aspect scanner passes.

Major conclusions of the multi-aspect investigation are as follows:

(1) Multi-aspect data may offer improved classification performance over that obtainable with conventional multispectral scanner data.

(2) Theoretical reflectance calculations for corn canopies under viewing conditions similar to those of the multi-aspect agricultural data show that reduced size (due to stress) and chlorosis of leaves, taken together, produce the most significant differences in reflectance as compared to mature healthy corn. Soil color becomes important only when the planting density is low, in which case it can have a substantial effect. Tassel effects were found to be discernible in multi-aspect data.

(3) The feasibility of extracting forest stand information (such as stand volume) from multi-aspect data was neither established nor rejected—in large part because the study was not completed. Encouraging progress was made, however, and trends predicted by theoretical reflectance modeling were found in the empirical data for one forest stand.

2
MULTISPECTRAL SIGNATURE ANALYSIS

If correct decisions are to be made in computer recognition processing, the multispectral signatures used in decision rules for discriminating between various material classes should accurately represent those classes. Because radiance signals (and hence, signatures) from a scene can vary in a number of ways for a variety of reasons, it is important to understand the nature of such variations and their causes.

A major objective of the work here reported was to investigate and determine systematic (as opposed to random) temporal (time-of-day) variations of signatures — and methods for predicting them — so that spectral pattern recognition procedures can be improved and better results obtained. Another objective was to determine how accurately variations associated with scan angle could be predicted. The testing and application of techniques for extending signatures by removing or compensating for systematic effects, such as those studied here, fell within the scope of other tasks under this contract [1, 2].

Appreciable variations in signatures at different times of day and at different scan angles were observed in empirical multispectral scanner data over an agricultural area. Classification tests on data from the same fields at successive times of day both quantified how rapidly recognition can degrade when fixed signatures are used and demonstrated that time-of-day trends in signals cannot be ignored.

Variations in signature means were analyzed both qualitatively and quantitatively, as a function of both time of day and scan angle, for a variety of ground cover types and a representative set of channels. Comparison of observed variations in the empirical data with the predictions of a radiative transfer model developed at ERIM by Dr. Robert E. Turner [3] shows the following: (1) the model is able to predict the trend of the short-wavelength data as a function of time of day and, less accurately, as a function of scan angle; (2) there are some residual discrepancies not accounted for by the model. Empirical analysis is also made of data in the thermal channel.

This in-depth study is unique in the extent of its direct comparisons, on matching graphs, between empirical data and theoretical predictions of variations; these comparisons are made in more detail for more times, fields, and ground covers and wavebands than in any other treatment of the subject we have seen. The extent of the analysis was made possible by the unique data set used: it was obtained in 14 successive passes over the same ground-truthed strip at different times on the same day. Previous time-of-day studies have compared only data taken over the same area during a few passes on one day, over different areas on the same day, or over different areas on different days. In contrast to these compromises, the availability of repeated data for identical fields, at the same scan angles and on the same day, eliminates many extraneous sources of data variation.

This data set was collected on 6 August 1971, in Ingham County, Michigan, near the time of maturity for most crops. A series of north-south passes was made at a 1.52-km altitude (5000 ft) over a single 11-km (7-mi) flight line at various times of day from 147 minutes before local solar noon to 170 minutes after. The area covered was primarily agricultural and contained 147 usable fields with 10 different crops (plus woods). Since it was entirely ground-truthed, the area provided abundant data for detailed analyses.

2.1 EMPIRICAL DATA PROCESSING

Data for six passes from the Ingham County flights made on 6 August 1971 were chosen to be digitized and processed for the temporal study; the same data also were analyzed in terms of scan angle, ground cover, and wavelength. The spectral channels available for analysis are listed in Table 1. Table 1 also lists flight times, corresponding local solar times, sun positions, and minutes between runs.

The first four runs were selected from among 12 recorded during the morning mission and are spaced approximately equally in time. The remaining eight morning run recordings (four between the first two and four between the third and fourth) are available for future analysis to obtain additional information about short-term run-to-run variations. No other afternoon mission runs were made along the flight line.

Noise was reduced during digitization by averaging over sets of eight scan lines which were partially redundant in the 1.52-km altitude (5000-ft) scanner signals. Some electronic filtering of the analog signals effectively combined two optical resolution elements along the scan line into each digitized sample; 160 video samples per scan line were taken. The signals were dynamically clamped to the dark level (i.e., that signal level obtained when the optics view the unilluminated interior structure of the scanner). Since the flight log indicates that the operator occasionally made gain changes between runs to keep the signals within the dynamic range of the recording system, appropriate coarse scaling factors were applied during data preparation to compensate for all such discrete gain changes between runs. Reference signals from an internal calibration lamp, from the sun and skylight irradiance sensor (hereinafter called the "sun sensor") and from thermal sources were retained on the tapes for later use.

Over 140 ground-truthed fields and forest plots were delineated on line-printer graymaps for the 10:10 EST run, and identifying line and point numbers were extracted. To provide a check on the accuracy of these delineations, we used a computer program (ADCHAN) developed for this work that, with a map program, allows the production of another map with the same gray tone symbols except that all points of the designated fields are over-printed in color with a letter denoting the ground cover type. This map permitted a rapid check of the delineation operation and reduced chances of human error.

TABLE 1. INGHAM COUNTY RUNS DIGITIZED FOR TIME-OF-DAY STUDY. Data Collected on 6 August 1971.

Eastern Standard Time (EST) at Middle of Run*	Local Solar Time (LST) (84.42° W Longitude)	Minutes from Local Solar Noon	Minutes Between Runs	Solar Elevation (°)	Solar Azimuth (°)	Difference from 180° (South) Solar Azimuth (°)
10:10	9:33	-147		49.3	117.7	-62.3
			34			
10:45	10:07	-113		54.6	127.9	-52.1
			48			
11:32	10:55	-65		60.5	145.8	-34.2
			38			
12:10	11:33	-27		63.6	164.7	-15.3
			143			
14:33	13:56	116		54.5	232.1	52.1
			54			
15:27	14:50	170		45.8	247.4	67.4

* For all runs the following M-7 scanner channels were used:

Digital Number	10% Passband (μm)
1**	0.46-0.49
2	0.48-0.51
3	0.50-0.54
4**	0.52-0.57
5	0.54-0.60
6	0.58-0.65
7**	0.61-0.70
8**	0.72-0.92
9	1.0-1.4
10	1.5-1.8
11	2.0-2.6
12**	9.3-11.7

** Used in intensive field-mean study.

Since hand-delineation of field boundaries on graymaps is a time-consuming and error-prone process, a computer-aided method was used to transform the field delineations from the first run to each of the other runs. Here, computer programs, developed this year under ERTS investigations [4, 5] to transform field coordinates from USGS maps or high-altitude aerial photography to digitized multispectral scanner data, were adapted for use. Precise spatial registration of the data set points was not undertaken. The spatial resolution of the aircraft data was fine enough, in comparison to field sizes, that errors in the location of field boundaries (up to several 25-ft image elements) were made acceptable by moving the field delineations in from the field boundaries.

In contrast to the first-order transformation usable for portions of ERTS frames, a quadratic transformation was found necessary in the Ingham County aircraft data and, in addition, the seven-mile-long run had to be broken into three sections. The break points were determined from marked discontinuities in a plot of the errors in the line numbers along the flight path given by a preliminary linear transformation applied to the entire length. The approach taken gave better results than did a single higher-order fit to the same 20 to 28 reference points over the entire length. Errors along the scan line were usually less than two to four resolution elements (acceptable on almost all fields), but some errors along the flight path amounted to as many as ten resolution elements over short stretches. The accuracy of the new field delineations was verified on one of the two-color digital maps described above, and detected errors were corrected manually. The computer-aided procedure saved only a modest amount of human time compared to delineating the fields by hand on each new run; its primary worth was in reducing the number of human errors made in recording and handling the delineations.

The individual fields were divided into subfields, each lying entirely within one of seven contiguous, non-overlapping ranges of scan angles. Comparing subfields within the same scan angle range allows the effects of scan angle variations to be minimized; it also allows study of the data as a function of scan angle per se (i.e., with scan angle as an independent parameter). A small computer program was written to take as input the initial field delineation cards for whole fields and to then punch cards for a larger number of subfields broken up into different scan angles. One initial whole field might overlap three or four scan angle ranges, in which case it would be divided into three or four subfields. Since the end of a field sliced off by a division in scan angles might be too small to give a reliable subfield mean, a lower bound of ten pixels was set for accepting any subfield.

These data were analyzed both by direct examination of field signal means and by classification tests, which are discussed later in Section 2.3. For the signal mean comparisons discussed in Sections 2.3 and 2.4, graphs were plotted using The University of Michigan's Interactive Data

Analysis System, a program available on the campus IBM 360/67 computer. The dependent variables plotted on the vertical scale are as follows:

(1) Total radiance (derived from the subfield means)

(2) Total downward irradiance at 1.52 km (5000 ft) (supplied by the sky sensor as a function of time of day only, there being no scan angle and crop dependence)

Of the four available parameters, the following levels were used in all data processing and graphing:

(1) Time of day (six levels)*

EST	LST (Local Solar Time)
10:10	9:33
10:45	10:07
11:32	10:55
12:10	11:33
14:33	13:56
15:27	14:50

(2) Scan angle (seven levels)

The -28^{o} to $+28^{o}$ range of scan angles was broken into seven ranges, with nominal central scan angles of -24^{o}, -16^{o}, -9^{o}, 0^{o}, $+9^{o}$, $+16^{o}$, $+24^{o}$ (using negative scan angles to denote the western side on both north- and south-bound flights). As discussed above, statistics were extracted from those parts of the fields lying within each range of scan angles. Since the ranges were chosen to include approximately equal numbers of pixels within each range along the scan lines, they include more degrees of angle around nadir. The ranges are approximate and were varied slightly from run to run (by less than one range total) to include about the same ground area in each. The plane did not follow exactly the same flight path each time, but it was felt that the changes made in scan angle would introduce less variation in the data than using different fields.

(3) Channels (five levels)

Channel #	Band Wavelengths (μm)
1	0.46 - 0.49
4	0.52 - 0.57
7	0.61 - 0.70
8	0.72 - 0.92
12	9.3 - 11.7

*See Table 1.

(4) Ground covers (up to 11 cases, some not always available)

(a) NS Corn (north-south row direction)
(b) EW Corn (east-west row direction)
(c) Pasture
(d) Trees
(e) Oats
(f) Hay
(g) Soybeans
(h) Field Beans
(i) Winter Wheat
(j) Rye
(k) Buckwheat

Two basic types of graphs were produced. They differ in the parameter chosen for the independent variable on the horizontal scale. In the first type, the six times of day are treated as the independent variables, and three of the seven scan-angle ranges—at nominal angles of -24^{o} (extreme west), 0^{o} (nadir), and $+24^{o}$ (extreme east)—are used as parameters on different graphs. In the second type of graph, the seven scan-angle ranges are plotted along the horizontal axis, and three times (9:33, 11:33, and 14:50 LST) are parameters. Graphs of both types were generated for each of the five wavelengths paired with each of the 11 ground covers. For several ground covers, sufficiently reliable data were not available at all scan angles.

Before plotting, a final fine-scaling adjustment based on the recorded calibration was made to the data. To compare the six empirical runs to each other, it was necessary only to match the lamp signals between runs in the first four channels. The signals from the first four runs (all on the morning flight) were within a few percent of one another, near the limit of accuracy; and because the variations exhibited no consistent pattern, no correction was applied. Lamp signals for the last two runs (both on the afternoon flight) were from 4% to 7% lower depending on the channel, so data from the afternoon runs were scaled up to match the morning runs. For analysis of thermal channel (No. 12) data, we compensated for adjustments the operators had made separately for the hot and cold reference-source temperatures throughout the day.

2.2 THEORETICAL CALCULATIONS

Radiance predictions for Lambertian surfaces were made, using the radiative transfer model developed at ERIM by Dr. Robert E. Turner [3] for comparison with the empirical data. The radiative transfer model computes quantities such as spectral irradiance at any given altitude within the atmosphere, spectral path radiance and transmittance for any observation path, and the total radiance received from a surface with a given reflectance. The quantities

of path radiance and irradiance depend on the reflectance (or albedo) of the background surface, as well as on the haze content of the atmosphere. The model incorporates a number of standard atmospheres, each designated by its particular horizontal visual range at sea level; one of these atmospheres is used for calculations when more detailed information on the atmospheric state is not available.

Graphs of the model calculations were made on a Calcomp X-Y plotter to the same scale as the plots of empirical data. This allowed overlaying various empirical and theoretical graphs for quick comparison of their agreement. Used as a parameter on the theoretical graphs, ground reflectance appears in increments of 4% from 0 to 32% in channels 1, 4, and 7, and of 4% from 0 to 64% in channel 8 (near-infrared) because of higher reflectances expected there. Target and background reflectances were set equal for all calculations. A standard atmosphere characterized by a horizontal visual range of 23 km was used for the calculations. There is no theoretical graph to match the thermal (channel 12) empirical data: the radiative transfer model used for this work* is inapplicable to this 9.3 to 11.7 μm band where the energy recorded is emitted thermal radiation rather than reflected sunlight. To match the predictions of ERIM's radiative transfer model to the empirical data, lamp calibration curves for the July through December 1971 period were used to convert the observed digital signals to spectral radiance in milliwatts per steradian-centimeter^2-micrometer [mW/(sr-cm^2-μm)].

For the analysis of scan-angle effects, we used programs developed at ERIM by Dr. Gwynn Suits [6] to make some theoretical calculations of bidirectional reflectance from corn canopies.

2.3 TIME-OF-DAY EFFECTS ON SIGNATURES AND CLASSIFICATION RESULTS

This section will show with empirical data from the Ingham County flights that there are sizable variations in the mean radiance from each crop as a function of time of day. Classification tests using signatures from the first run (9:33 LST) at later times in the day reveal a serious degradation of classification accuracy; this effect cannot be ignored because, with time, it becomes progressively worse until by noon essentially nothing is recognized.

A radiative transfer model will then be demonstrated as able to predict these changes with moderate accuracy, doing best at the shortest wavelengths. We attribute two evident types of discrepancy—higher afternoon brightness and extra anti-solar peaking—to factors not included in the model.

* Different models developed at ERIM apply to thermal radiation but were not used here because of limited resources.

2.3.1 COMPARISON OF FIELD SIGNAL MEANS

Clear-cut systematic trends as a function of time of day are evident in ground radiance signals measured for the multispectral scanner data set for Ingham County. We first analyze the behavior of these signals in the visible and near-infrared channels in comparison with that predicted by the radiative transfer model. Since the behavior of the far-infrared (or thermal-radiance) channel is intrinsically different and cannot be compared to predictions of the short-wavelength radiative transfer model used, it is analyzed separately later.

Figures 1 and 2 portray the temporal variation of the mean radiance for some important ground covers compared to theoretical predictions. Data for channel 1, which is the shorter waveband used (0.46 - 0.49 μm), are presented in the first figure, while the next presents data for channel 8, the near-infrared waveband (0.72-0.92 μm, the longest wavelength band utilized for this portion of the study). For each channel, results are shown for fields within one of three selected scan-angle ranges nominally centered at -24^{o} (westward), 0^{o} (nadir), and $+24^{o}$ (eastward). The empirical multispectral scanner measurements are indicated for the six different times by symbols for each of four ground covers:

Corn (planted in north-south rows)
Corn (planted in east-west rows)
Pasture
Trees

Each symbol represents the average signal over all fields satisfying the conditions, each field weighted equally. The solid lines depict the theoretical predictions of the radiative transfer model for Lambertian surfaces with different reflectances.

In the visible and near-infrared channels, the signal means rise until about noon, then tend to fall off later in the afternoon. We would have expected, a priori, that the afternoon decline would roughly match the morning rise, at least at the nadir scan angle—assuming the predominant influence is the total downward solar (plus sky) irradiance which should fall off symmetrically on each side of local solar noon.

Two apparent forms of deviation occur. First, the measured radiances on the two afternoon runs stay noticeably brighter than expected. Our conjecture is that scattered radiation from high altitude clouds increased the overall illumination in the afternoon. This hypothesis is supported by readings from the sun (and sky) irradiance sensor on top of the airplane, relative to those of the calibration reference sources. A second observed effect is additional brightness in the direction opposite the sun, hereinafter called "anti-solar peaking," which is most evident at the extreme westward and eastward scan angles. This is believed mostly the result of atmospheric back-scattering of direct solar irradiance for the shorter wavelengths and bidirectional reflection at the surface for the longer ones. The radiative transfer model

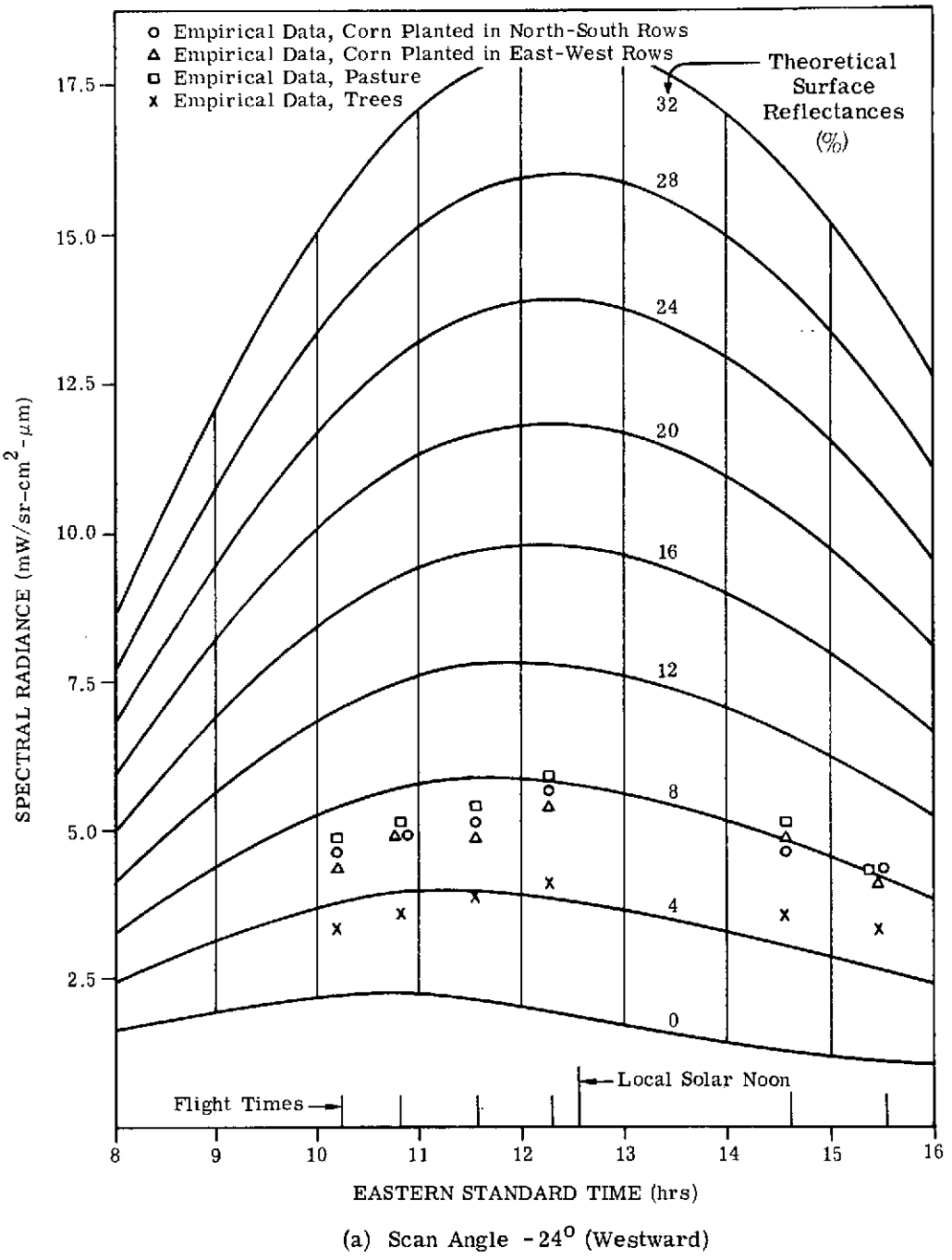

(a) Scan Angle -24° (Westward)

FIGURE 1. RADIANCE AS A FUNCTION OF TIME, CHANNEL 1 (0.47-0.49 μm). Empirical data for four crops and theoretical data for various Lambertian surface reflectances. 6 August 1971, altitude 1.5 km (5000 ft), visibility 23 km. (Continued)

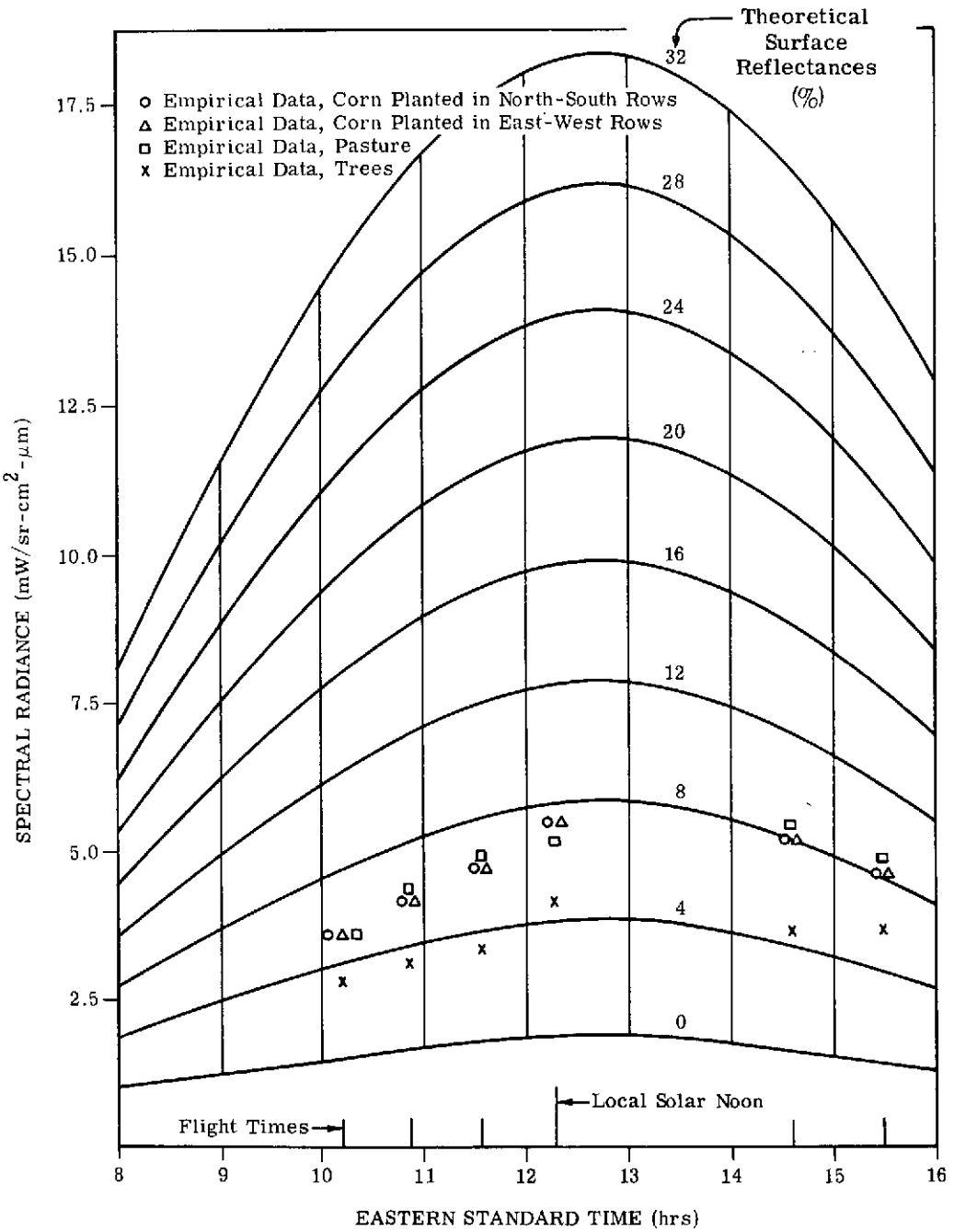

(b) Scan Angle 0^{o} (Nadir)

FIGURE 1. RADIANCE AS A FUNCTION OF TIME, CHANNEL 1 (0.47-0.49 μm). Empirical data for four crops and theoretical data for various Lambertian surface reflectances. 6 August 1971, altitude 1.5 km (5000 ft), visibility 23 km. (Continued)

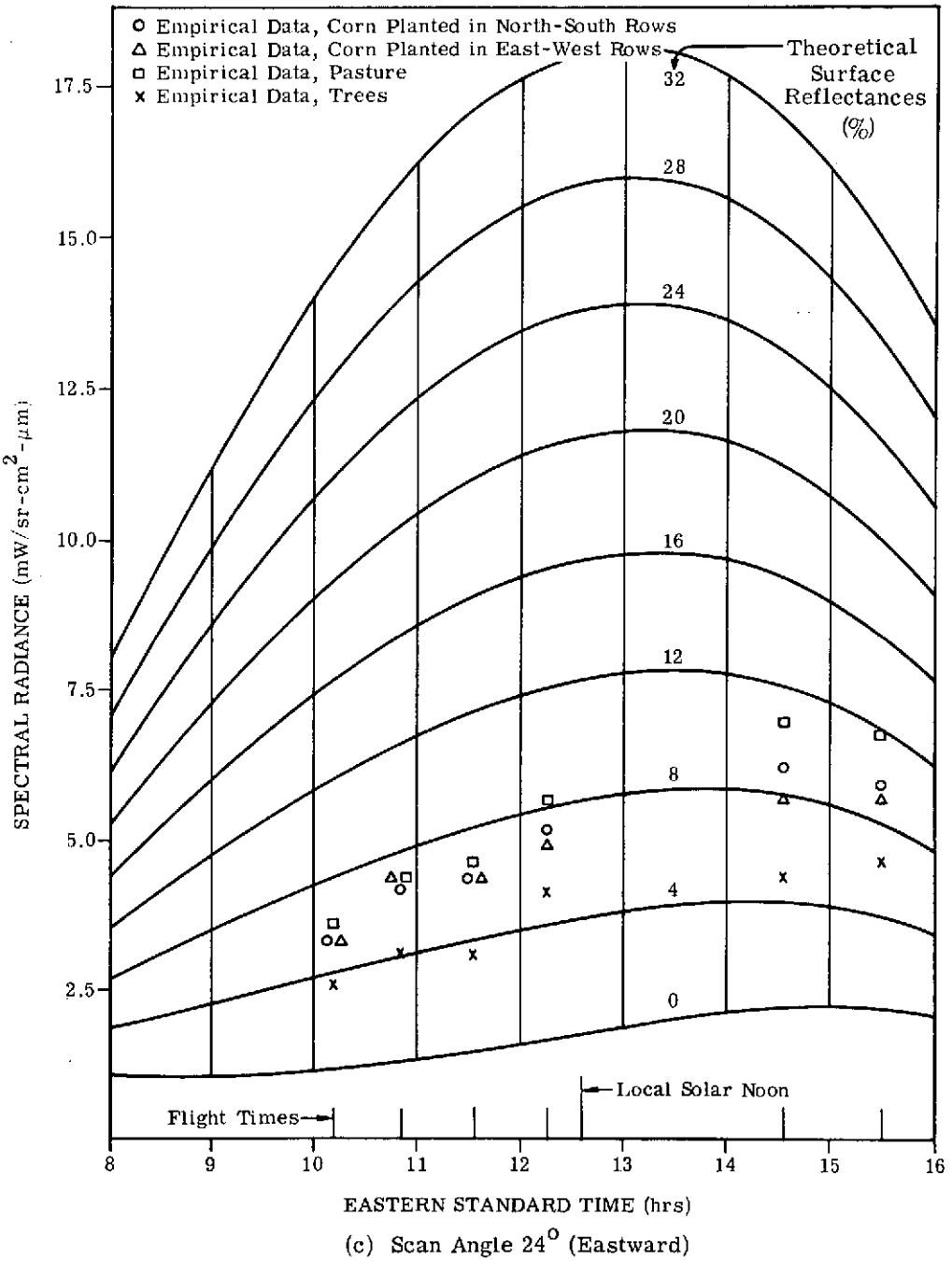

(c) Scan Angle 24° (Eastward)

FIGURE 1. RADIANCE AS A FUNCTION OF TIME, CHANNEL 1 (0.47-0.49 μm). Empirical data for four crops and theoretical data for various Lambertian surface reflectances. 6 August 1971, altitude 1.5 km (5000 ft), visibility 23 km. (Concluded)

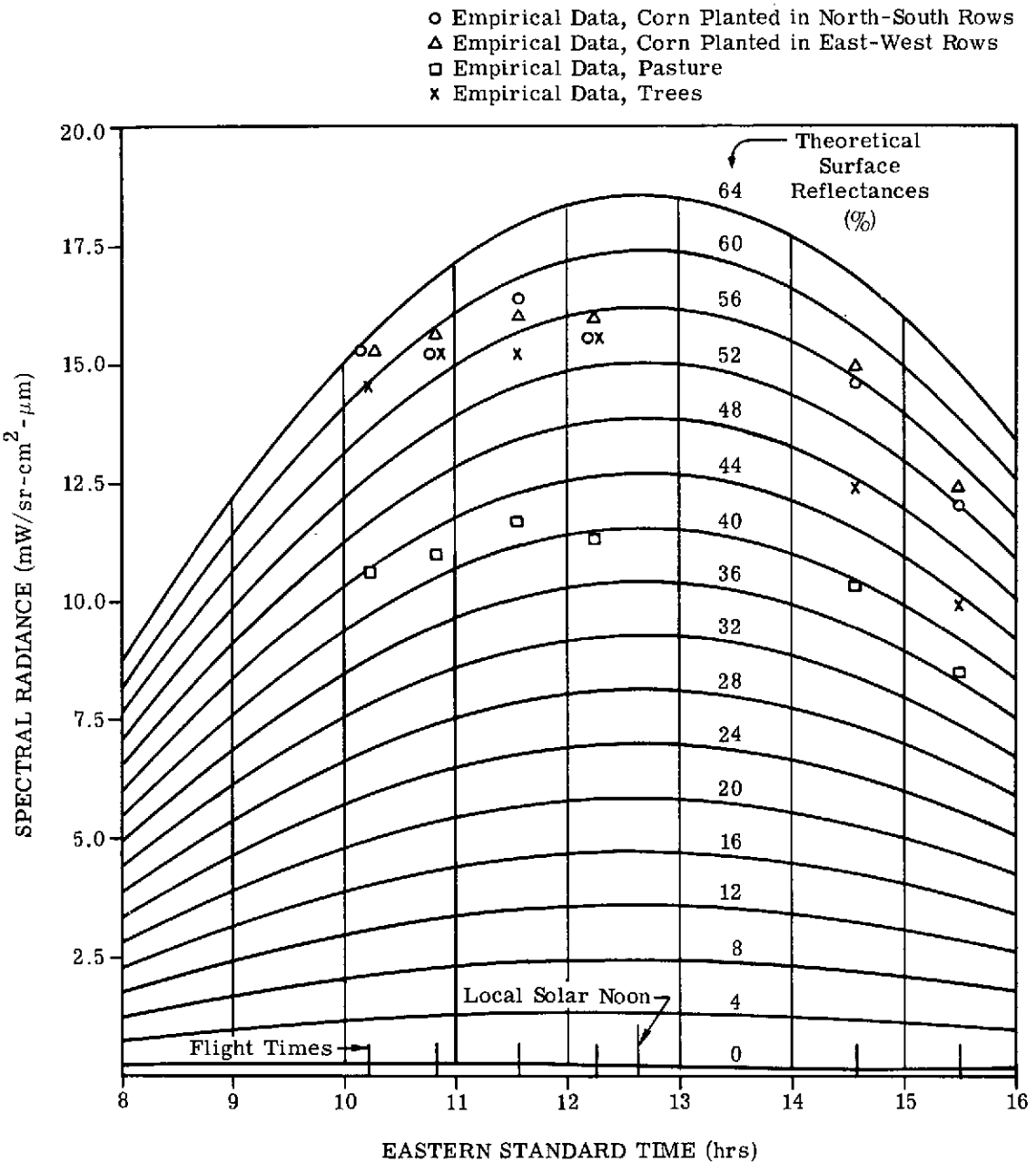

(a) Scan Angle - 24° (Westward)

FIGURE 2. RADIANCE AS A FUNCTION OF TIME, CHANNEL 8 (0.72-0.92 μm). Empirical data for four crops and theoretical data for various Lambertian surface reflectances. 6 August 1971, altitude 1.5 km (5000 ft), visibility 23 km. (Continued)

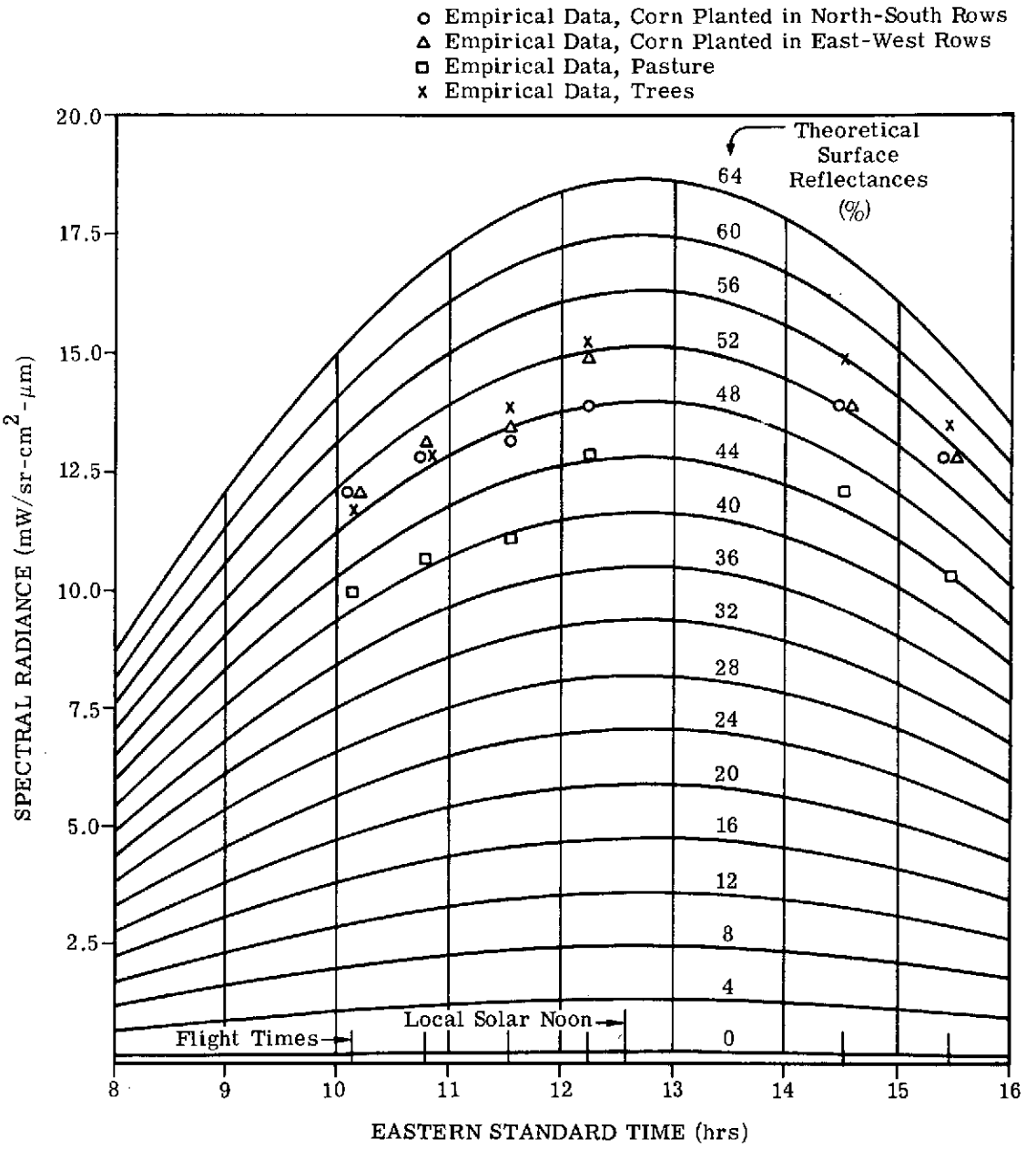

(b) Scan Angle 0^o (Nadir)

FIGURE 2. RADIANCE AS A FUNCTION OF TIME, CHANNEL 8 (0.72-0.92 μm). Empirical data for four crops and theoretical data for various Lambertian surface reflectances. 6 August 1971, altitude 1.5 km (5000 ft), visibility 23 km. (Continued)

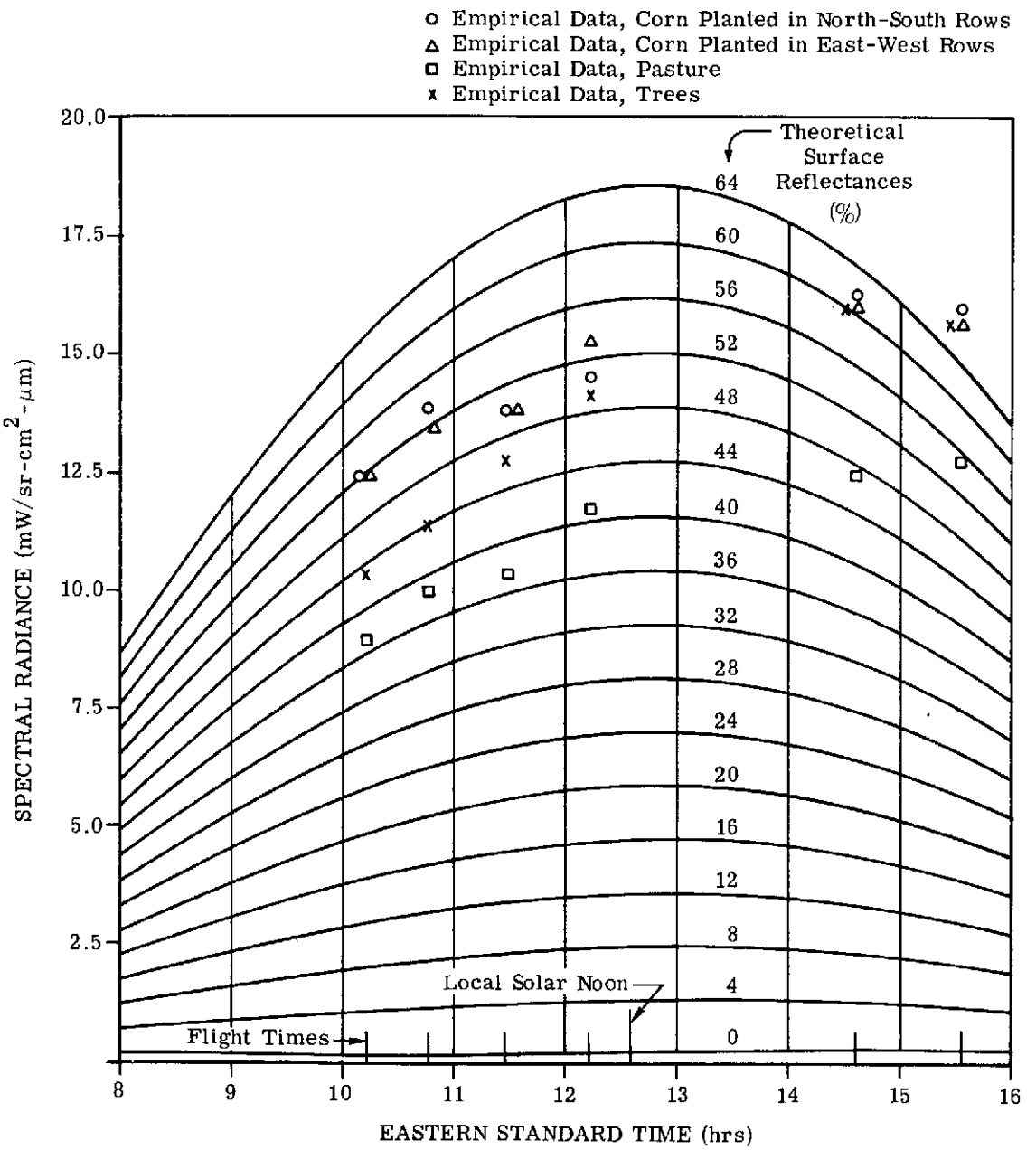

(c) Scan Angle 24° Eastward)

FIGURE 2. RADIANCE AS A FUNCTION OF TIME, CHANNEL 8 (0.72-0.92 μm). Empirical data for four crops and theoretical data for various Lambertian surface reflectances. 6 August 1971, altitude 1.5 km (5000 ft), visibility 23 km. (Concluded)

is reasonably successful in predicting both the effects of the changing total downward irradiance and the atmospheric contribution to anti-solar peaking at the shorter wavelengths, but it does not include a bidirectional reflectance effect and fails to account for the majority of the anti-solar peaking noted at the longer wavelengths.

We should note that any absolute overall errors in the model, as opposed to differential errors between different conditions, would not significantly affect interpretations based on the relative curve shapes. For pure Lambertian surface reflectors, the empirical curve shapes should ideally match those of the theoretical curves. Deviations of the empirical curve shapes from the theoretical shapes can be attributed to bidirectional reflectance effects or, perhaps, to variations in atmospheric phenomena, illumination, and run-to-run calibration of the scanner data —assuming that differential errors in the model are small by comparison. We might also note that the effective (equivalent Lambertian) reflectance of the ground cover can be estimated by comparing the magnitude of the empirically measured scanner signals with the nearby theoretical curves for different Lambertian surface reflectances.

Some effects seen in these figures are typical of those in most if not all graphs generated. The theoretical predictions of the radiative transfer model show peaking in the anti-solar direction (e.g., in the afternoon at the eastward-looking scan angle). This is caused by backscattering of incident solar irradiation in the atmosphere. Atmospheric scattering is strongest in the short-wavelength blue channel (No. 1), but it decreases with increasing wavelength until in channel 8 any differences are almost indiscernible.

The empirical data partially follow the theoretical curves except for the two forms of deviation previously noted. Data for the last two times of the afternoon mission are consistently higher in amplitude compared to the theoretical curves than data of the first three times of day; the fourth time, near noon (11:33 LST), also tends to be higher than the first three. On the graphs plotted versus time of day for channel 1 (Figs. 1 through 3), empirical signals for trees at nadir can be seen to correspond to about 3 to 4% theoretical reflectance at the first three morning times, rising to 5 to 6% in the afternoon. Similarly, the other three ground covers shown rise from 5 to 7% at morning times to about 8% in the afternoon (and to 11% for the anti-solar eastward graph). For channel 8, the graph at nadir scan angle in Fig. 5 shows similar apparent increases in effective reflectance in the afternoon. This afternoon rise, apparently, is also present at the extreme westward and eastward scan angles for channel 8 (see Figs. 4 and 6), but substantially masked by additional empirical anti-solar peaking.

We have conjectured that the higher afternoon measurements were caused by the presence of high, thin cirrus clouds that increased the total downward irradiance by reflecting additional light to the ground. Flight logs and ground observations a few miles from the test area

show that there were scattered, high, thin cirrus clouds in an otherwise clear sky for the afternoon flight. Flight logs indicate the presence of high cirrus clouds in the morning as well, but none was observed from the ground. Run-to-run variations may also have been caused by changes in scanner system response, but an examination of calibration lamp signals showed insufficient variation to explain the observed morning-to-afternoon data difference. However, at the time of this analysis, the run-to-run stability of the scanner calibration system had not been studied thoroughly. (Another task under the parent contract includes a study of the system calibration for a more recent version of the M-7 scanner system [7].)

Examination of data from the sun sensor on top of the airplane at 1.52-km (5000-ft) altitude supports the conclusion that the afternoon illumination was brighter. Figures 3 and 4 show empirical measurements (relative) from the sun sensor as a function of time of day, along with the theoretical total downward irradiance at the aircraft altitude as calculated by the radiative transfer model. Theoretical irradiances for channel 1 are presented in Fig. 3 for three background albedos (0%, 16%, and 32%), while Fig. 4 shows irradiances for channel 8 with 0%, 32%, and 64% albedos (only one figure per channel is supplied, since there is no scan-angle dependency in the sun sensor). Unlike the preceding graphs, the measured data here were not absolutely calibrated (e.g., in spectral irradiance units) since the sun sensor is known to have a non-Lambertian response and sufficient calibration data for the particular configuration were not available. Instead, the measured data were adjusted relative to the theoretical curves by using the same scaling factor for all times of day such that the measured data nearest local solar noon (the fourth run) matched the theoretical value. Ignoring atmospheric effects, we can say that the theoretical curves decline away from local solar noon according to the cosine law—assuming an ideal horizontal planar detector. Since the detector is not perfect, we expect additional falloff, relative to theory, of the sensor measurements away from noon, particularly at lower sun-elevation angles. After allowing for this effect, it can be seen from the graphs that the sun-sensor readings confirm the situation observed in the empirical data from crops (i.e., higher than expected values in the afternoon).

The second form of deviation is that the data tend to be brighter in the anti-solar direction than is predicted by the theory. This is most evident in channel 8 for which the theory predicts minimal atmospheric anti-solar peaking: at the westward scan angle in Fig. 4, the morning data are higher, relative to theory, than the afternoon data; while at the eastward scan angle in Fig. 6, the afternoon data are higher than expected—even considering the brighter afternoon illumination. There also seems to be a little additional anti-solar brightness, relative to theory, in channel 1; when this is examined as a function of scan angle in Section 2.4, however, the difference does not seem clear-cut.

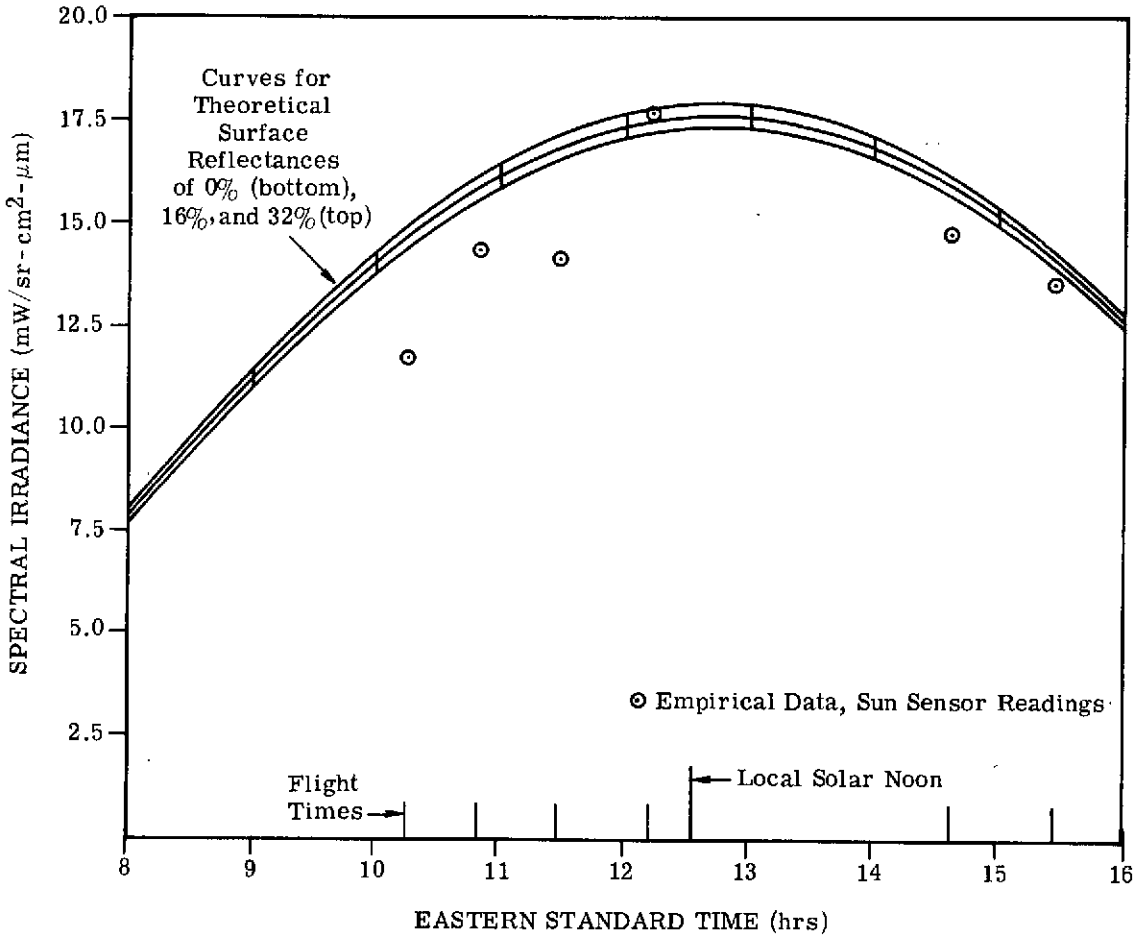

FIGURE 3. IRRADIANCE AS A FUNCTION OF TIME, CHANNEL 1 (0.47-0.49 μm). 6 August 1971, altitude 1.5 km (5000 ft), visibility 23 km.

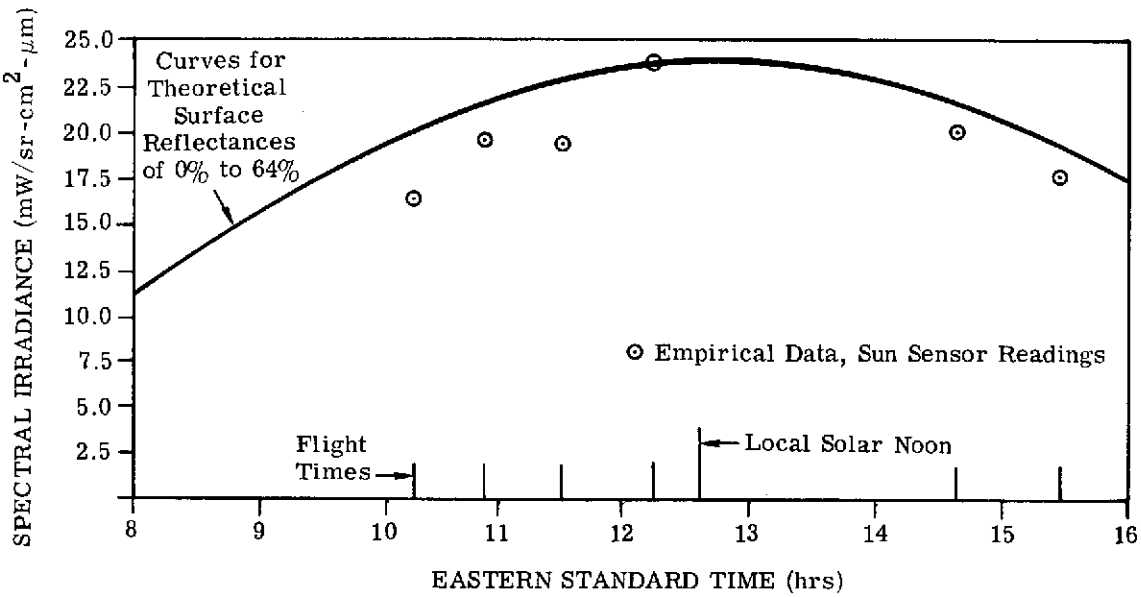

FIGURE 4. IRRADIANCE AS A FUNCTION OF TIME, CHANNEL 8 (0.72-0.92 μm). 6 August 1971, altitude 1.5 km (5000 ft), visibility 23 km.

The additional anti-solar increase in the empirical data relative to the theoretical anti-solar peaking noticed is apparently attributable to bidirectional reflectance. The scan-angle-dependency analysis in Section 2.4 discusses bidirectional reflectance effects in some detail, making the distinction between the case at shortest wavelengths when anti-solar peaking is mostly contributed by atmospheric scattering and the case at longest wavelengths when bi-directional reflectance effects may predominate. The effects of bidirectional reflectance need further investigation.

The two forms of deviation probably can be attributed to causes specifically excluded from the theoretical model we used. This model includes neither the effect of clouds, which we believe caused an overall irradiance increase in the afternoon, nor bidirectional reflectance, which we believe caused anti-solar peaking in addition to that predicted by the model from atmospheric scattering. Even without excluding these two supposed additional effects, however, it can be seen that the radiative transfer model adequately predicts major trends in the empirical data. The theory predicts about the expected increase at later times throughout the morning, and the predictions for the afternoon come closer than the changes in absolute radiance in most cases. In channel 1, then, when we compare the first run of the morning with the afternoon runs, we see that the effective reflectances interpolated from the model rise about the same at all scan angles (i.e., increases of 30-60% depending on the ground cover). Yet, the increase in absolute radiance from morning to afternoon is near zero at the westward scan angle, 35% at nadir, and almost 90% at the eastward angle.

For the far-infrared thermal channel (No. 12, from 9.3 to 11.7 μm), the time-dependent behavior of the measured signals is shown in Fig. 5 for the same three scan-angle ranges used before. Note that the measured radiance is a function of ϵT^4, where ϵ is the emittance, $0 \leq \epsilon \leq 1$, and T is the absolute temperature. The apparent temperature scale on the figures is an approximation which neglects atmospheric effects and assumes that target emittances are roughly constant and about the same as those of hot and cold calibration plates. There are no matching theoretical curves here. The short-wavelength radiative transfer model used for the earlier work is inapplicable at these wavelengths, since the signal is preponderantly direct thermal radiation from the target with negligible reflected radiation. Resource limitations precluded the use of thermal models that exist at ERIM.

One would expect that all ground covers should rise in temperature throughout the morning and be consistently warmer in the afternoon than they were for corresponding sun elevation angles in the morning. Observation of the data shows that this is mainly the case. It can be seen that the temperatures rise through the morning and stay comparatively constant from about the fourth run on—near-noon (11:33 LST). There is a significant dependence of the observable effective temperatures on the ground cover type. Trees are always cooler than

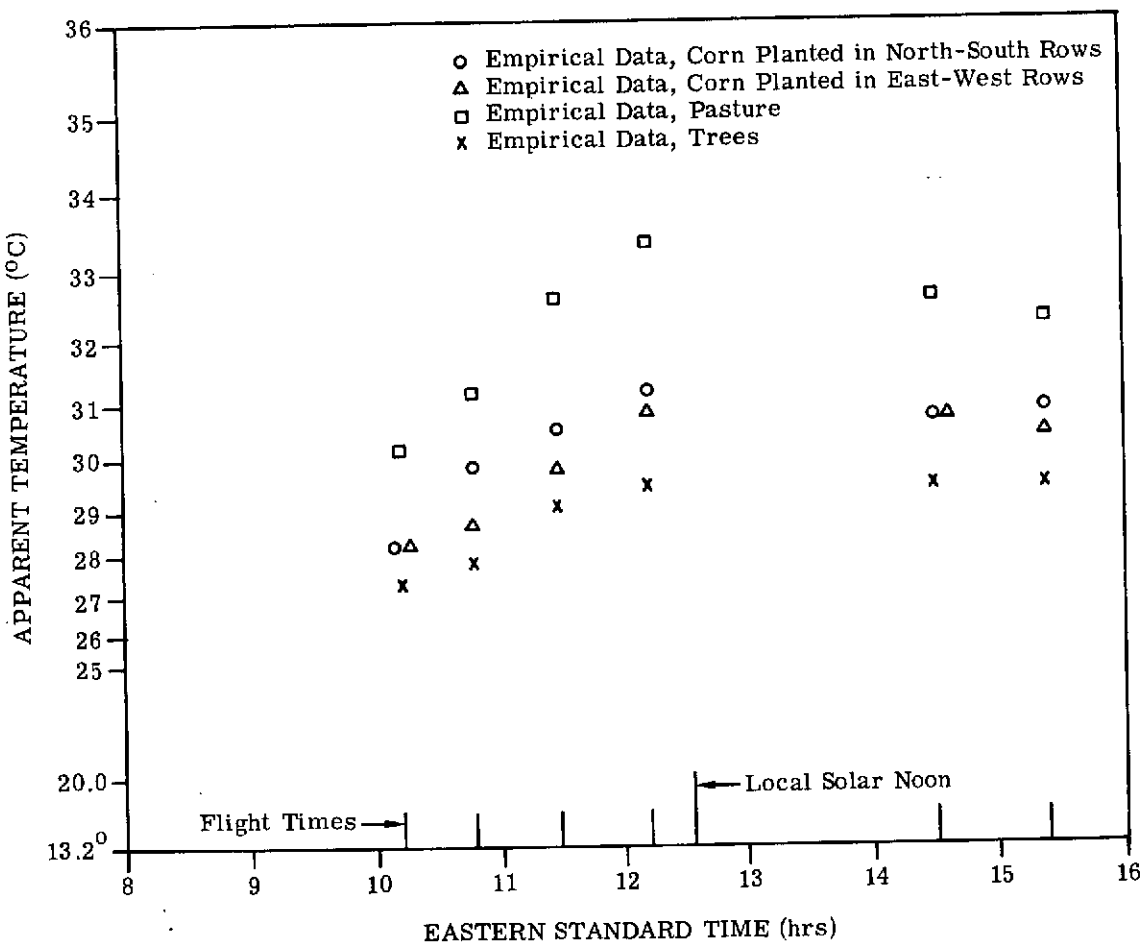

(a) Scan Angle -24° (Westward)

FIGURE 5. APPARENT TEMPERATURE AS A FUNCTION OF TIME, CHANNEL 12 (9.3-11.7 μm). 6 August 1971, altitude 1.5 km (5000 ft), visibility 23 km. (Continued)

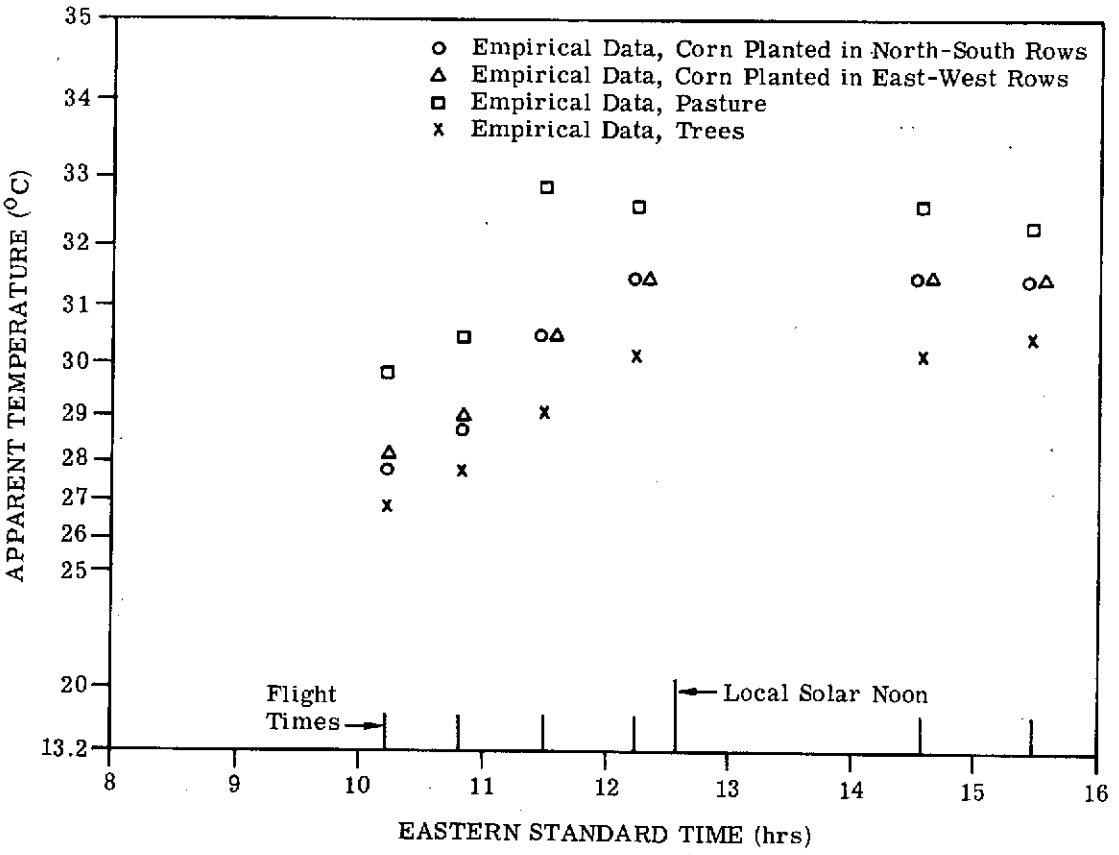

(b) Scan Angle 0° (Nadir)

FIGURE 5. APPARENT TEMPERATURE AS A FUNCTION OF TIME, CHANNEL 12 (9.3-11.7 μm). 6 August 1971, altitude 1.5 km (5000 ft), visibility 23 km. (Continued)

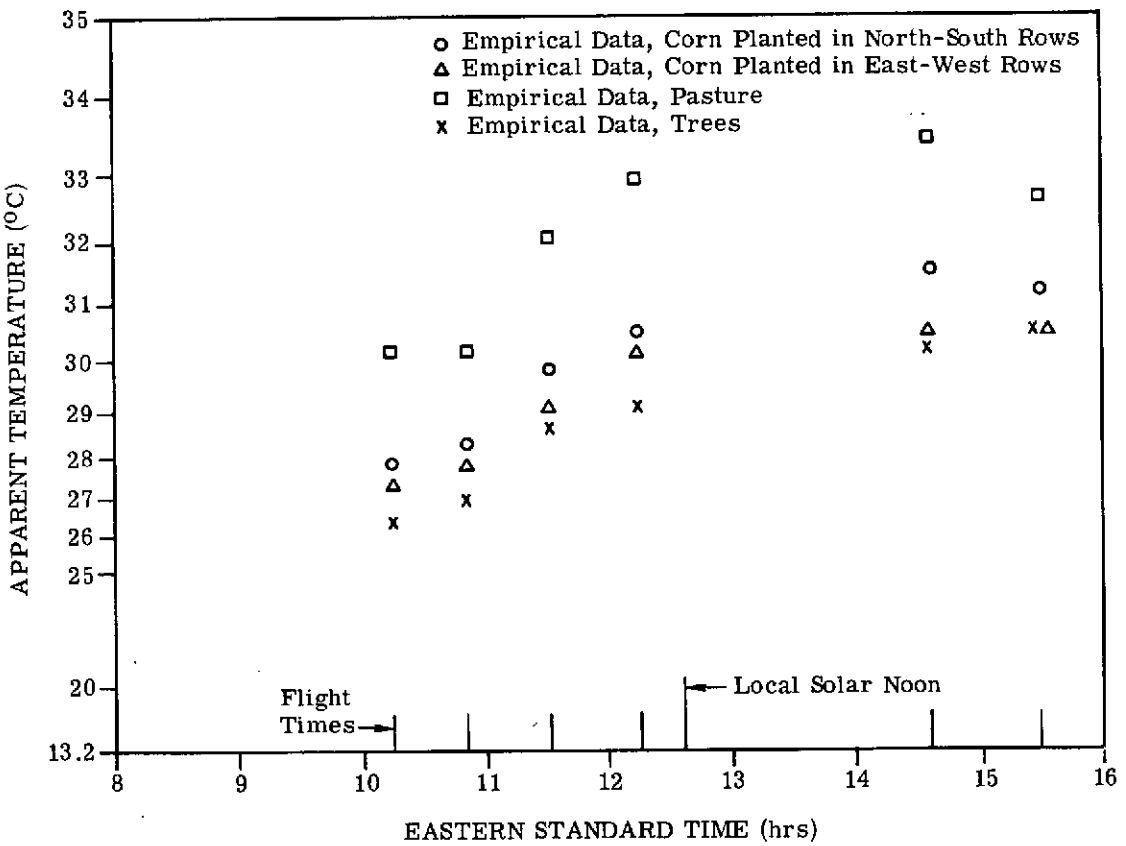

(c) Scan Angle +24° (Eastward)

FIGURE 5. APPARENT TEMPERATURE AS A FUNCTION OF TIME, CHANNEL 12 (9.3-11.7 μm). 6 August 1971, altitude 1.5 km (5000 ft), visibility 23 km. (Concluded)

corn (in both east-west and north-south row directions), while pasture is always hotter. The differences are reasonable in physical terms of the actual temperatures expected. The tree tops can be expected to stay cooler since their height above the ground exposes them to more cooling breezes; in addition, trees transpire well (cool by evaporating moisture). At the other extreme, the pasture and grasses are nearest the hot ground and exposed to the least breeze; furthermore, their shallow root systems provide less moisture for transpiration under extreme conditions —the flight was made on a hot August day with temperatures as high as 30°C (86°F).

Even within the micro system for one ground cover, temperatures were not uniform. Comparison of the same ground covers on different scan-angle graphs shows the sunlit side was somewhat warmer. The afternoon measurements at the eastward (anti-solar) scan angle are particularly warmer than afternoon measurements at the other scan angles. But at the westward scan angle, the afternoon measurements are only slightly cooler than the near-noon run, especially for pasture (which, however, is not as reproducible as the other ground covers shown). This will be discussed further in connection with the subject of scan-angle dependencies in Section 2.4.

2.3.2 RECOGNITION RESULTS

The empirical and theoretical data presented in the preceding section clearly exhibit systematic trends associated with the time of day. It is important to determine the degree to which classification performance is affected by such changes in signal levels. A series of classification tests was made in which signatures obtained from the first run of the day (9:33 LST) were applied to data from that run and from each of the other five runs. The application of signatures to a run other than that for which they were extracted is hereinafter called "non-local" classification. "Local" classification, i.e., classification with signatures extracted from the same run, was carried out for each of the other five runs to provide a standard for comparison with the performance achieved with the non-local signatures.

Thirty-two nadir fields were used to form combined signatures for eight ground covers — EW corn (i.e., corn with east-west rows), NS corn (i.e., corn with north-south rows), trees, pasture, hay, oats, field beans, and soybeans —for each of the six times of day. Only fields in the nadir scan-angle range (±5° in most cases) were used for training and testing, so that scan-angle effects would not be a factor in the results. One combined signature was established for each of six classes, with the subsignatures within a class given equal weights.

The ERIM linear-classification algorithm [8] was used with a classification threshold corresponding to a 0.001 probability of false rejection (under the assumption of multivariate normal distributions). Eleven of the twelve available channels were used. The thermal

channel (No. 12, 9.3 to 11.7 μm) was excluded because it measures emitted radiation which behaves in an intrinsically different way from the primarily reflected radiation we wanted to study in the other eleven channels, as discussed earlier in Section 2.3.1. Reflected radiation (including some scattered radiation from the atmosphere) theoretically should decrease in proportion to the solar irradiance in the afternoon to match the morning level at the corresponding sun elevation angle (as noted in Section 2.3.1, though, afternoon measurements declined only slightly). One of our objectives, therefore, was to determine how well morning signatures would perform on data collected under corresponding solar positions in the afternoon.

Figure 6 portrays graphically the degradation in classification results when the first-run signatures were used on later runs. The lower values in all cases represent correct classifications with the non-local signatures from the first run, while the higher values represent the reference performance achieved with the local signatures (there is of course only one value for the first run). The exact pattern varies from crop to crop, but the trend is one of consistent decline in performance as time progresses. The results are also presented in tabular form in Tables 2 (summary averages over all classes) and 3 (values for individual classes).

From an average classification accuracy of 84% on the first run (ranging from 77 to 99% for the six classes), the results decrease to an average of 36% (ranging from 29 to 52%, except for an anomalously low 3% for soybeans) for the second run (10:07 LST) which is only 35 minutes later than the first. By the third run (10:55 LST), some 82 minutes after the signature-extraction run, the average classification accuracy is only 14% (ranging from 0 to 33%). Recognition is virtually 0% for all ground covers by the fourth run (11:33 LST), which is 120 minutes after signature extraction and only 27 minutes from local solar noon. By comparison, except for oats on the second run which was anomalously low at 55%, the local classification accuracy ranged from 77 to 99%, averaging 85%.

False detection and unclassified percentages, averaged over all classes, are also noted in Table 2. It can be seen that most of the incorrectly classified data were unclassified rather than misclassified as a different ground cover. One exception noted during the analysis was corn, for which 13.6% of corn pixels on the second run were classified as soybeans, as opposed to only 0.8% on the first.

The oat recognition extrapolated to later times better than any other ground cover. Its 32.8% on the third run is about twice the next best of 16.6% obtained for combined hay and pasture; and 1.4% of oats was still recognized on the fourth run, versus 0 to 0.2% for the other classes. Soybeans, on the other hand, are the best (at 99.1%) on the first run; yet they are by far the worst under extrapolation, with only 3.1% by the second run and 0% from then

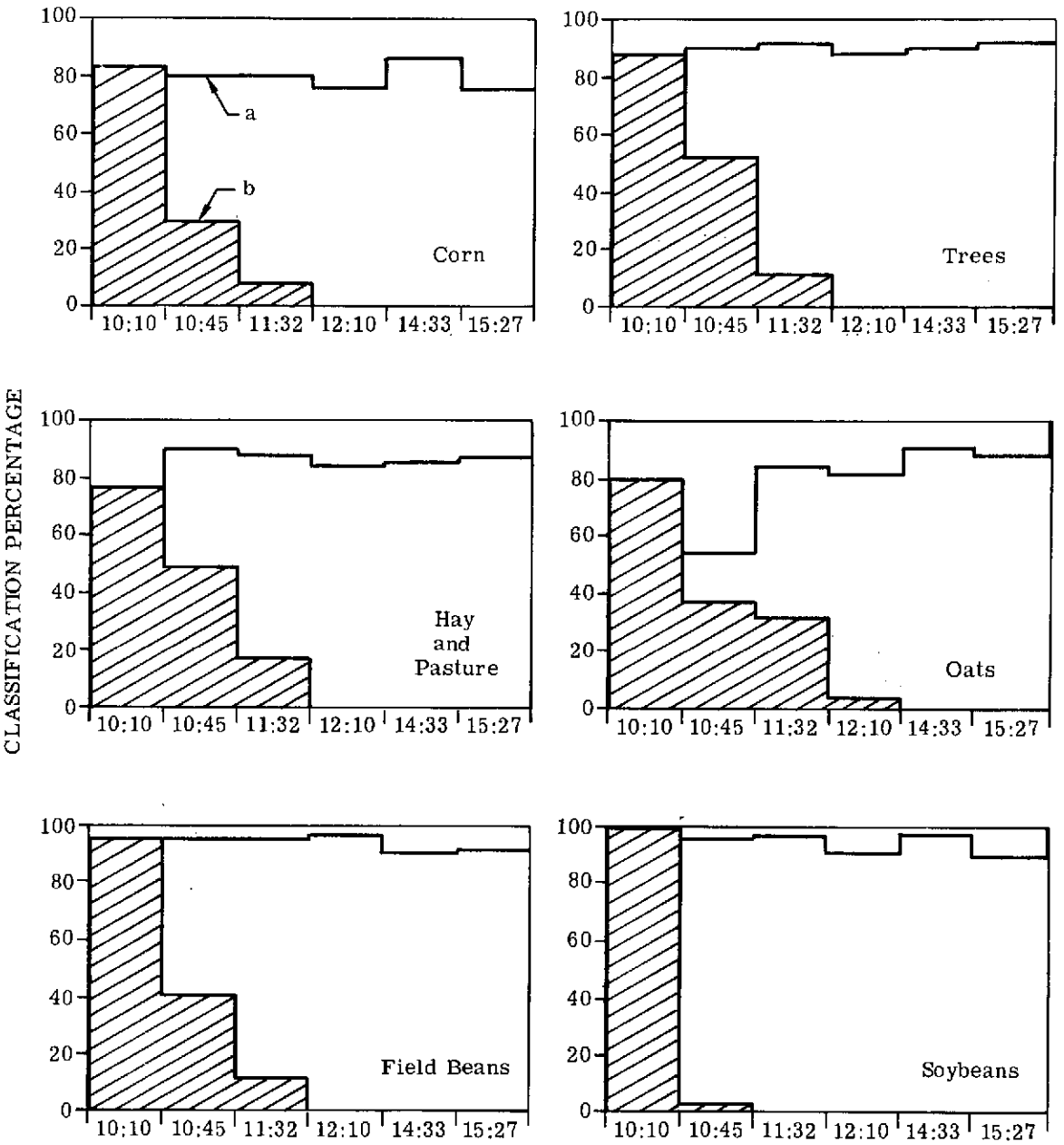

a - percent correct crop classification with signatures from same run as classified

b - percent correct crop classification with signatures from 10:10 EST

FIGURE 6. CORRECT CLASSIFICATION ON NADIR TRAINING FIELDS. Both non-local combined and local combined signatures from the first run were used.

TABLE 2. TIME-OF-DAY EFFECTS ON CLASSIFICATION, RESULTS AVERAGED OVER SIX CLASSES

Data: Ingham County, Michigan
6 August 1971
1.5-km (5000-ft) altitude
North-South headings

		Times of Run (EST)					
		10:10	10:45	11:32	12:10	14:33	15:27
Own-Run Signatures	Correct (%)	84	83	88	84	88	86
10:10-Run Signatures	Correct (%)	84	36	14	0.2	0	0
	Incorrect (%)	11	10	5	0	0	0
	Unclassified (%)	5	53	81	99.8	100	100

Class	Number of Fields	Average Number of Data Points
Corn	14	2100
Trees	2	160
Pasture and Hay	7	1400
Oats	4	640
Field Beans	3	1200
Soybeans	2	220

TABLE 3. TIME-OF-DAY EFFECTS ON CLASSIFICATION, SPECIFIC RESULTS FOR EACH CLASS

Data: Ingham County, Michigan, 6 August 1971, 1.5-km (5000-ft) altitude, North-South headings, 11 channels (thermal omitted), nadir training and test fields, single combined signature for each class, threshold for 0.001 probability of false rejection for normal distributions.

Classification Run	LST	Using Signatures from Run	Percentage-Correct Classification For: Corn	Trees	Pasture and Hay	Oats	Field Beans	Soybeans	Average Over Classes
1	(9:33)	1	83.3	87.6	77.4	81.1	95.2	99.1	84.4
2	(10:07)	1	29.3	52.4	49.3	36.7	40.7	3.1	36.4
		2	80.1	89.3	90.2	55.8	95.2	97.5	82.8
3	(10:55)	1	6.8	11.4	16.6	32.8	11.1	0	13.5
		3	80.6	90.8	87.6	85.2	95.0	98.4	87.6
4	(11:33)	1	0	0	0.2	1.4	0.2	0	0.2
		4	75.4	87.2	84.8	82.8	96.0	87.6	83.5
5	(13:56)	1	0	0	0	0	0	0	0
		5	85.4	90.0	85.7	90.5	90.8	98.6	87.7
6	(14:50)	1	0	0	0	0	0	0	0
		6	79.1	91.5	86.4	87.2	96.3	90.0	86.1

on. We suspected that oats might have a broader-than-average signature distribution in most channels and that soybeans might have an unusually narrow signature in at least one channel. However, channel-by-channel calculations of the standard deviations divided by the mean signature value for each material were made (see Table 4), and no such clear-cut differences between ground-cover signatures are apparent. We presently do not understand why these classification differences occurred, although correlations between channels were not examined at this point.

The results of the four morning runs are roughly in accordance with our expectations. But, the last two runs (afternoon) in all cases give 0% recognition with the signatures from the first run, although we had expected that classification results would improve again in the afternoon as the sun geometry became comparable to that of the first run. Note in Table 1 that the first run is 147 minutes before local solar noon, about two-thirds of the way between the 115 and 170 minutes after local solar noon for the fifth and sixth run. The fifth run is nearly the mirror image (around local solar noon) of the second, differing by two minutes in time, 0.07^{o} in solar-elevation angle, and 0.04^{o} in solar-azimuth angle from 180^{o} (due South). Also note that the sixth run is fairly near the mirror image of the first run, since the solar elevation angles differ by only 3.5^{o}, and the azimuth angles by only 5.2^{o} from 180^{o} (due South). Hence, considering only the effects of the solar angle and noting that all ground areas used are from subfields restricted to a few degrees around nadir, one would expect that at worst the classification results on runs 5 and 6 would be commensurate with those on run 2. Instead, there is absolutely no correct classification of any ground cover tried on either afternoon run.

There are several possible explanations as to why the morning signatures gave poor results on the near mirror-image afternoon runs. Among them are the following:

(1) Changes in crop leaf attitude, reflectance, etc., perhaps the result of heating and moisture losses later in the day

(2) The suspected changes in illumination caused by partial cloud cover in the afternoon, as previously discussed

(3) Run-to-run calibration differences

Before the poor results can be attributed to one of the first two causes, it is necessary to establish that they cannot be blamed solely on differences stemming from inadequate correction for run-to-run calibration differences. We have some indications that any remaining calibration discrepancies are insufficient in magnitude, and apparently of the wrong sign, to account for the observed differences on the afternoon runs; however, we have not examined possible calibration differences in sufficient detail to allow a firm conclusion. We do have cause to suspect some of the coarse-adjustment scaling changes made, particularly on channels

TABLE 4. FIRST-RUN SIGNATURE SPREADS FOR INGHAM COUNTY TIME-OF-DAY STUDY, STANDARD DEVIATION, σ, DIVIDED BY MEAN, μ

Ground Cover		Channel 1	2	3	4	5	6	7	8	9	10	11	12	Average of Channels 1-11
NS Corn	μ	88.81	64.01	71.39	113.69	92.94	75.70	65.68	214.77	179.67	113.34	75.59	122.13	
	σ	7.57	6.03	7.03	12.35	11.33	10.75	10.21	11.95	7.65	9.93	7.78	9.97	
	σ/μ%	8.5	9.4	9.8	10.9	12.19	14.2	15.5	5.6	4.3	8.8	10.3	8.2	9.8
Trees	μ	64.65	44.93	49.75	81.48	63.35	47.31	37.14	211.60	181.06	92.25	63.66	103.84	
	σ	5.03	4.19	5.73	12.00	9.44	7.24	5.45	36.77	27.84	17.28	6.65	11.50	
	σ/μ%	7.8	9.3	11.5	14.7	14.9	15.3	15.7	17.4	15.4	18.7	10.4	11.1	13.5
Pasture	μ	87.77	63.93	70.66	110.64	94.22	81.75	75.60	178.67	182.69	145.37	93.78	162.96	
	σ	12.42	9.77	8.51	10.63	11.05	14.23	17.81	28.68	16.42	17.66	14.32	32.53	
	σ/μ%	14.2	15.3	12.0	9.6	11.7	17.4	23.6	16.1	9.0	12.1	15.3	20.0	14.7
Oats	μ	123.42	94.57	100.70	149.76	137.78	135.94	140.54	172.86	178.67	175.75	126.34	176.59	
	σ	16.63	13.31	12.92	17.81	18.05	21.48	25.30	10.76	11.50	25.48	20.25	22.78	
	σ/μ%	13.5	14.1	12.8	11.9	13.1	15.8	18.0	6.2	6.4	14.5	16.0	12.9	12.9
Soybean	μ	105.00	76.66	82.58	127.63	106.12	90.55	82.34	241.38	201.23	137.16	95.20	144.71	
	σ	17.70	14.42	14.73	20.65	21.01	23.32	24.55	12.14	7.36	10.32	11.42	12.12	
	σ/μ%	16.9	18.8	17.8	16.2	19.8	25.8	29.8	5.0	3.7	7.5	12.0	8.4	15.1

other than the four (Nos. 1, 4, 7, and 8) chosen for intensive study under the preceding analysis of field-signal means. Channel 3, in particular, is suspect. The coarse scale changes recorded in the flight log did not agree well with the scaling calculated by comparing the channel 3 calibration lamp signals between run 1 and the afternoon runs. The scaling adjustments recorded in the flight log were used to correct the data. It can also be seen that the changes in means from run 1 to run 6 seem anomalously large for channel 3, as shown in Table 5. One indication of the possible magnitude of calibration differences is the fine (4 to 7%) calibration adjustment derived from the calibration lamp signals from run 1 to the afternoon runs for the four channels studied. These adjustments had been made previously on the afternoon runs for the field signal mean studies already discussed. Since similar adjustments were not available for the other seven channels at the time classification was tested, none was applied—however, note that the adjustments for the four channels studied are all increases which would have moved the afternoon data even farther from the morning signatures if they had been applied. The possible magnitudes of any necessary fine scaling calibration corrections apparently are not large enough (nor the signs correct) to account for the degraded performance, as can be seen by comparing these 4 to 7% adjustments with the typically 5 to 20% σ/μ values shown for various run-1 signatures in Table 4. However, these calibration discrepancies warrant further study to determine whether they can be more precisely determined. Furthermore, since we have evidence that the afternoon illumination was higher, it would be desirable to investigate the use of scaling according to the sun sensor.

Also, it now seems desirable to repeat the temporal classification test using fewer channels. The main reason for this is that some χ^2 tests of the separation between later-run signal means and first-run signatures point to improved results on runs 5 and 6 with four channels instead of 11. Furthermore, results on another task [1] under this contract show drastically improved signature extension to another area when fewer channels are used.

Since the χ^2 calculation takes into account the correlations between channels, in general it is different from values that could be computed from Table 5. The distance of a point from a multivariate normal distribution can be measured by the exponent of the distribution's likelihood function evaluated at that point. This exponent value, which herein is called the χ^2 value, is the squared distance between the distribution mean and the point in question, measured in standard deviation units of the distribution. Thus, a large χ^2 value indicates a large separation. The χ^2 value also increases with the number of channels used.

In Table 6 some χ^2 values for the field-weighted means of various ground covers on later runs are compared with signatures for the same ground covers from the first run. The χ^2 values given are both for the 11 channels used in the classification test and for the subset of four channels selected for intensive study in Section 2.3.1 (channels 1, 4, 7, and 8—again

TABLE 5. COMPARISON OF GROUND-COVER MEANS ON FIRST AND SIXTH INGHAM COUNTY RUNS. Standard deviations of first-run combined signatures, $(\mu_6 - \mu_1)/\sigma_1$.

	Channel										
Ground Cover	1	2	3	4	5	6	7	8	9	10	11
Corn, N-S Rows	3.10	2.53	4.70	1.62	1.67	1.48	1.20	0.69	1.09	0.83	0.67
Trees	4.41	3.25	4.76	3.60	1.99	1.92	1.93	0.67	0.95	1.57	0.40
Pasture	2.29	1.90	4.25	2.12	1.92	1.42	1.02	-0.06	-0.03	0.42	0.58
Oats	1.07	0.93	1.82	0.88	0.88	0.75	0.60	0.46	0.65	0.39	0.39
Soybeans	1.56	1.31	2.23	1.36	1.24	0.97	0.76	0.41	0.53	0.31	0.38
Average	2.49	1.98	3.55	1.92	1.54	1.31	1.10	0.97	0.64	0.70	0.48

TABLE 6. χ^2 VALUES OF GROUND COVER MEANS ON LATER INGHAM COUNTY RUNS. Combined signatures for matching ground covers from first run of the day.

Ground Cover	Run	χ^{2*} 11 Channels	χ^{2*} 4 Channels
Corn, E-W Rows	2	27.41	15.12
	3	48.49	28.38
	4	156.37	107.08
	5	713.91	38.53
	6	612.21	51.46
Corn, N-S Rows	2	18.74	8.83
	3	32.67	12.83
	4	94.64	63.71
	5	548.17	19.90
	6	491.68	33.38
Trees	2	20.84	11.43
	3	33.82	17.66
	4	121.69	87.59
	5	508.62	18.83
	6	549.93	51.32
Pasture	2	16.82	7.46
	3	25.31	15.78
	4	63.06	38.55
	5	616.83	21.00
	6	521.49	28.10
Hay	2	43.80	11.27
	3	38.79	14.13
	4	150.02	79.48
	5	692.20	25.27
	6	575.21	47.39
Oats	2	19.67	13.00
	3	22.20	11.92
	4	63.14	34.81
	5	581.34	13.93
	6	421.80	8.28
Field Beans	2	23.32	13.63
	3	34.02	17.09
	4	128.05	82.66
	5	704.56	31.05
	6	645.11	36.12
Soybeans	2	48.38	21.00
	3	62.08	27.95
	4	156.56	104.01
	5	590.34	18.55
	6	750.23	57.91

*With a probability of 0.001, for example, a sample from a multivariate normal distribution will have $\chi^2 > 31.26$ for 11 channels and $\chi^2 > 18.47$ for 4 channels. Therefore, the magnitude of χ^2 values for 11 and 4 channels should not be compared directly.

excluding the thermal channel). The unexpectedly high 11-channel χ^2 values between 400 and 750 for the two afternoon runs corroborate the zero-correct classification results obtained earlier; these values are much higher than even the 62 to 156 values on the fourth run (nearest noon) at 11:33 LST. Yet, for four channels the afternoon χ^2 values of 8 to 58 are lower than the noon values of 35 to 107 and more commensurate with the run 2 values of 7 to 21 (the low and high extremes occurred on different ground covers, however). Hence, the four-channel χ^2 values for the afternoon runs imply that classification, after degrading toward noon, should indeed improve in the afternoon.

We need to further study the reasons for the exceptionally large 11-channel χ^2 values compared with the decreasing four-channel χ^2 values on the two afternoon runs. There might be a calibration problem with the two afternoon runs in one or more of the seven channels excluded in the four-channel subset, or there might be some actual physical differences.

The results obtained to date, even if only the morning runs are considered, demonstrate that temporal effects can seriously degrade classification performance with airborne-multispectral-scanner data. We believe, however, that one of the first priorities for continued work should be to provide a better quantitative assessment of performance degradation by repeating the temporal classification tests, which would include using a suitably selected subset of channels and giving careful attention to their individual calibration.

2.4 SCAN-ANGLE AND BIDIRECTIONAL-REFLECTANCE EFFECTS IN SIGNATURES

When empirical data from the Ingham County flights are considered as a function of scan angle, it can be seen that there are sizable variations. In the shortest wavelength channel, the predictions of the radiative transfer model closely follow the empirical data; but at the longer visible and near-infrared wavelengths, there are strong scan-angle dependencies not accounted for by this model. Predictions of bidirectional reflectance variations at the longer wavelengths, made with a different theoretical model developed at ERIM by Dr. Gwynn Suits [6], show similar variations with scan angle under somewhat different conditions. In the far-infrared thermal channel, there are small scan-angle variations which show that the ground covers are slightly warmer on their sunlit side.

Figures 7-9 present both the theoretical radiation-transfer model predictions for Lambertian reflectors and the empirical data for four ground covers, all plotted as a function of scan angle for channels 1 (0.46-0.49 μm), 7 (0.61-0.70 μm), and 8 (0.72-0.92 μm). Each figure is for one of three selected times of day (corresponding to different data-collection runs): the first run, 9:33 AM LST ("morning"); the fourth run, 11:33 AM LST ("noon"); and the sixth and last run, 2:50 PM LST ("afternoon"). These figures are similar to the graphs of radiance versus time-of-day in Figs. 1 and 2 already discussed, except in the choice of scan angle for

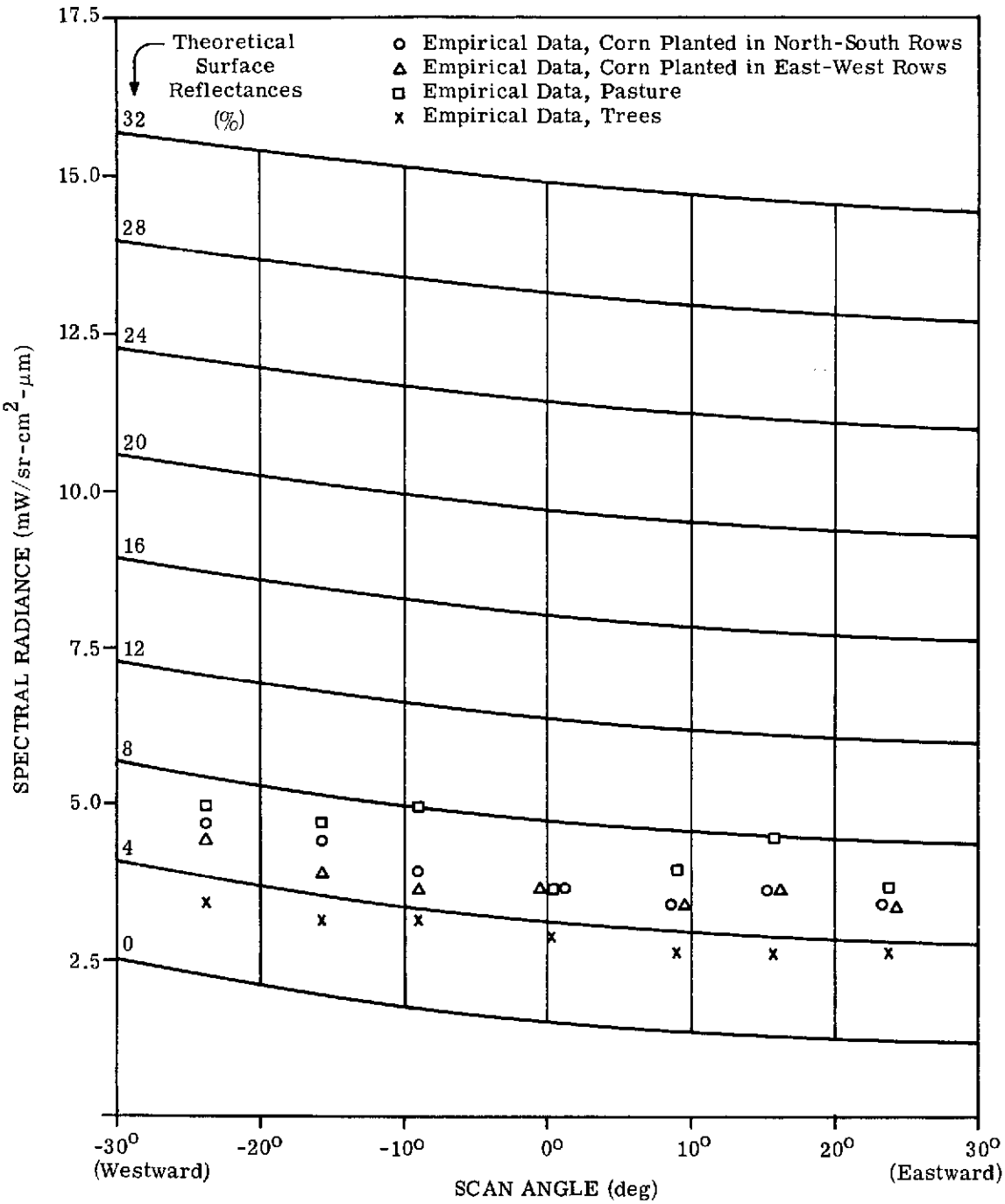

(a) 9:33 LST

FIGURE 7. RADIANCE AS A FUNCTION OF SCAN ANGLE, CHANNEL 1 (0.47-0.49 μm). Empirical data for four crops and theoretical data for various Lambertian surface reflectances. 6 August 1971, altitude 1.5 km (5000 ft), visibility 23 km. (Continued)

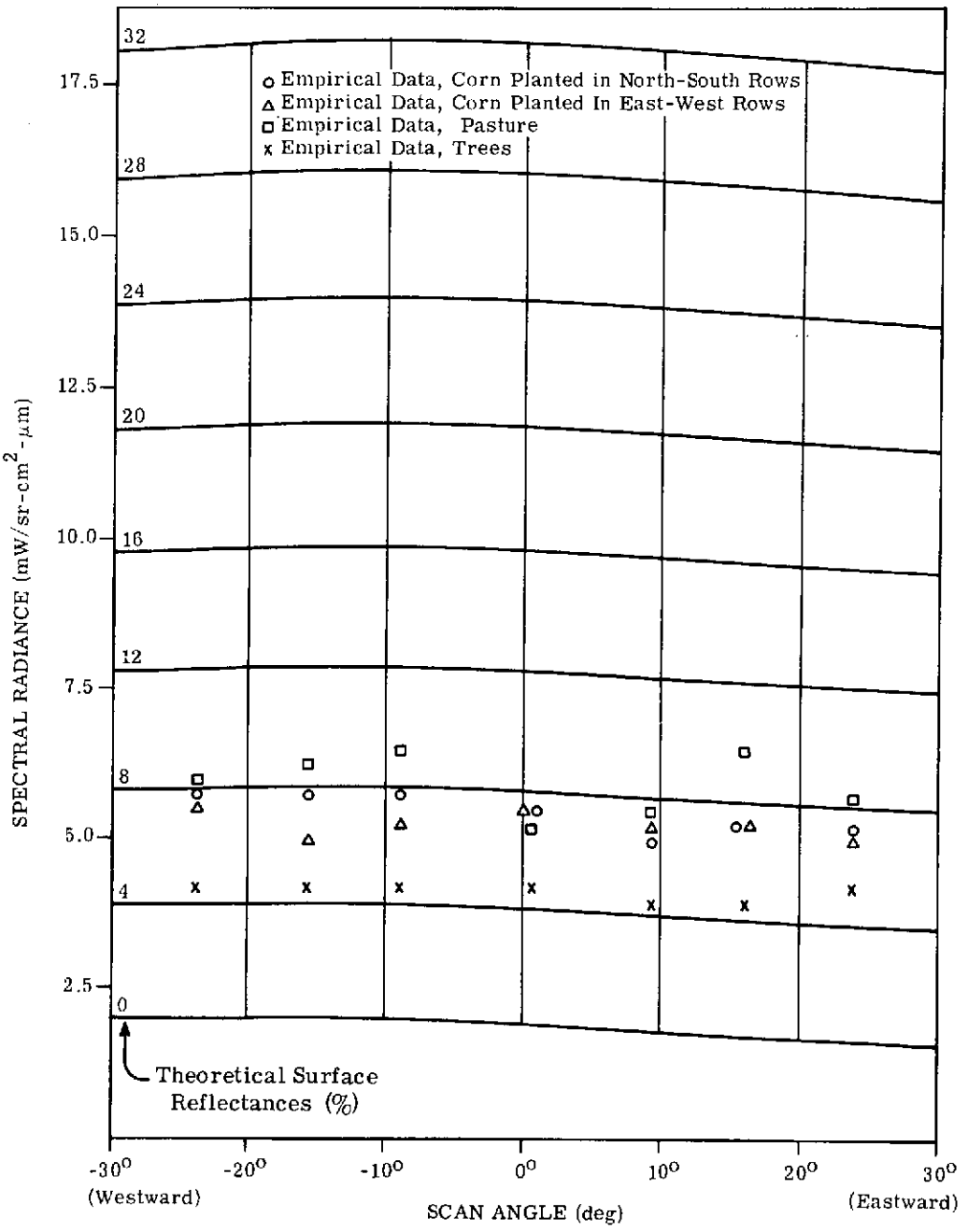

(b) 11:33 LST

FIGURE 7. RADIANCE AS A FUNCTION OF SCAN ANGLE, CHANNEL 1 (0.47-0.49 μm). Empirical data for four crops and theoretical data for various Lambertian surface reflectances. 6 August 1971, altitude 1.5 km (5000 ft), visibility 23 km. (Continued)

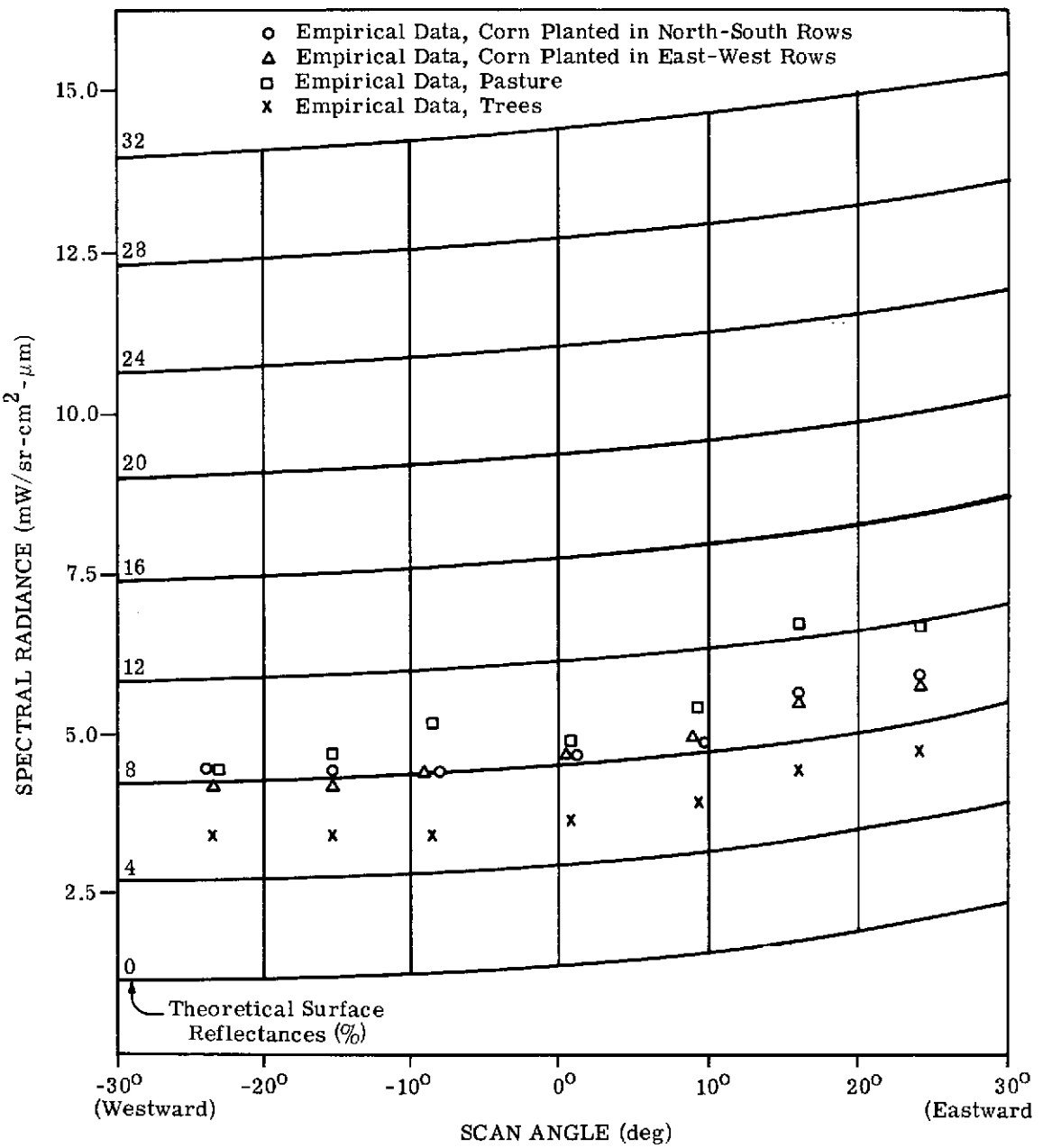

(c) 14:50 LST

FIGURE 7. RADIANCE AS A FUNCTION OF SCAN ANGLE, CHANNEL 1 (0.47-0.49 μm). Empirical data for four crops and theoretical data for various Lambertian surface reflectances. 6 August 1971, altitude 1.5 km (5000 ft), visibility 23 km. (Concluded)

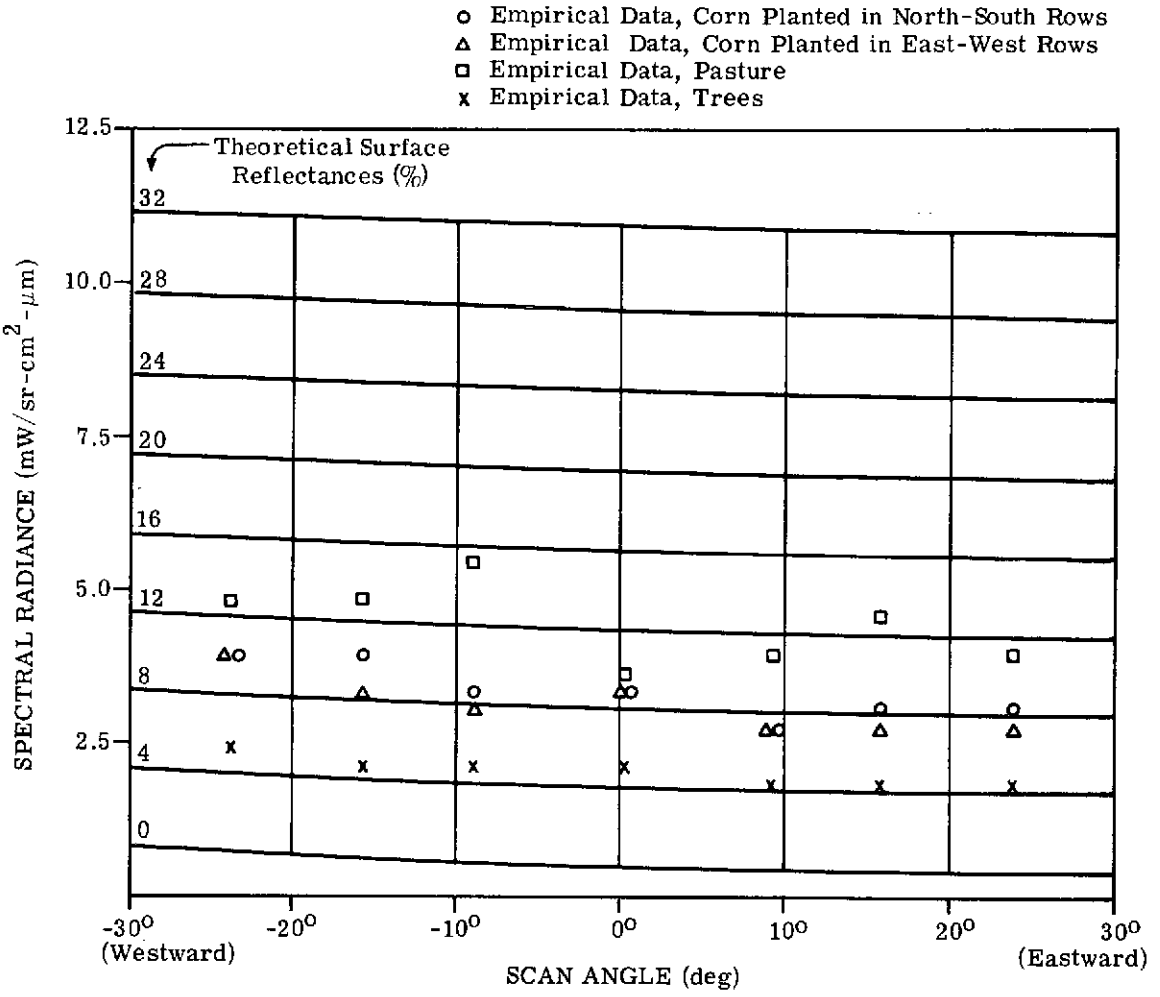

(a) 9:33 LST

FIGURE 8. RADIANCE AS A FUNCTION OF SCAN ANGLE, CHANNEL 7 (0.61-0.70 μm). Empirical data for four crops and theoretical data for various Lambertian surface reflectances. 6 August 1971, altitude 1.5 km (5000 ft), visibility 23 km. (Continued)

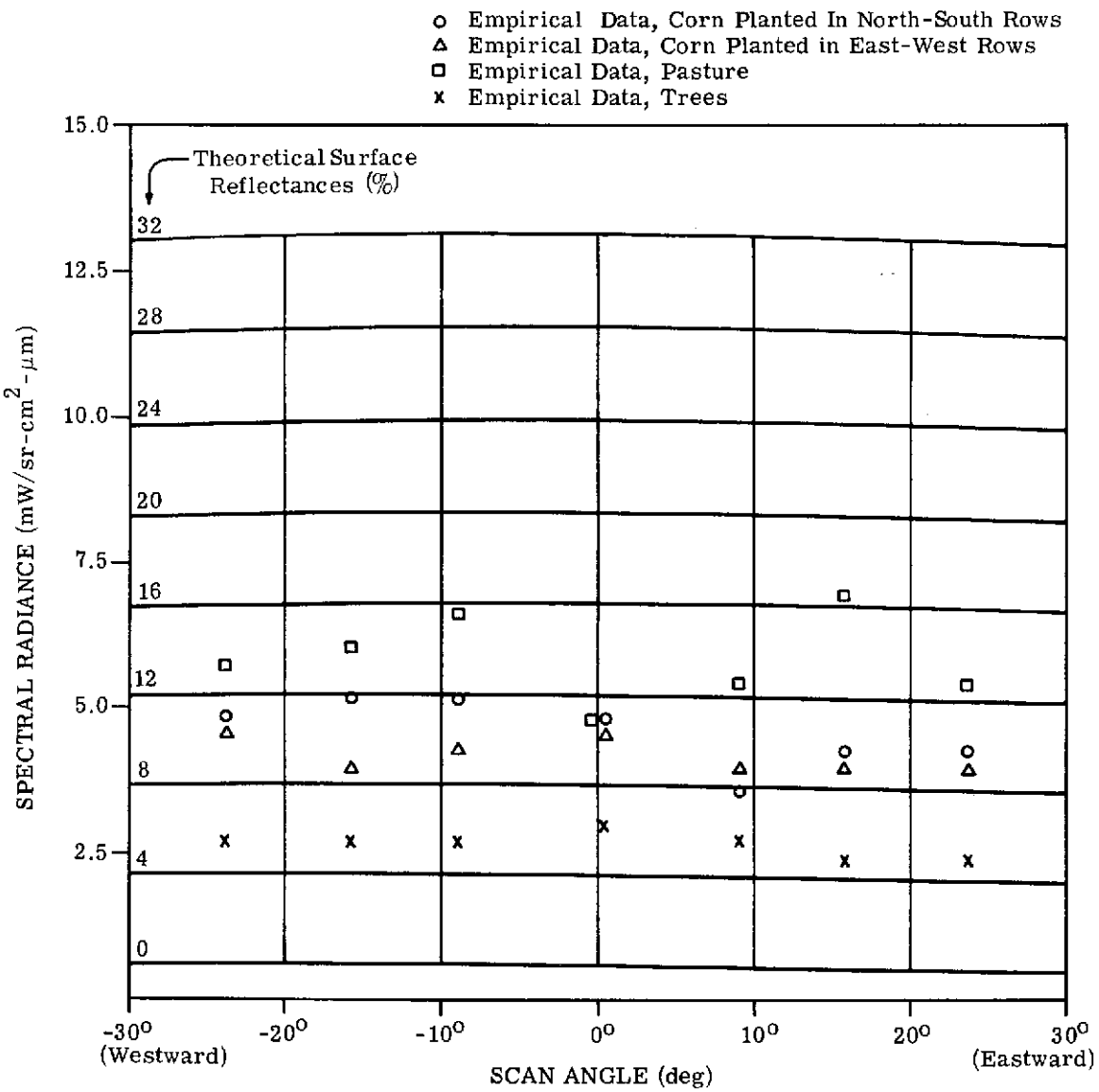

(b) 11:30 LST

FIGURE 8. RADIANCE AS A FUNCTION OF SCAN ANGLE, CHANNEL 7 (0.61-0.70 μm). Empirical data for four crops and theoretical data for various Lambertian surface reflectances. 6 August 1971, altitude 1.5 km (5000 ft), visibility 23 km. (Continued)

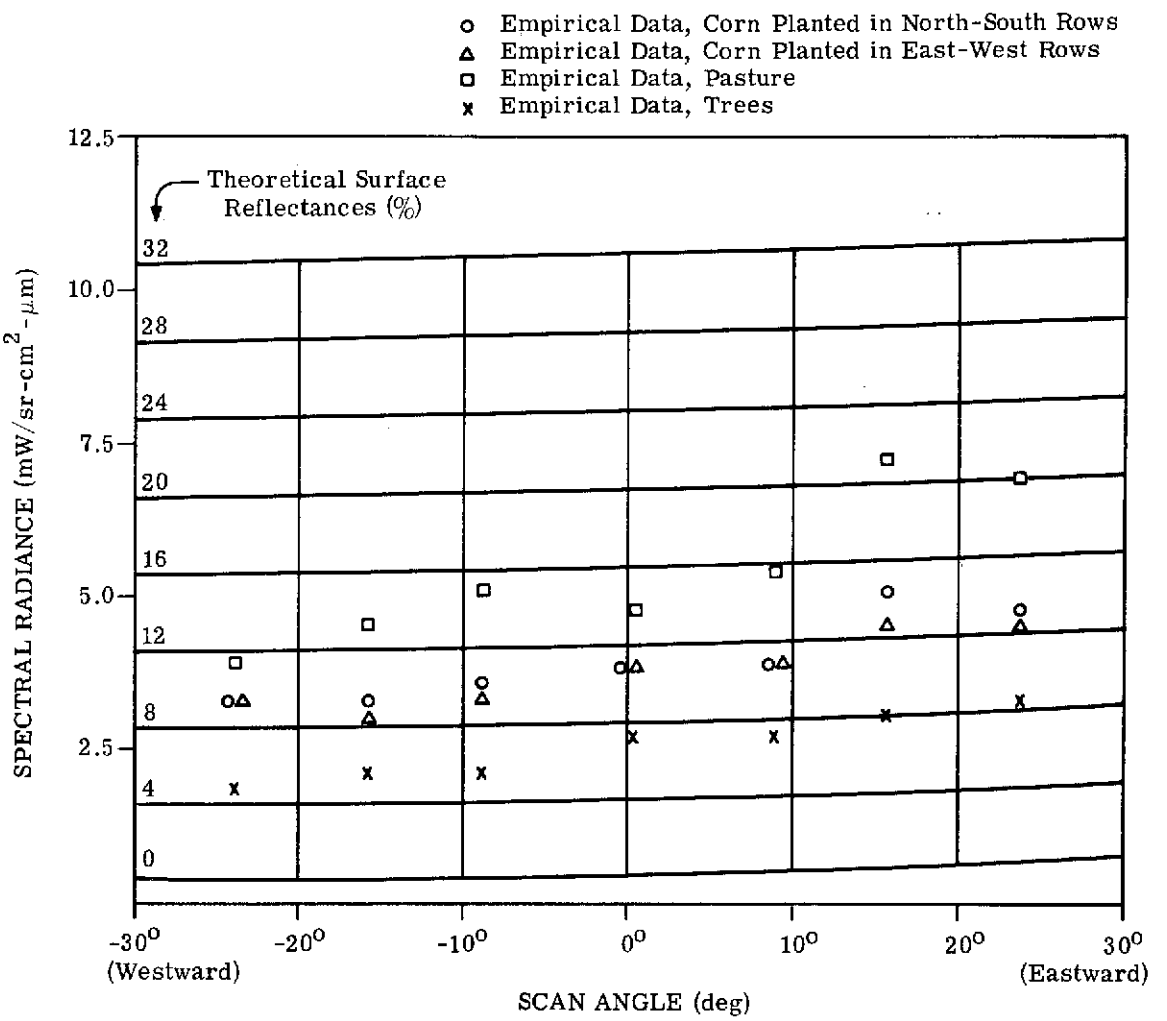

(c) 14:50 LST

FIGURE 8. RADIANCE AS A FUNCTION OF SCAN ANGLE, CHANNEL 7 (0.61-0.70 μm). Empirical data for four crops and theoretical data for various Lambertian surface reflectances. 6 August 1971, altitude 1.5 km (5000 ft), visibility 23 km. (Concluded)

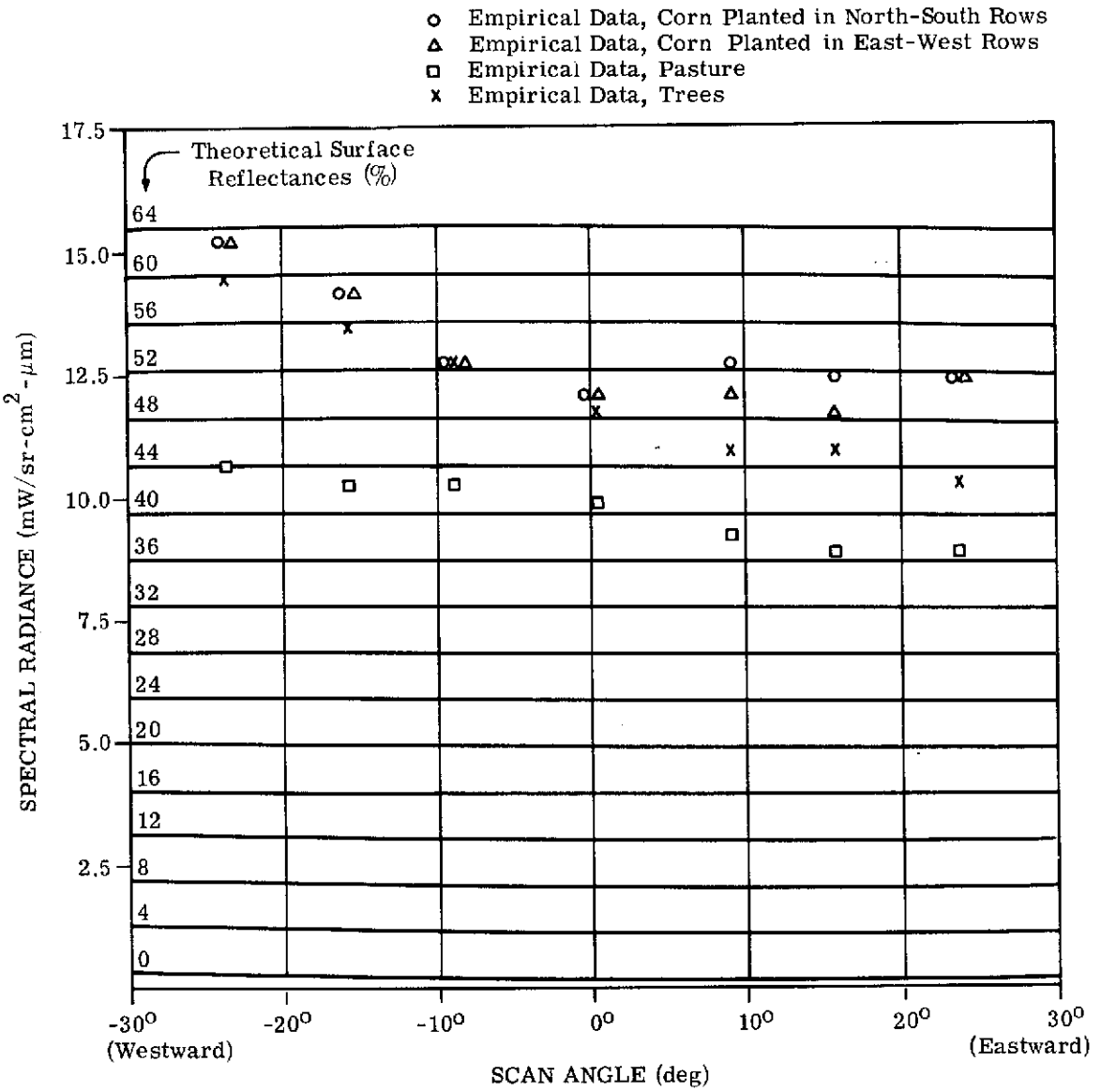

(a) 9:33 LST

FIGURE 9. RADIANCE AS A FUNCTION OF SCAN ANGLE, CHANNEL 8 (0.72-0.92 μm). Empirical data for four crops and theoretical data for various Lambertian surface reflectances, 6 August 1971, altitude 1.5 km (5000 ft), visibility 23 km. (Continued)

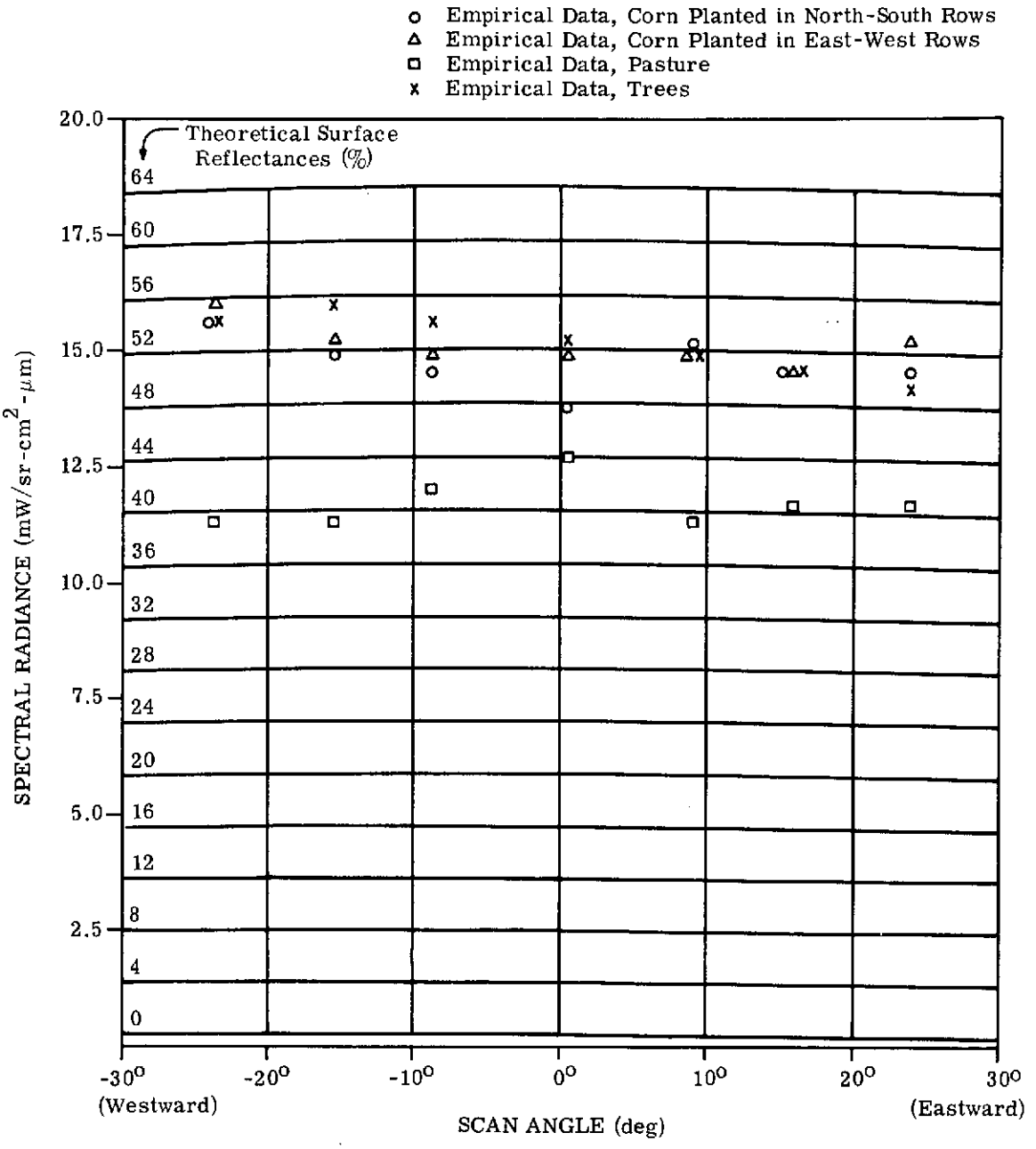

(b) 11:30 LST

FIGURE 9. RADIANCE AS A FUNCTION OF SCAN ANGLE, CHANNEL 8 (0.72-0.92 μm). Empirical data for four crops and theoretical data for various Lambertian surface reflectances, 6 August 1971, altitude 1.5 km (5000 ft), visibility 23 km. (Continued)

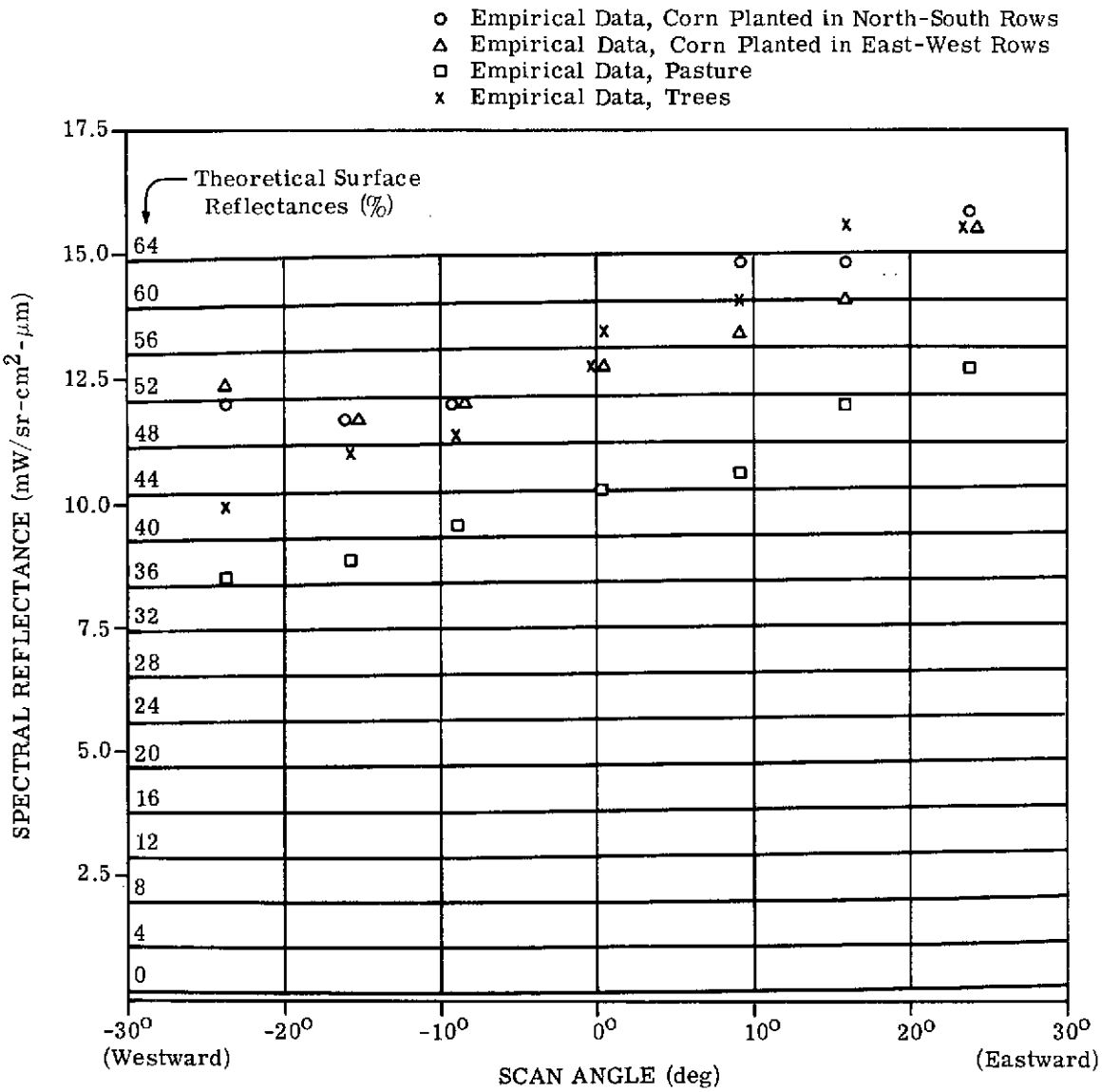

(c) 14:50 LST

FIGURE 9. RADIANCE AS A FUNCTION OF SCAN ANGLE, CHANNEL 8 (0.72-0.92 μm). Empirical data for four crops and theoretical data for various Lambertian surface reflectances, 6 August 1971, altitude 1.5 km (5000 ft), visibility 23 km. (Concluded)

the independent variable. Since the same data are plotted in both sets of graphs, many conclusions are related; however, the plots of radiance versus scan angle are better suited for studying scan-angle effects, particularly those that might be attributable to bidirectional reflectance variations.

Again it can be noted that the shortest wavelength (blue, or channel 1) shows the strongest theoretical atmospheric effects, with anti-solar backscatter peaking in the west on the morning run and in the east on the afternoon, and with less scan-angle effect at noon. In this channel, the radiative transfer model comes very close to predicting the trend of the empirical data for trees and for corn planted in both row directions. The empirical curve shape for pasture is irregular and dips around nadir, contrary to the predictions. But this can probably be attributed to the different ground areas covered in the different scan-angle ranges, since pasture is typically a less uniform ground cover than the others on this data set. There also appears to be a slight tendency for the empirical data to be a little brighter than predicted by theory in the anti-solar direction, especially for the corn, but this effect is not consistent or strong enough to be clearly separable. Hence, we conclude that the scan-angle variations exhibited by the data in this blue channel can be attributed predominantly to atmospheric contributions, and that any variations caused by bidirectional reflectance are too small to be independently observable.

Atmospheric influence, as predicted by theory, decreases with increasing wavelength until there is virtually no scan-angle dependency in predictions for the near-infrared channel (No. 8). Hence, channels 7 (0.61-0.70 μm and 8 (0.72-0.92 μm) are best for examining bidirectional reflectance effects per se, since the minimal atmospheric contribution should not mask surface reflectance changes. The empirical data observed in channels 7 and 8 show scan-angle dependencies, particularly increases in the anti-solar direction of 40% or more over the minimum value—far stronger than predicted by the radiative transfer model. The data for pasture are still irregular, but despite this, the trends noticed in the other ground covers are now strong enough to be seen in pasture as well.

The deviations from the model may be interpreted in any of three ways: The additional empirical variations might be atmospheric contributions not properly predicted by the model; they might be the result of bidirectional reflectance effects excluded from this Lambertian reflector model; or, they might be caused by some other factor such as non-uniform instrument response, although this last possibility is not considered likely.

The model calculations were made using an assumed average atmospheric visibility of 23 km (15+ mi, considered a typically clear atmosphere at mid-latitudes and low elevations). While with lower visibilities, the model would predict more atmospheric scattering, the assumed visibility was reported by the closest airport, and both flight logs and independent

ground observations indicate a clear atmosphere (except some high thin cirrus clouds in the afternoon, which should not affect the visibility or haze content in the lower atmosphere). In other tests of the radiative transfer model [9], it accurately predicted the angular and wavelength dependencies of sky radiance. Accordingly, we believe that most of the difference noted between the empirical data and predictions of the radiative transfer model must be attributed to reflectance variations.

An empirical argument in favor of this bidirectional reflectance source of variation is the difference observed between the behavior of corn versus trees and pasture in the solar direction (opposite the anti-solar peak); such divergence between two ground covers cannot be explained by any atmospheric contributions and, hence, must be a ground-based phenomenon. On the anti-solar side, all four ground covers have similar increases above nadir values; but on the solar side, the corn radiances start to rise away from nadir while the radiances for trees and pasture are still declining. This is especially visible for channel 8 (see Fig. 9), in the east for the morning and in the west for the afternoon.

Some theoretical calculations of the expected bidirectional reflectance variations, which we made using the Suits model, are shown in Fig. 10 for corn canopies under roughly comparable conditions on another data set. The shapes of the bidirectional reflectance curves agree approximately with the empirical curve shapes. At 0.65 μm (within the channel-7 waveband, 0.61-0.70 μm) these calculations predict a monotonic increase toward the anti-solar side of 14% (i.e., 3.55 to 4.05% equivalent Lambertian reflectances) from the extreme eastward scan angle, $+24^{\circ}$, to the extreme westward scan angle, -24°, of the Ingham County data. This compares with the increase of over 40% in equivalent reflectances (as interpolated from the adjoining radiative transfer model curves) for the corn in channel 7 on the morning and afternoon runs, with a roughly monotonic increase toward the anti-solar side. Similarly, for 0.76 μm (within the channel-8 waveband, 0.72-0.92 μm) a dip in reflectance around nadir with a 10% increase to the extreme scan angles, $\pm 24^{\circ}$, is predicted, versus an observed clear-cut minimum on the solar side and an increase of over 30% toward the anti-solar side. The predicted bidirectional reflectance variations should not be expected to show as strong a variation as is observed in the empirical data, since the solar-elevation angle used for the bidirectional reflectance calculations is about midway between the elevations for noon and the extreme morning or afternoon runs analyzed for Ingham County. The predicted minimum in channel 8 would be expected to shift more toward the solar side at the more extreme times.

The problem of bidirectional reflectance deserves more study. For example, to determine whether this model can be more closely related to the observed deviations between the Lambertian radiative transfer model and the empirical data, more calculations need to be made using the bidirectional reflectance canopy model for matching conditions.

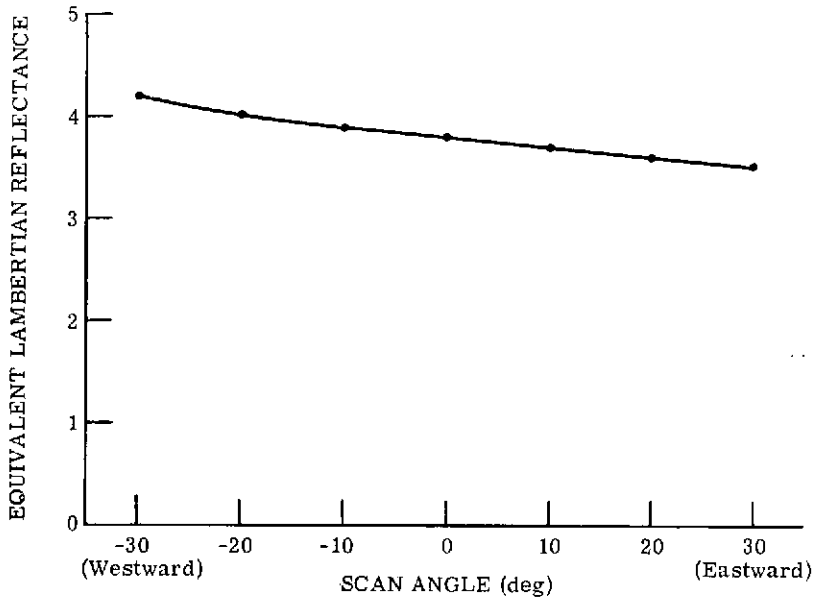

(a) Channel 7 (λ = 0.65μm)

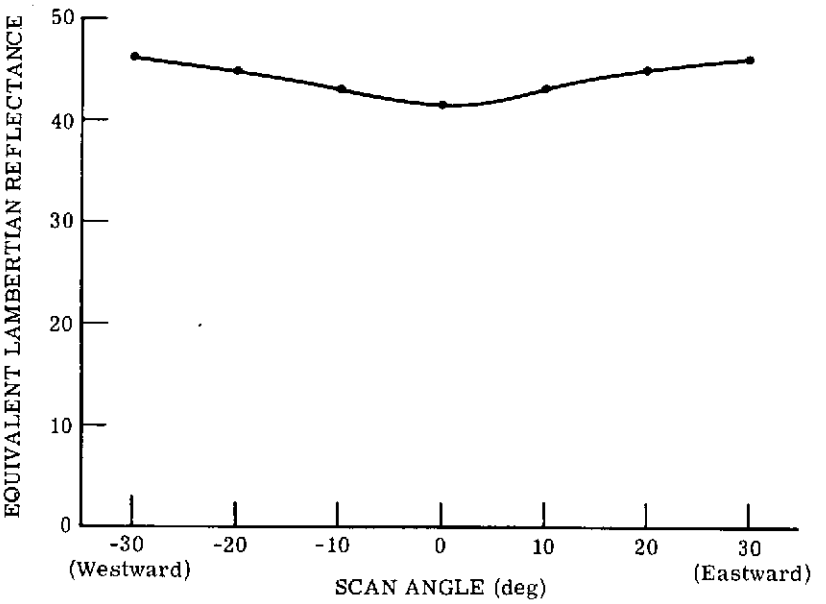

(b) Channel 8 (λ = 0.76μm)

FIGURE 10. THEORETICAL CALCULATIONS OF CORN CANOPY REFLECTANCES. Healthy, mature canopy, no tassels, plant density 28,000/acre, dark soil. Sun azimuth 135°, sun elevation 57°.

The variation of the direct thermal radiation in the far-infrared channel (No. 12) as a function of scan angle is shown for the same three times of day in Fig. 11. These curves confirm the observations made in Section 2.3 about time-of-day variations, namely that different ground covers stay at distinctly different temperatures and that they are in general slightly warmer on the sunlit side. This latter effect is clearly present, although it is mild compared to the variations, primarily in reflected radiation, seen in the near-infrared. Overall, then, the data show a consistency of temperature patterns (since the drop around nadir for pasture is probably attributable to differences between the fields in each angle range, as noted for the visible and near-infrared channels, it is probably meaningless).

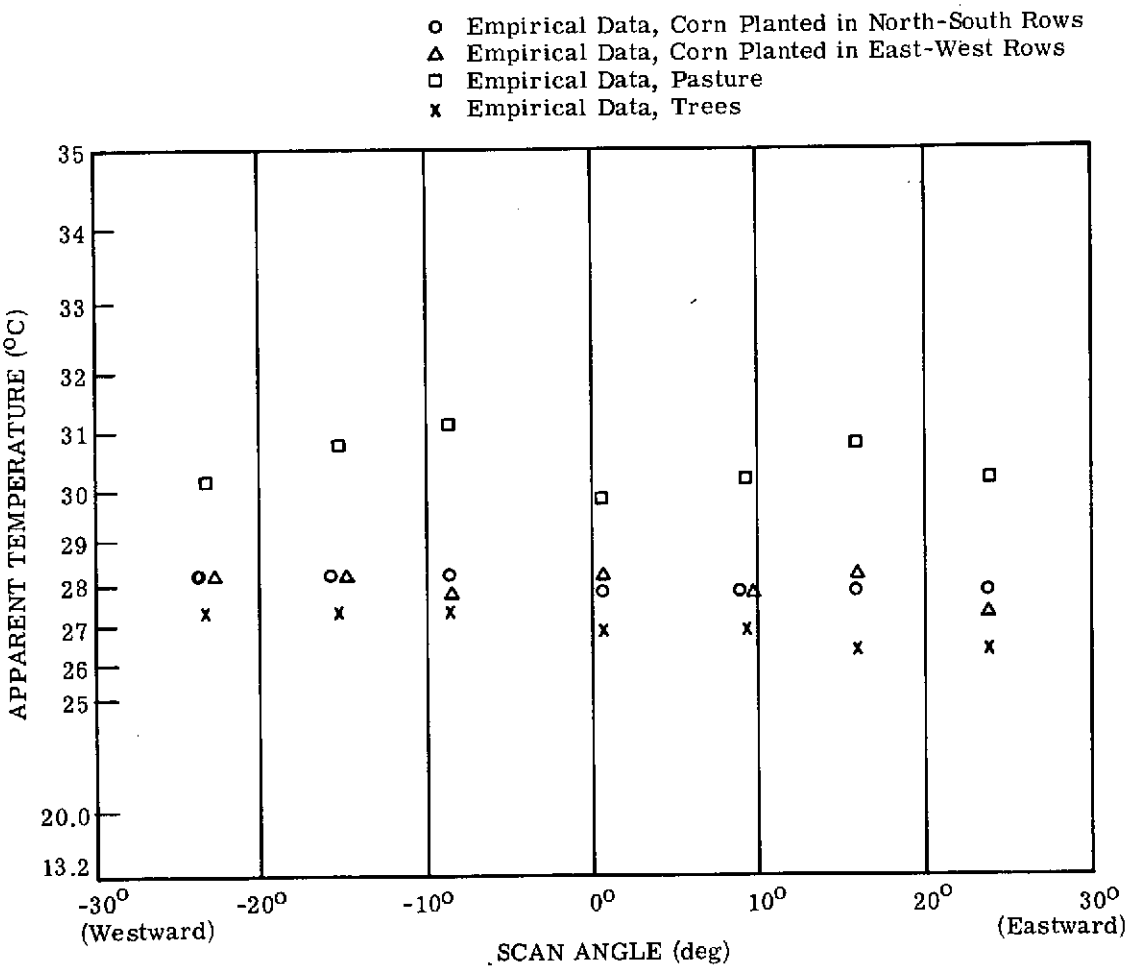

(a) 9:33 LST

FIGURE 11. APPARENT TEMPERATURE AS A FUNCTION OF SCAN ANGLE, CHANNEL 12 (9.3-11.7 μm). 6 August 1971, altitude 1.5 km (5000 ft), visibility 23 km. (Continued)

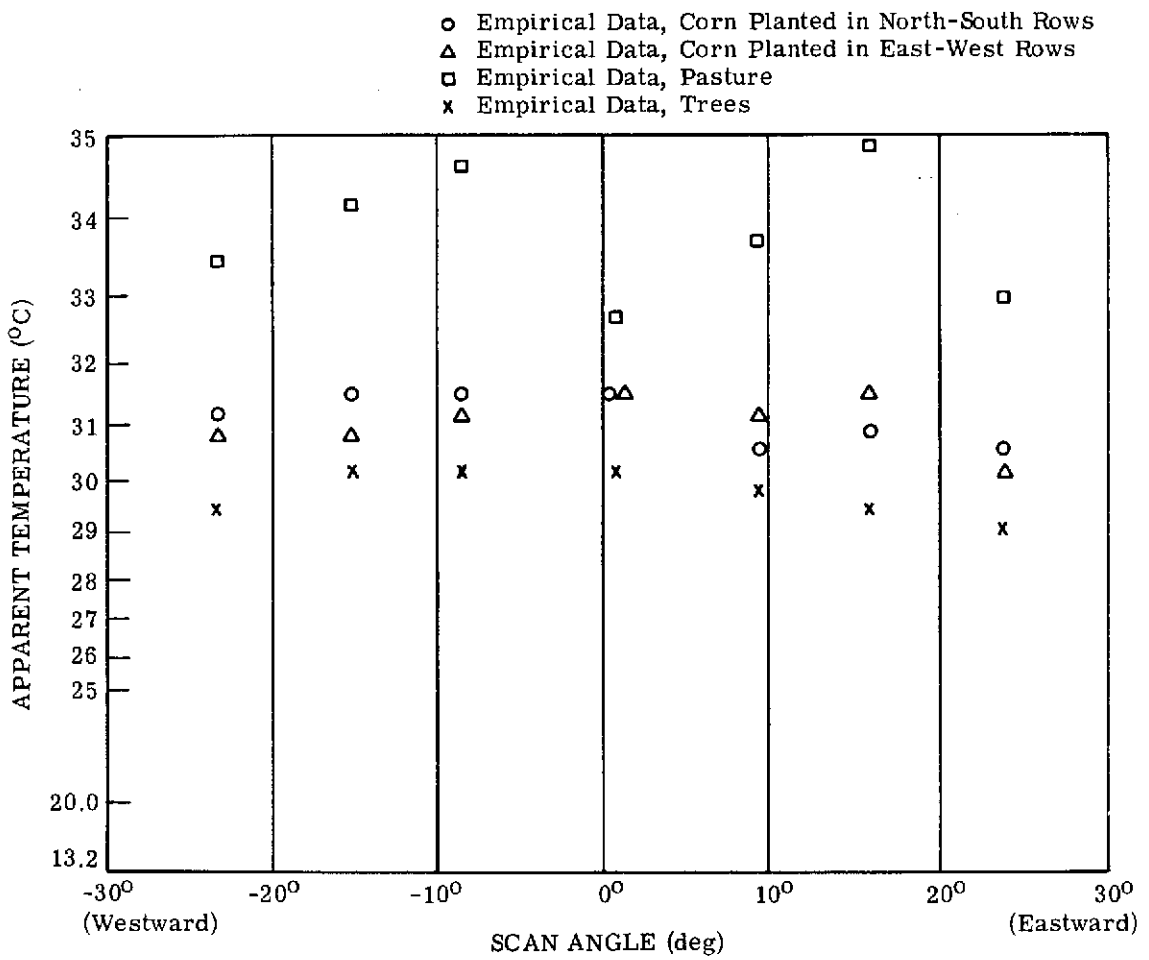

(b) 11:33 LST

FIGURE 11. APPARENT TEMPERATURE AS A FUNCTION OF SCAN ANGLE, CHANNEL 12 (9.3-11.7 μm). 6 August 1971, altitude 1.5 km (5000 ft), visibility 23 km. (Continued)

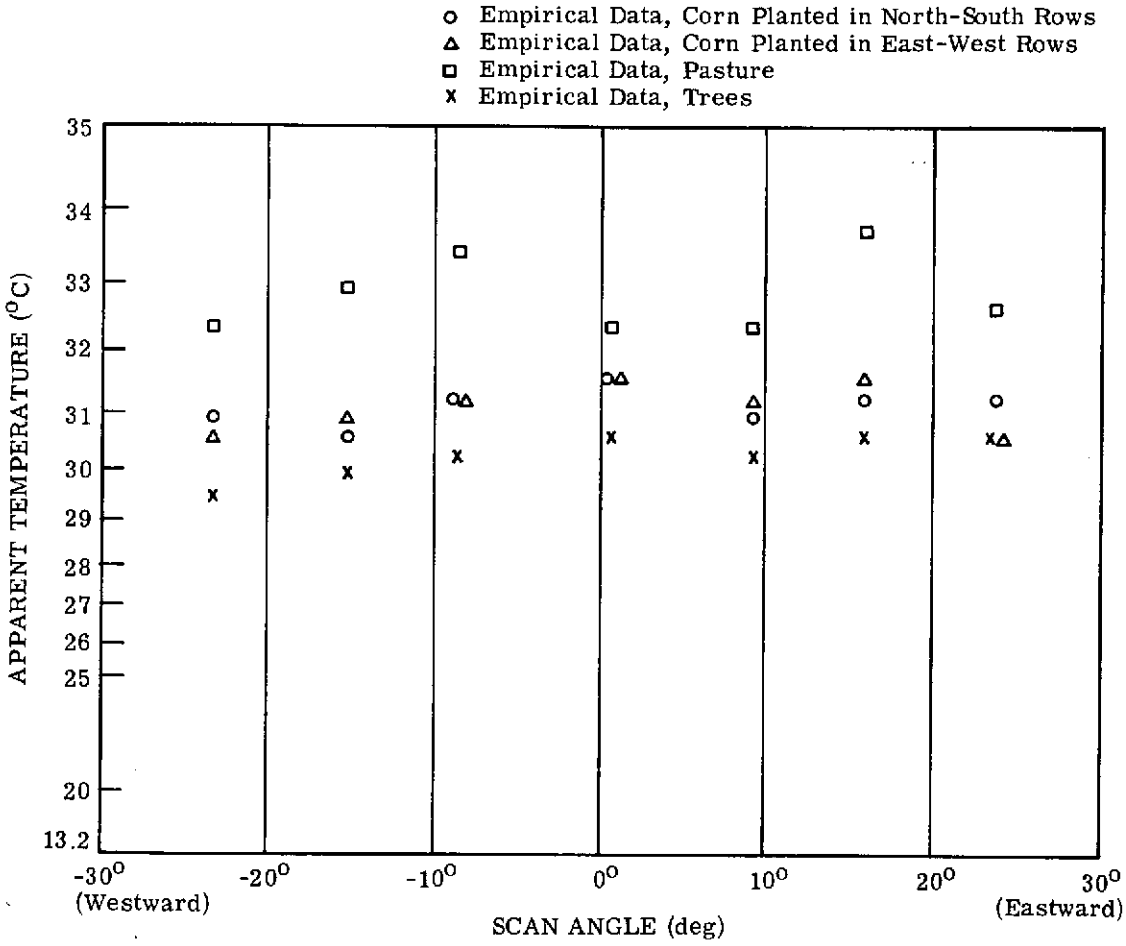

(c) 14:50 LST

FIGURE 11. APPARENT TEMPERATURE AS A FUNCTION OF SCAN ANGLE, CHANNEL 12 (9.3-11.7 μm). 6 August 1971, altitude 1.5 km (5000 ft), visibility 23 km. (Concluded)

3
MULTI-ASPECT REMOTE SENSING TECHNIQUES

The trend in the development of remote sensing technology has been toward the inclusion of additional information channels or recording media. For example, early aerial cameras used black-and-white film with a single spectral filter function. Though single film-filter combinations are still employed, we now have color film with dyes sensitive to three different spectral bands of light in common use. Today's multispectral cameras and scanners collect data in even more spectral bands. Yet another example of this trend is the past development of stereographic techniques whereby overlapping photographs of terrain taken from different camera stations and resulting in different angles of view permit the measurement of terrain elevation differences not easily measured in individual aerial photographs.

This section introduces remote sensing techniques that collect multispectral scanner data at two or more different view (or aspect) angles over the same scene. These multi-aspect remote sensing techniques are directed toward the improved extraction from scanner data of two major types of information: (a) accurate classification information and (b) useful information about the condition or state of surface materials. Both are discussed and illustrated below.

3.1 GENERAL

General observation and experience show that the observed color and brightness of vegetation canopies and other surface materials depend on the angle of view, as well as on the location of the sun relative to the observer. Calculations made with a vegetation-canopy reflectance model developed at ERIM substantiate that there are spectral differences at different view angles, and that these differences can be linked to the canopy structure as well as to the spectral reflectance and transmittance characteristics of the canopy components. To enable study of techniques for exploiting such differences in remote sensing, the ERIM M-7 multispectral scanner installation in the C-47 aircraft was modified so that it can be tilted forward at angles up to 55°.

Figure 12 illustrates typical data collection geometry for a multi-aspect mission. Two or more passes are made over the flight line, the first with the scanner in its normal position; the second and any succeeding passes are made with the scan plane tilted forward to a selected tilt angle (e.g., 45°). Differences will be produced in signals by differences in both tilt angle and flight heading. In flying the tilted-scanner passes, there are two altitude options. One is to fly the tilted scanner at the same altitude as that of the standard pass; the other option is to fly at that lower altitude which gives both the standard and the tilted-scanner passes the same slant range to the ground for a 0° scan angle. The latter case produces the same atmospheric path length for the received radiance signals and results in ground spatial

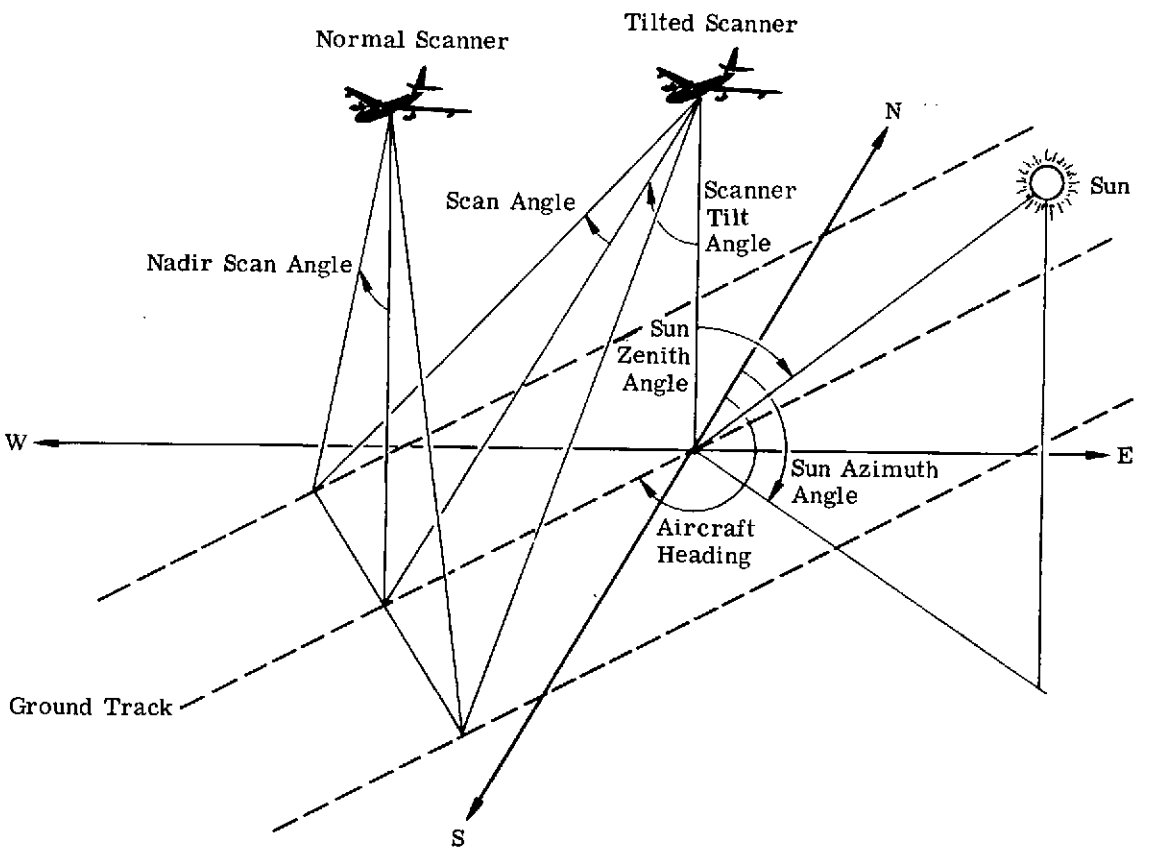

FIGURE 12. NORMAL AND TILTED GEOMETRIES

resolution elements approximately equal in size. Obviously an operational system could be designed to record both aspects simultaneously, thus requiring only a single pass over the ground area being scanned.

In describing the geometry of tilted scanner data, several angles are important. Three are of principal interest for modeling studies: the zenith angle of the sun, the zenith angle of the scanner's view direction, and the difference between the sun and the view azimuth angles. These angles, in turn, depend on angles that describe the operational configuration of the scanner—namely, the tilt angle, the aircraft heading angle, and the scan angle which is measured from the nadir ground track within the scan plane.

Multi-aspect scanner data collected over two areas are discussed in this report. One is an agricultural site in Eaton County, Michigan, southwest of Lansing; the other is a forested site, the University of Michigan School of Natural Resources' Saginaw Forest near Ann Arbor. The agricultural data were collected on 13 August 1972, the latter part of the growing season, while the forest data were collected on 20 March 1973 when deciduous trees were leafless and ground and forest litter were snow-covered. Analyses of these data are reported in later sections.

In addition to empirical analyses of multi-aspect scanner data, complementary theoretical analyses were carried out using radiative transfer as well as canopy reflectance models both to predict and simulate scanner signals and to explore the correlation between canopy biological characteristics and observable radiation.

The radiative transfer model, discussed earlier in Section 2.2, was used to compute path radiance, path transmittance, and surface irradiance for several wavelengths.

The majority of our theoretical analysis was devoted to calculation of canopy characteristics using the bidirectional canopy reflectance model developed by Dr. Gwynn Suits of ERIM [6]. The computer program that implements his model was modified in several ways under this contract. The principal modification was the addition of operational scanner geometry to the input section, including the capability for specifying a scanner tilt angle and for computing the angles needed for reflectance calculations.

Suits assumes a multi-layered canopy model, each layer being of infinite extent and characterized by randomly distributed and homogeneously mixed constituents with different spectral properties. Both the spectral transmittance and spectral reflectance for each constituent are required inputs to the computer program. Also, the physical structure of the canopy can be characterized by specifying optical cross-sections for horizontal and vertical components of each constituent material in each layer. The bottom layer of the canopy is bounded by the ground surface, bare soil or snow for example. The important feature of the model is that it

predicts the bidirectional reflectance properties of a canopy in a way that can be traced to the geometric and spectral properties of identifiable canopy components while still allowing the parametric variation of canopy constituents and observation geometry.

3.2 MULTI-ASPECT TECHNIQUES IN CLASSIFICATION

Multispectral classification algorithms depend on the differences between signals received from scene materials in various spectral channels. In a more general context, the spectral channels are merely information channels upon which the classifier operates, and the fact that the observed differences have spectral origins is of little or no consequence. An information channel that differs from another one could just as well do so because of viewing geometry, temporal, or polarization differences. In addition to spectral differences, this report deals with information channel dissimilarities originating from differences in viewing geometry, (i.e., it deals with multi-aspect remote sensor data).

A common method of describing multispectral classification techniques is to use two-dimensional scatter diagrams, that is, plots of data in one channel versus the corresponding values in another. Figure 13 presents three scatter diagrams of data from a multi-aspect scanner flight over Eaton County, a mission analyzed extensively in this section. Here, mean signals from approximately 50 fields are plotted: one scatter diagram for the same spectral channel at two aspects, one for different spectral channels at a 45^{o} aspect, and the third for different spectral channels at a 0^{o} (non-tilted) aspect. Differences between signals from the various classes are readily apparent. Multispectral classification algorithms partition such signal spaces into regions in which specific decisions are made regarding the class identities of observation vectors.

3.2.1 DATA SET DESCRIPTION

The agricultural test area overflown is in Eaton County, Michigan, along Cochran Road just north of Charlotte. The major crops in the area are corn, wheat, hay (alfalfa and red clover), beans (field beans and soybeans), and oats. There also are pastures and wood lots.

A 16-km (ten-mi) flight line was flown on 13 August 1972, at 10:23 AM EST from an altitude of 1.52 km (5000 ft) above terrain, with the scanner in its normal vertical configuration. The aircraft heading was due north. The scanner was tilted forward by 45^{o} and the flight line was flown again at 10:43, this time from an altitude of 1.07 km (3500 ft) so that the path length to the ground was again about 1.52 km. The sun positions at these times are listed in Table 7.

A major reason for selecting this site for the multi-aspect flight was its use as a test area for two ERTS investigations (MMC 321 and MMC 136). At the time of site selection, extensive ground observations were being collected by Michigan State University personnel for

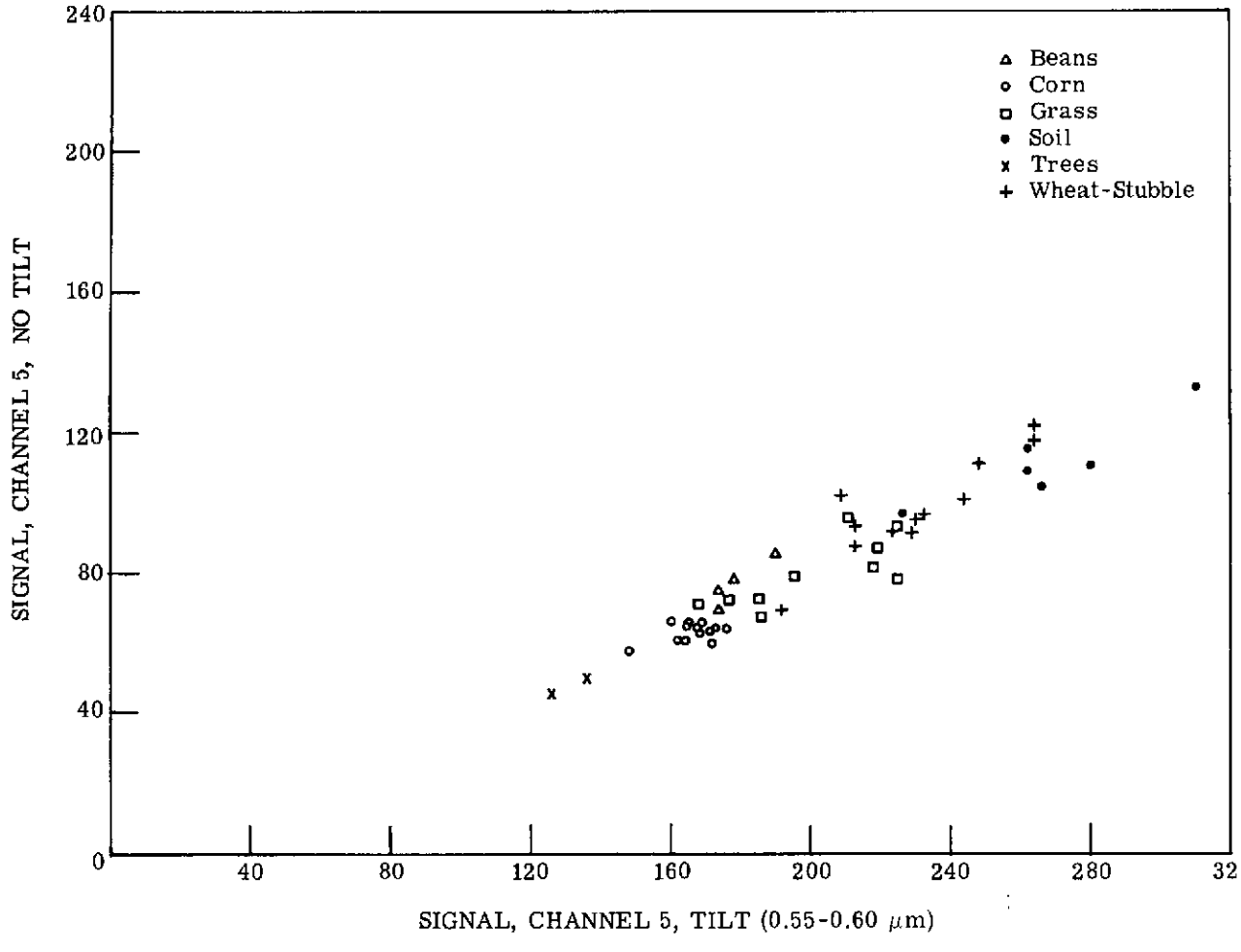

(a) Same Channel, Two Aspects (0° and 45°)

FIGURE 13. SCATTER DIAGRAMS OF MULTI-ASPECT AGRICULTURAL DATA FROM EATON COUNTY (Continued)

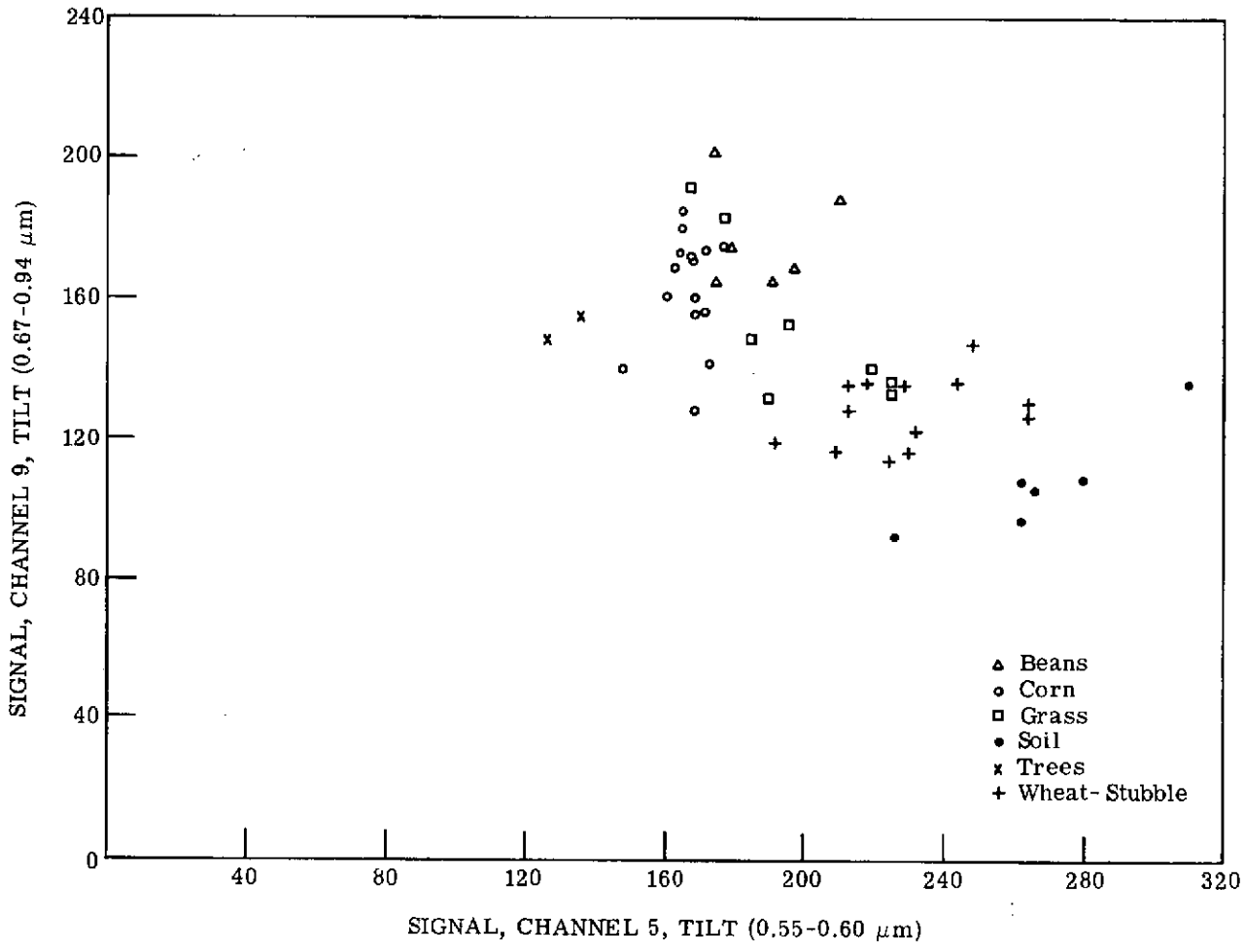

(b) Two Channels, Tilted Aspect (45°)

FIGURE 13. SCATTER DIAGRAMS OF MULTI-ASPECT AGRICULTURAL DATA FROM EATON COUNTY (Continued)

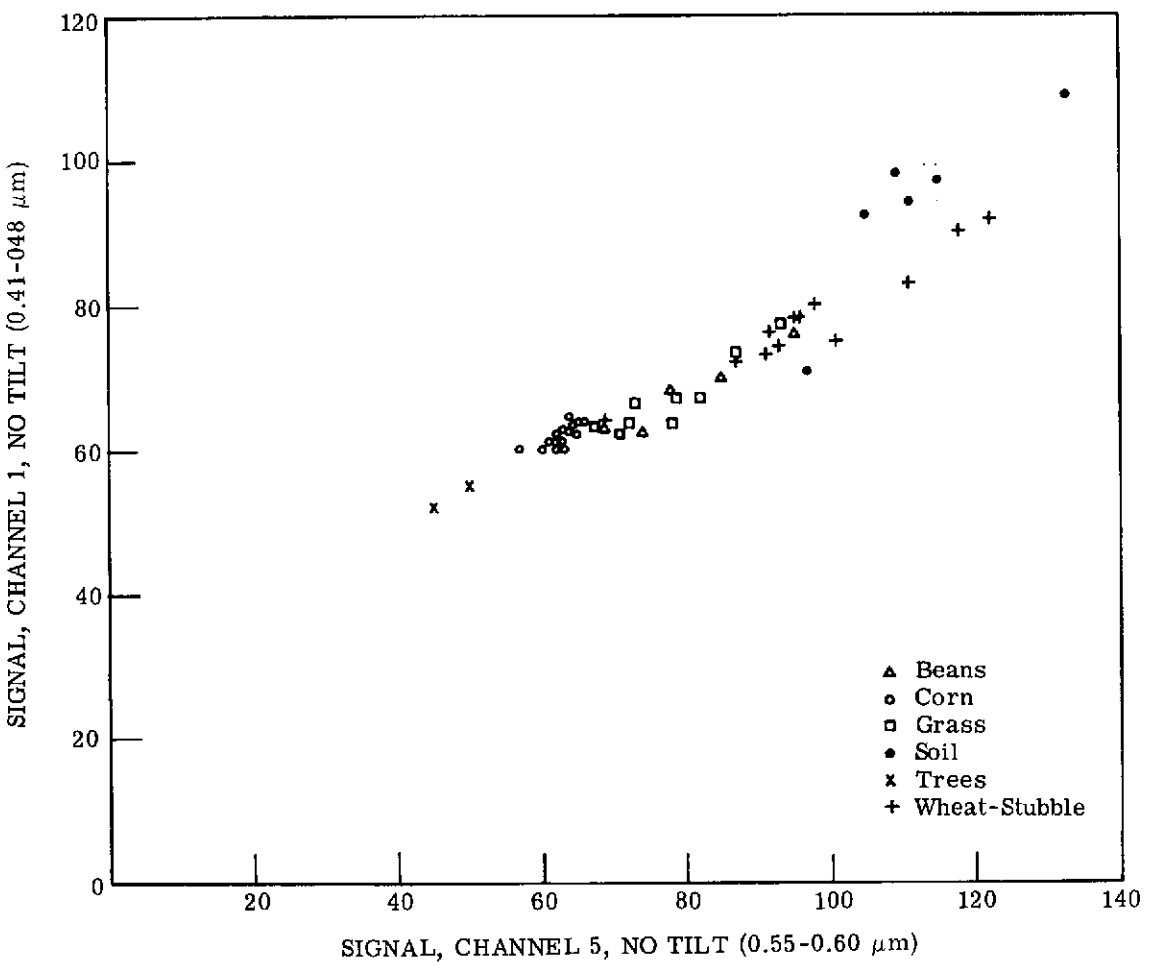

(c) Two Channels, Non-Tilted Aspect (0°)

FIGURE 13. SCATTER DIAGRAMS OF MULTI-ASPECT AGRICULTURAL DATA FROM EATON COUNTY (Concluded)

these investigations, so the limited resources available on this task for such work were applied in increasing the amount of data gathered for the first half of the flight line.

3.2.2 DATA SET PREPARATION

A number of data preparation steps were necessary before classification processing could take place. The key step was to place data from the two passes into spatial registration so that multi-aspect and multispectral information channels could be used jointly for classification. Two registration procedures were employed—manual and semi-automatic. Semi-automatic machine registration was accomplished through the courtesy of Digital Image Systems Division, Control Data Corporation (CDC), Minneapolis, but it was not completed until late in the period. Consequently, manual registration was done at ERIM on a field-by-field basis for selected fields and plots, and much of the analysis was carried out on data so registered.

Additional preparation was necessary for the data sets, both before and after registration. The first step, common to both procedures, was analog-to-digital conversion of the original scanner data. Averaging was accomplished during conversion in a manner similar to that described in Section 2.1 for the Ingham County data,except that groups of five scan lines were averaged.

3.2.2.1 Semi-Automatic Registration

CDC used their semi-automatic warp (SAW) process [10]. It entails the use of manually selected control points to determine a two-dimensional warp function that is applied to data points of the collateral image to register them with the reference image. The ten-mile flight line was divided into several overlapping sections, warp functions were determined and applied separately for each, and the warped collateral outputs were pieced together to form a corrected and registered collateral image tape for the entire flight line.

CDC first attempted to use their automatic TRAK process (which reportedly has been successfully used on other data sets), but the data set had several characteristics that complicated its application. Therefore, they used the semi-automatic process described above. The ground swath was just over one-mile wide, and there were portions in which the size and frequency of identifiable features were unsatisfactory. Also, a roll-stabilization failure on the conventional no-tilt run, which resulted in crooked roads and field boundaries, led to selection of the tilted-scanner data for the reference image. Distortions caused by aircraft pitch motions were more pronounced in the tilted scanner data, especially in the scale along the ground track; another complicating factor was the effect of height displacements in the tilted data.

The CDC algorithm uses only a single channel for determining the warp function, and we had two tapes of 12-channel data to be registered. Therefore, a program was written at ERIM

to produce reformatted data tapes which had the 12-channel values packed into two 60-bit words (for the CDC-6600)—a duplicate of channel-7 values (0.62 to 0.70 μm) was used in the first nine bits for warp determination. CDC used a nearest-neighbor rule in applying the warp because this rule does not require interpolation calculations and because the pixel (picture element) shifting algorithm could be modified easily to shift pairs of words instead of conventional single-channel pixel values.

Another computer program was written at ERIM to convert the 12 channels of collateral tape data back to the standard ERIM format and, at the same time, merge these data with the reference data to produce a 24-channel multi-aspect data tape. The spectral passband definitions of the ERIM M-7 multispectral scanner channels used are listed in Table 8.

Before any other processing was performed, groups of two points on four consecutive lines of data on the 24-channel tape were averaged to minimize the effects of any errors in spatial registration. A program called SMOOTH, implemented on the 7094 computer under this task, was used (see Appendix A).

Finally, the program ACORN4 was used to determine an average signal-versus-scan angle function over the entire flight line for each channel. Correction functions were applied (using program APPLY) to produce the 24-channel, angle-corrected, multi-aspect data tape used for classification runs. A tape of 12 difference images was also produced by CDC. It too was subjected to 2×4 averaging before further analysis was carried out.

3.2.2.2 Manual Registration

For manual registration, data from the no-tilt run were first processed to straighten the roads and field boundaries. A program, DESNAKE, was developed under this task to accomplish this correction (see Appendix A). Next, angle-correction functions were determined and applied to both data tapes. Field-center regions were then identified for fields selected on line printer graymaps of both the tilt and no-tilt data. The program MERGE, also developed for this task (see Appendix A), was used to combine the two 12-channel data sets and create a 24-channel, multi-aspect data file for each field-center rectangle. The procedure relied on the manual choice of rectangles on the two data sets for point-by-point matching within field centers. Effects of any misregistrations were reduced by averaging groups of two points and two lines within each data file.

3.2.3 EXAMPLES OF MULTI-ASPECT SCANNER DATA

Figure 14 presents an aerial photograph of a representative portion of one section of the Eaton County flight line. A corresponding ground-truth map also is presented in the figure.

TABLE 7. SUN POSITION FOR MULTI-ASPECT FLIGHT OVER EATON COUNTY

Time (EST)	Tilt Angle (°)	Sun Zenith (°)	Sun Azimuth (°) (from North)
10:23	0	41.4	122.4
10:45	45	38.1	128.7

TABLE 8. M-7 SCANNER CHANNELS USED FOR MULTI-ASPECT AGRICULTURAL STUDY

Digital Number	Channels Collected 10%* Passband (μm)	Channels Used in Analysis to Date
1	0.41 - 0.48	X
2	0.48 - 0.52	
3	0.50 - 0.54	
4	0.52 - 0.57	X
5	0.55 - 0.60	X
6	0.58 - 0.64	
7	0.62 - 0.70	X
8	0.71 - 0.73	
9	0.67 - 0.94	X
10	1.5 - 1.8	X
11	2.0 - 2.6	
12	9.3 - 11.7	

*The spectral passbands here differ slightly from those listed in Table 1 because the data were collected in different years, changes were made in the scanner system between years, and different selections of channels for recording were made from those available.

(a) Aerial Photograph

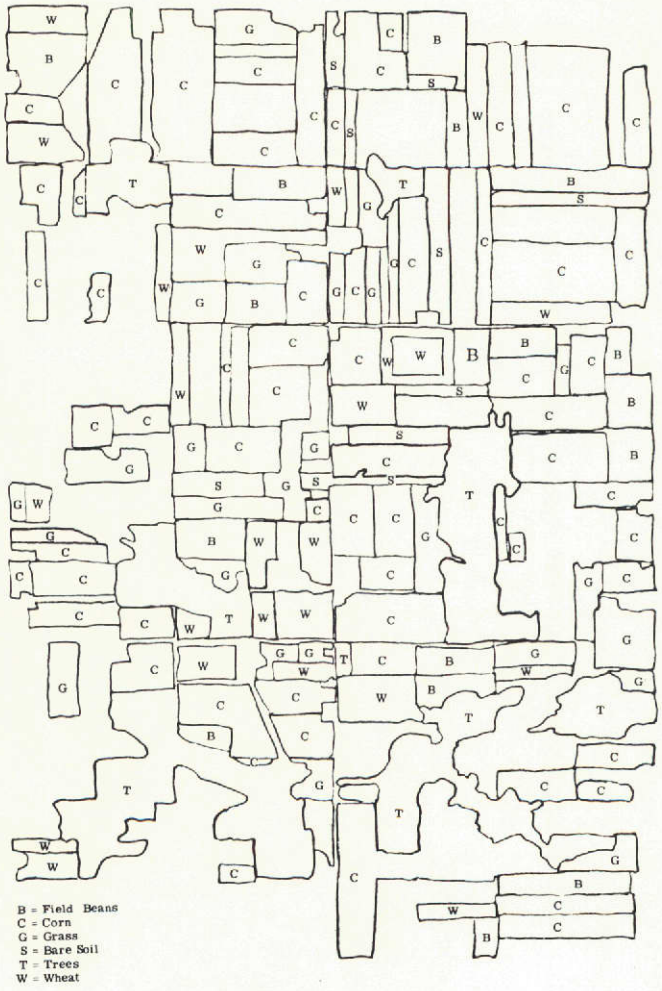

(b) Ground-Truth Map

FIGURE 14. EATON COUNTY TEST SITE

Analog images of scanner data collected over the site were examined, and differences in the tonal patterns, which are exploitable by classification processors, were noted on tilt/no-tilt pairs of images.

Such dissimilarities between two images can be made more evident by producing a difference image (i.e., by subtracting the datum value at each scene point in the non-tilted data from the corresponding datum value in the tilted data). Figure 15 presents digital difference images for channels 5, 7, and 9 (0.55 to 0.60, 0.62 to 0.70, and 0.67 to 0.94 μm, respectively) taken from the averaged version of the CDC-merged difference tape* (without correction for scan angle). The area covered corresponds to that presented in the photograph and map of Fig. 14.

An examination of these images shows that trees are the darkest material on the 0.55 to 0.60 μm difference image (D5). Also, the tonal pattern of many fields in the 0.62 to 0.70 μm image (D7) is nearly the negative of that on D5. That is, bare soil and wheat stubble fields that are lightest on D5 tend to be darkest on D7. The difference image for 0.67 to 0.94 μm (D9) does not have tonal patterns as distinctive as those on the other two images.

The above results are understandable if one examines scatter diagrams in which mean signals of the no-tilt class in each channel are plotted versus the corresponding tilt values. Figure 16 presents such diagrams for channels 5, 7, and 9. Also shown on the diagrams are families of lines drawn at 45° to the axes. These are lines of constant difference between the values of the two axes. Each symbol on a difference image represents points that lie between two similar lines. Note that for each channel shown and every channel analyzed, the tilted scanner data had a higher average signal level than did the standard data. The intervals assigned to each symbol were set automatically to approximately equalize the number of points printed in each symbol. The map tones then represent only departures from the average differences.

The scatter diagram patterns on Fig. 16 confirm the observations made previously, but the associated physical reasons need further discussion. Bare soil shows the greatest aspect dependence of any of the materials in channel 5 (0.55 to 0.60 μm). There appears to be a steady progression toward a lesser-aspect effect as one moves to crops with more vegetation biomass and/or green vegetation (i.e., in going from bare soil to wheat stubble, grass, field beans, corn, and trees, the difference value decreases).

In channel 7 (0.62 to 0.70 μm), the vegetation signatures have nearly equal difference values, but bare soil has a markedly lower difference value; it has been determined that this is a result of saturation in tilt channel 7.

*The values on the difference tape actually are scaled and offset differences [i.e., $V_{Difference} = 0.5(V_{Tilt} - V_{No\text{-}Tilt}) + 255$], to allow representation of the entire possible range of difference values.

(a) Channel 5 (0.55-0.6 μm)

(b) Channel 7 (0.62-0.7 μm)

(c) Channel 9 (0.67-0.94 μm)

*Data Spatially Registered Courtesy of Control Data Corporation

FIGURE 15. MULTI-ASPECT SIGNAL DIFFERENCE (D) IMAGES: 45^{o} (TILT) - 0^{o} (NO-TILT). 13 August 1972, 10:30 EST, altitude 1.5 km (5000 ft), flight direction North.

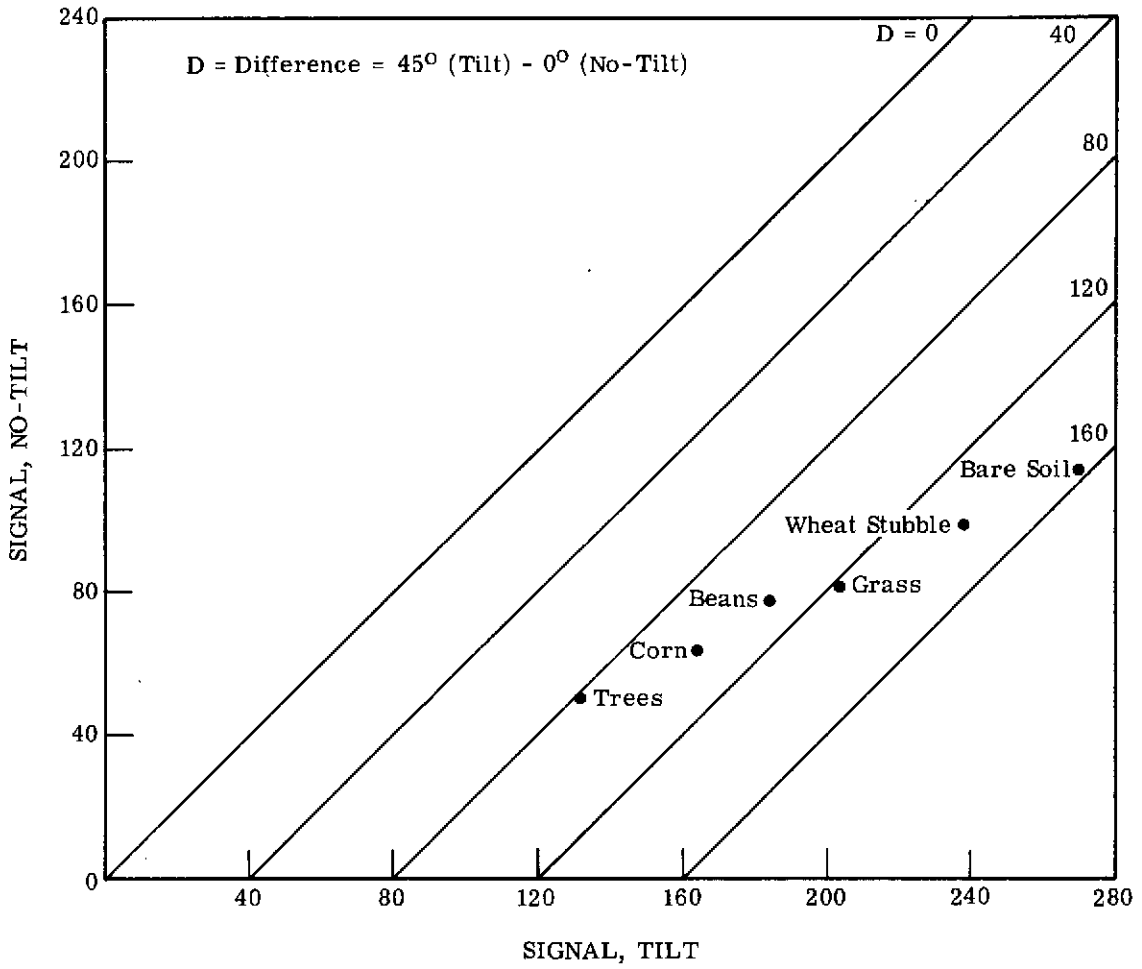

(a) Channel 5 (0.55-0.6 μm)

FIGURE 16. SINGLE-CHANNEL MULTI-ASPECT SCATTER DIAGRAMS CORRESPONDING TO SIGNAL DIFFERENCE (D) IMAGES IN FIG. 15 (Continued)

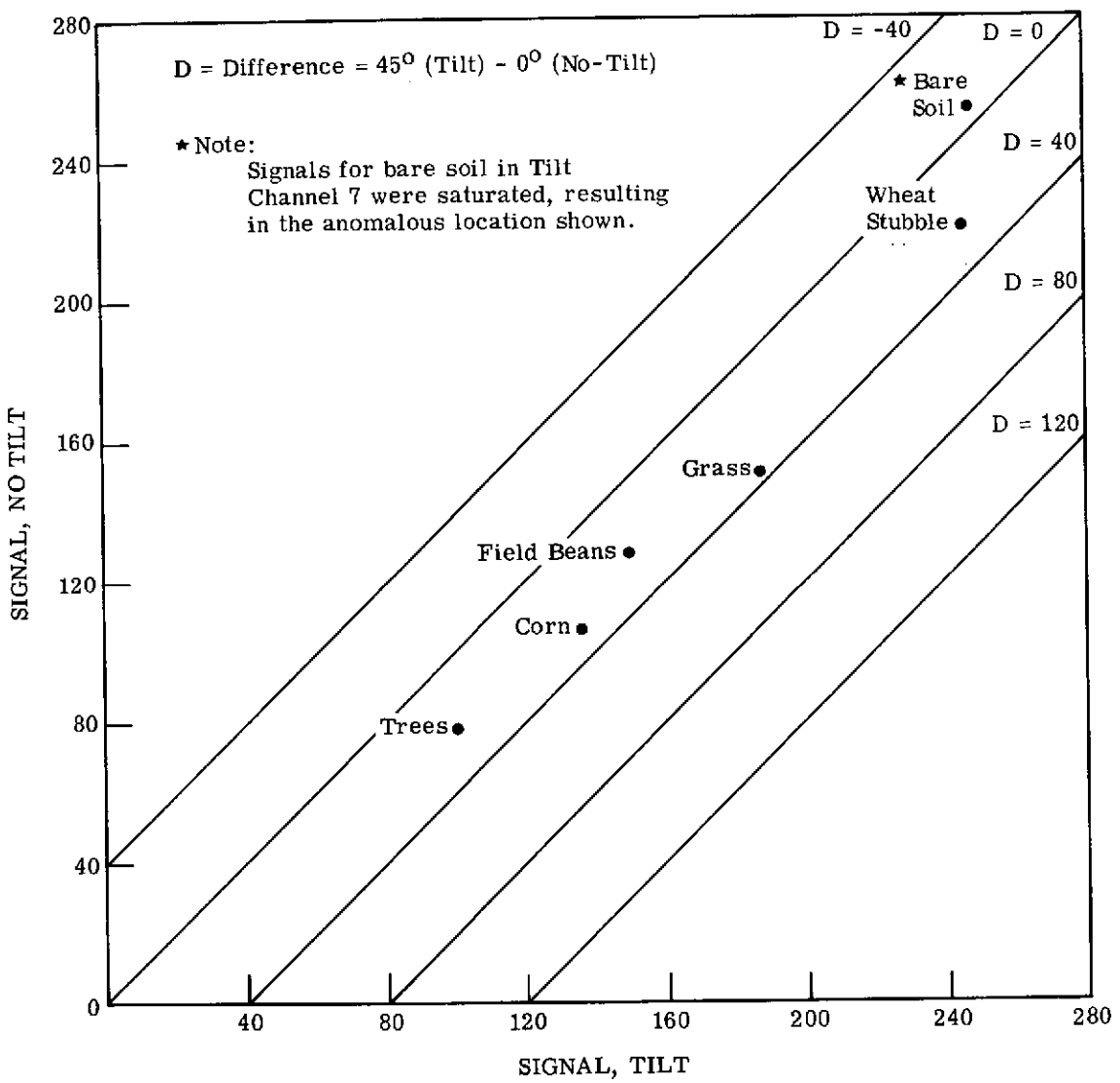

(b) Channel 7 (0.62-0.7 μm)

FIGURE 16. SINGLE-CHANNEL MULTI-ASPECT SCATTER DIAGRAMS CORRESPONDING TO SIGNAL DIFFERENCE (D) IMAGES IN FIG. 15 (Continued)

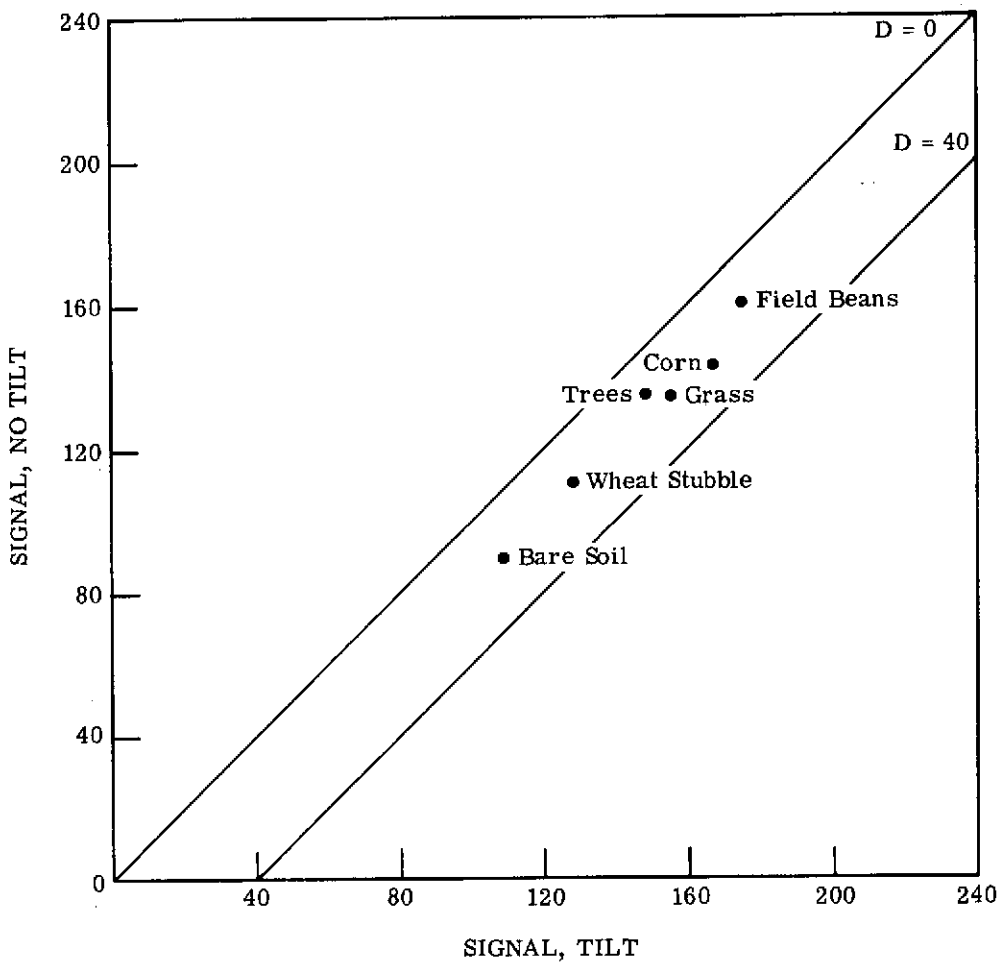

(c) Channel 9 (0.67-0.94 μm)

FIGURE 16. SINGLE-CHANNEL MULTI-ASPECT SCATTER DIAGRAMS CORRESPONDING TO SIGNAL DIFFERENCE (D) IMAGES IN FIG. 15 (Concluded)

The trends seen in the scatter diagrams of class signatures become less evident in scatter diagrams of means of individual fields within these classes. As an example, the field scatter diagram presented earlier in Fig. 13(a) may be compared with the corresponding class scatter diagram in Fig. 16(a). It can be seen that Fig. 13(a) shows a substantial amount of overlap between fields of different classes.

Additional analysis should be performed in order to better explain the observed signal differences and, at the same time, to develop human intuitional abilities essential in image and data interpretation. Ratios and other signal combinations should be examined, both with and without prior subtraction of path radiance contributions, to find, for example, a transformation that provides optimum differentiation of scene materials.

3.2.4 MULTI-ASPECT CLASSIFICATION RESULTS

The first step in classification processing required extracting signal statistics from fields of the various classes and establishing signatures for the classifier. Based on qualitative analysis of signal statistics for all 12 tilted-scanner channels for a sample of fields, six of the 12 spectral channels were chosen as a subset to be used in subsequent analysis.

Signal statistics for 69 fields, extracted from both tilt and no-tilt data for the six spectral channels noted in Table 9, were divided into two sets, one with 36 fields and the other with 33. To avoid the introduction of bias, no analysis of the signatures was made to assist the selection procedure. One set was used for training and the other for testing, with the two roles reversed for some analyses.

A signature combination program —SIGCOM (see Appendix A) —developed under this task was used to combine individual field statistics and form signatures for EW corn, NS corn, EW beans, NS beans, wheat stubble, alfalfa, grass-weeds, grass-pasture, red clover, trees, brush, and bare soil. Since output from the program LINDIST, implemented under this task, indicated that there was a large probability of misclassification among the grasses and clover, between EW and NS corn, and between EW and NS beans, classification results from each of these similar sets of ground covers were combined to get six classes.

Classification was carried out for the 12 signatures associated with six classes* by using the ERIM linear-classification algorithm for three selections of data channels: (1) the six standard no-tilt channels, (2) the six tilt channels, and (3) all 12 multi-aspect channels (six tilt and six no-tilt). Results are separately summarized in Table 10 for training and test fields. The average percentage of points from other classes that were falsely assigned to each class is also listed. Each percentage correct, except as noted, is an over-class

* The brush class was excluded because there were no test fields.

TABLE 9. MULTI-ASPECT CHANNELS RANKED FOR DISCRIMINATING AMONG SIX AGRICULTURAL CLASSES, EATON COUNTY

Order of Selection*	No-Tilt (NT) Data Channel	Tilt (T) Data Channel	Multi-Aspect Channel	
			Aspect	Number
1	5	5	T	5
2	1	9	T	9
3	10	1	NT	10
4	9	10	NT	1
5	7	4	NT	4
6	4	7	T	7**

*Based on lowest probability of misclassification, according to program STEPLIN.

**Channel T7 was a close runner-up to NT9 for sixth choice and was substituted for it in the analysis.

TABLE 10. SUMMARY OF MULTI-ASPECT CLASSIFICATION RESULTS FOR HAND-REGISTERED DATA FROM EATON COUNTY

Number of Signatures	Training Set	Channels Used Number and Aspect*	Classification Results Averaged Over All Classes*** Percent Correct Training	Test	Percent False Detections Training	Test
6 12 (Classes)	A	12(6T + 6NT)	95.9	78.2	0.8	3.3
		6(NT)	93.3	73.6	1.2	4.4
		6(T)	86.6	72.5	2.8	4.8
6 6 (Classes)	B	12(6T + 6NT)	92.5	78.8	1.2	2.8
		6(NT)	90.3	82.8	2.0	3.9
		6(T)	87.6	81.6	2.6	4.9
		6(3T + 3NT)**	91.6	86.0	1.9	3.0

*T = Tilted (45° Aspect)
NT = Non-Tilted (0° Aspect)

**The entries in all other rows are for a χ^2 value of ≤ 99.9, giving a rejection threshold with a very small probability of false rejection. For the "best six" runs, a threshold of 0.001 probability of false rejection was used inadvertently, so the designated number is the percent correct based upon the 75% of all points that were classified.

***The percentage correct classified of all points in each plot was computed. These percentages were averaged over all plots in a class to obtain the class average. The overall result given is an average over the six classes.

average of the average correct classification in individual plots (or fields) within each class (based on all points in each plot). It is seen that classification percentages are higher in training than in test data (e.g., 96% as compared to 78% for the multi-aspect case). The performance differences between the three selections are not especially great; however, the multi-aspect correct percentages are higher for both training and test data, and false detection percentages are lower.

A more detailed breakdown of these classification results is presented in Table 11, in which averages are presented separately for each of the six classes. The classes best recognized on all training cases are trees and bare soil. Trees were correctly identified 95% of the time, except for the no-tilt case (77%). The recognitions for soil were 100%, except for a slightly lower tilt performance (90%). The multi-aspect result is the best on both trees and bare soil, as well as on corn (79%). Test results are poorest on field beans (~50% for multi-aspect and no-tilt, and 35% for tilt), which is explainable by the large variability of the spectral signatures of beans which were in varying stages of yellowing; tilt data performed poorly even on the bean training fields. Accuracies on grasses and wheat stubble test fields ranged from 68 to 76%, with no clear difference between channel sets.

The use of combined signatures is an alternative to multi-modal signatures. The program SIGCOM was used to combine the mode signatures for each of the classes. However, since the role of the training and test sets was reversed at the same time, the effects of the two changes became intermixed and precluded separate analysis. We then performed classification using the six combined signatures—corn, beans, wheat stubble, trees, grasses, and bare soil. The 69 fields were classified four ways using the new combined signatures for the following subsets of channels: (1) the six tilt channels, (2) the six no-tilt channels, (3) all 12 multi-aspect channels, and (4) the six best multi-aspect channels (3 tilt + 3 no-tilt).

The choice of the six best multi-aspect channels was based, except for one minor adjustment, on a rank-ordering of channels by program STEPLIN according to their ability to separate the six signatures. The first two channels selected were tilt channels (5 and 9); the next four were no-tilt (10, 1, 4, and 9). The minor adjustment for classification was this: we substituted tilt channel 7 for no-tilt channel 9 as the sixth channel (tilt channel 7 was a very close runner-up to no-tilt channel 9). The substitution gave us three channels chosen from each of the tilted and non-tilted sets, and also, by avoiding double use of channel 9, permitted single usage of each spectral channel.

The overall classification results for six signatures also are presented in Table 10. The results for the different channel selections again are close to one another. On training data, the percentages correct are slightly lower than for the 12-signature cases, while the test values are slightly higher. Values for the six best channels, unfortunately, are not exactly

TABLE 11. DETAILED TABULATION OF MULTI-ASPECT CLASSIFICATION RESULTS FOR HAND-REGISTERED DATA FROM EATON COUNTY

Number of Signatures	Training Set	Channels Used Number and Aspect*	Classification Results for Individual Crops (Averages Over Plots of Percents of Total Number of Points in Each Plot) Percent Correct and Percent False Detections											
			Corn		Field Beans		Trees		Grasses		Wheat Stubble		Bare Soil	
			Training	Test	Training	Test	Training	Test	Training	Test	Training	Test	Training	Test
12 (6 Classes)	A	12 (6T + 6NT)	98.8 (0)	78.9 (0.2)	96.8 (1.0)	51.2 (3.6)	100.0 (0)	95.8 (0)	93.4 (3.3)	67.5 (13.8)	86.7 (0.2)	75.5 (0.9)	100.0 (0.3)	100.0 (1.7)
		6 (NT)	96.7 (0.4)	71.1 (0.3)	90.0 (1.4)	53.6 (6.4)	98.3 (0)	77.4 (0)	85.5 (4.1)	69.8 (14.1)	89.7 (0.3)	69.5 (1.7)	99.5 (0.8)	100.0 (3.6)
		6 (T)	93.0 (0.2)	69.8 (1.8)	67.5 (2.5)	35.4 (6.2)	97.8 (0.4)	95.6 (2.1)	88.6 (10.5)	70.9 (17.6)	77.2 (2.5)	73.1 (1.1)	95.4 (0.5)	90.0 (0)
6 (6 Classes)	B	12 (6T + 6NT)	96.4 (0.1)	90.2 (0.5)	91.1 (3.1)	68.0 (5.6)	99.6 (0.1)	91.5 (0.1)	82.9 (2.7)	56.4 (4.7)	90.7 (1.2)	92.2 (5.6)	94.3 (0)	74.4 (0.1)
		6 (NT)	97.6 (0.7)	96.9 (1.6)	87.0 (4.5)	68.5 (3.9)	94.6 (0.1)	97.6 (1.5)	79.0 (4.2)	57.6 (8.4)	84.3 (1.7)	93.4 (7.8)	99.5 (1.0)	82.5 (0.3)
		6 (T)	96.5 (1.8)	93.0 (0.9)	81.2 (5.5)	75.6 (10.8)	94.8 (0.6)	95.9 (0.2)	67.6 (3.7)	37.8 (5.8)	94.0 (4.2)	88.1 (11.2)	91.7 (0)	99.1 (0.6)
		6** (3T + 3NT)	90.0 (0)	97.1 (0.1)	91.8 (6.2)	62.5 (5.0)	100.0 (0.3)	100.0 (0.5)	84.9 (4.2)	76.7 (9.3)	84.4 (0.7)	79.8 (2.6)	100.0 (0)	100.0 (0.2)

*T = Tilted (45° Aspect)
NT = Non-Tilted (0° Aspect)

**The values in all other rows are for a χ^2 value of ≤99.9, giving a rejection threshold with a very small probability of false rejection. For the "best six" run, a 0.001 probability of false rejection threshold was used inadvertently, so the designated number is the percent correct based upon the 75% of all points that were classified.

comparable to the others because a different rejection threshold was used for those runs than for the others.

Detailed classification results for the individual classes are presented in Table 11. All performances for test trees were again good (92 to 100%); and performances for bare soil were at or near 100% for the tilt set and six-channel multi-aspect set, but they dropped somewhat for both the 12-channel multi-aspect and six no-tilt channel sets (74 to 83%). The recognition accuracies of test corn and wheat stubble improved over those obtained with multi-modal signatures from the other training set—values of 90% and greater were obtained in most instances. Even performances for field beans were higher (at 68 to 75%) with the newer combined signatures than with the older multi-modal signatures.

Results from our analysis of manually registered data indicate that multi-aspect data hold some promise for improving classification performance, but the case for the use of such data will require additional demonstration. As always, in machine-processing studies, the training of the classifier is important, as well as the inherent separability of the classes. Two of the scatter diagrams in Fig. 13 represent the first two channels selected in runs of program STEPLIN to rank-order the available channels (see Table 9). Figure 13(b) represents the top pair for both tilt-only and multi-aspect data, while Fig. 13(c) represents the choice for no-tilt data. Considerable overlap can be seen between several of the classes. If an analysis of signature variability were made part of the training procedure, it might improve results and lead to increased understanding of real multi-aspect data.

Results in tabular form do not always provide a complete description of classification performance. Valuable insights and observations can also be gained from examination of recognition maps. The manually registered data do not lend themselves to mapping, but the machine-registered data are well suited to the purpose.

Because of the late availability of the machine-registered data, the six combined signatures extracted from the hand-registered data were used for classification on the machine-registered data to produce recognition maps for the entire flight line. Recognition maps were made using the six no-tilt, six tilt, and six best channels for comparison. Maps for a 4.8-km (3-mi) section of the flight line are presented in Fig. 17. A threshold ($\chi^2 = 99.9$) with a very low probability of rejection was used. Quantitative analysis on a field-by-field basis was not completed, but some qualitative conclusions have been drawn from an examination of these maps.

First, the classification patterns are more spotty on the no-tilt map than on the others. Second, mature trees appear to be most accurately delineated on the multi-aspect map (see bottom third of map). Third, corn was less often missed on the tilt map, and most corn fields appear to be well delineated, but false detection of corn within trees is a problem.

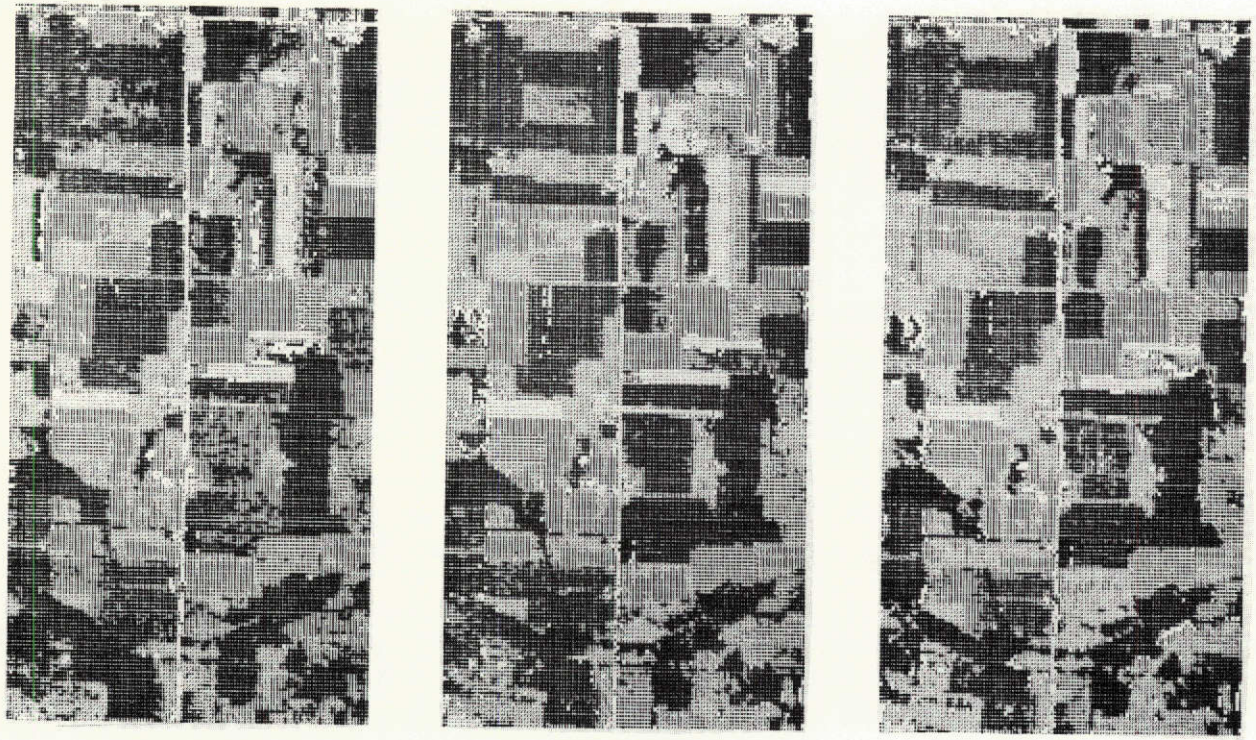

(a) Standard, No-Tilt (6 Channels)

(b) 45° Tilt (6 Channels)

(c) Multi-Aspect (3 Channels Tilt and 3 Channels No-Tilt)

Trees | Wheat Stubble | Corn | Field Beans | Grass | Bare Soil

*Data Spatially Registered Courtesy of Control Data Corporation.

FIGURE 17. STANDARD AND MULTI-ASPECT RECOGNITION MAPS.* 13 August 1972,10:30 EST, altitude 1.5 km (5000 ft), flight direction North.

Fourth, corn was recognized nearly as well with multi-aspect data as with tilt data, with fewer false detections. Examples of poorer corn field recognition with no-tilt data are seen in the top left corner and across the middle of the maps. With the multi-aspect and tilt data, individual field recognition is more of an "either-or" situation than for no-tilt data, in which variations across fields are more pronounced.

3.3 MULTI-ASPECT TECHNIQUES IN INFORMATION EXTRACTION

Classification techniques are used on remote sensor data to identify one or more classes of material in a scene. In addition to identity, other types of information can be extracted from the data. For example, having identified a field as belonging to a particular class of agricultural crop, one might wish to determine its condition, either absolutely or in comparison to other fields of the same crop. There are sometimes large differences in condition within a class, for which separate signatures are established (e.g., mature and recently harvested alfalfa, or healthy and severely blighted corn). At other times, the differences are less extreme and a continuous range of variability can be encompassed in a single signature for identification (e.g., density of plant cover, or level of stress). If additional information is to be extracted regarding the condition of the identified members of a class, we must establish relationships between the remotely sensed radiation and the conditions of interest. Multi-aspect data promise to add a new dimension to remotely sensed data, one that is related to the structure of vegetation canopies and/or the macro- and micro-structure of other reflecting surfaces.

This section discusses initial studies of the use of multi-aspect data for agricultural and forestry applications. Our studies primarily involved calculations made with the Suits bidirectional-reflectance model for vegetation canopies. The agricultural reflectance calculations were made for observation conditions comparable to those of the Eaton County data set analyzed in Section 3.2. Corn field reflectances were calculated for a variety of canopy characteristics.

The forest reflectance calculations were made for a variety of canopy characteristics under conditions that matched a flight made in March 1973 over an experimental forest with deciduous trees in a leafless condition and snow cover on the ground. These theoretical calculations are compared with the empirical scanner data.

3.3.1 AGRICULTURAL APPLICATIONS

We made a series of reflectance calculations to explore the ways in which corn field spectra depend upon the structure and composition of the canopy. The structural characteristics and component reflectances and transmittances for corn were obtained from Dr. Gene Safir of Michigan State University and Dr. Suits [11].

The first effect explored was that of differences in planting density in healthy corn canopies. Two density values were selected, one higher (~69,200 plants/hectare or 28,000 plants/acre) than the average planting density for corn and the other lower (~34,600 plants/hectare or 14,000 plants/acre). Calculations at wavelengths of 570 and 760 nm (two of 13 wavelengths for which calculations were made) are plotted with open and closed circles in Fig. 18. Figure 18(a) is a multi-aspect scatter diagram for 570 nm (i.e., the reflectances for a 45°-tilt geometry are plotted versus the corresponding reflectances for a no-tilt geometry). An aircraft heading of 360° (i.e., due North) was assumed for these calculations, as well as a sun zenith angle of 33° and a sun azimuth angle of 135°. The seven points plotted are for scan angles of -30°, -20°, -10°, 0°, 10°, 20°, and 30°. It can be seen that the reflectances are less for the denser canopy along both axes. The situation is different in the scatter diagram for 760 nm (see Fig. 18(b)). Here, reflectances for the denser canopy generally are greater than those for the thinner canopy. But, while the separation is complete in the 45° tilt data, there is some overlap in the no-tilt direction.

The 13 wavelengths selected for the calculations approximately correspond to the band centers of M-7 scanner channels. The optimum two channels selected from a subset of 12 multi-aspect channels in Section 3.2 were tilt channel 5 and tilt channel 9. The nearest wavelengths from the corn canopy reflectance calculations are 570 and 760 nm, respectively. A scatter diagram for these wavelengths is presented in Fig. 19. It should be compared to Fig. 13(b), the corresponding empirical scatter diagram.

Still considering only the healthy canopy, plotted in both open and closed circles, one notes that the density differences again are greater than the scan-angle differences. A lower density decreases the 760-nm reflectances while it increases the 570-nm reflectances for the given soil type (see the discussion of soil color effects below).

The next effects explored were those of moisture stress and chlorosis (yellowing) of the leaves. The canopy structural parameters measured by Suits and Safir for a moisture-stressed corn field were used; basically, the stressed canopy had a shorter height and different distribution of leaf surfaces than healthy corn. Severe chlorosis was simulated by changing the spectral characteristics of 50% of the healthy leaves to those of chlorotic leaves. The results of reflectance calculations for stressed and chlorotic corn are plotted in Figs. 18 and 19 with open and closed triangles. The combined effect is to shift the reflectances from the dense canopy in the same general direction as the less dense canopy but substantially farther away. Also, since the stressed chlorotic canopies are distinctly separated from the healthy canopies on all diagrams, density differences do not cause any overlap between reflectance patterns for the two conditions.

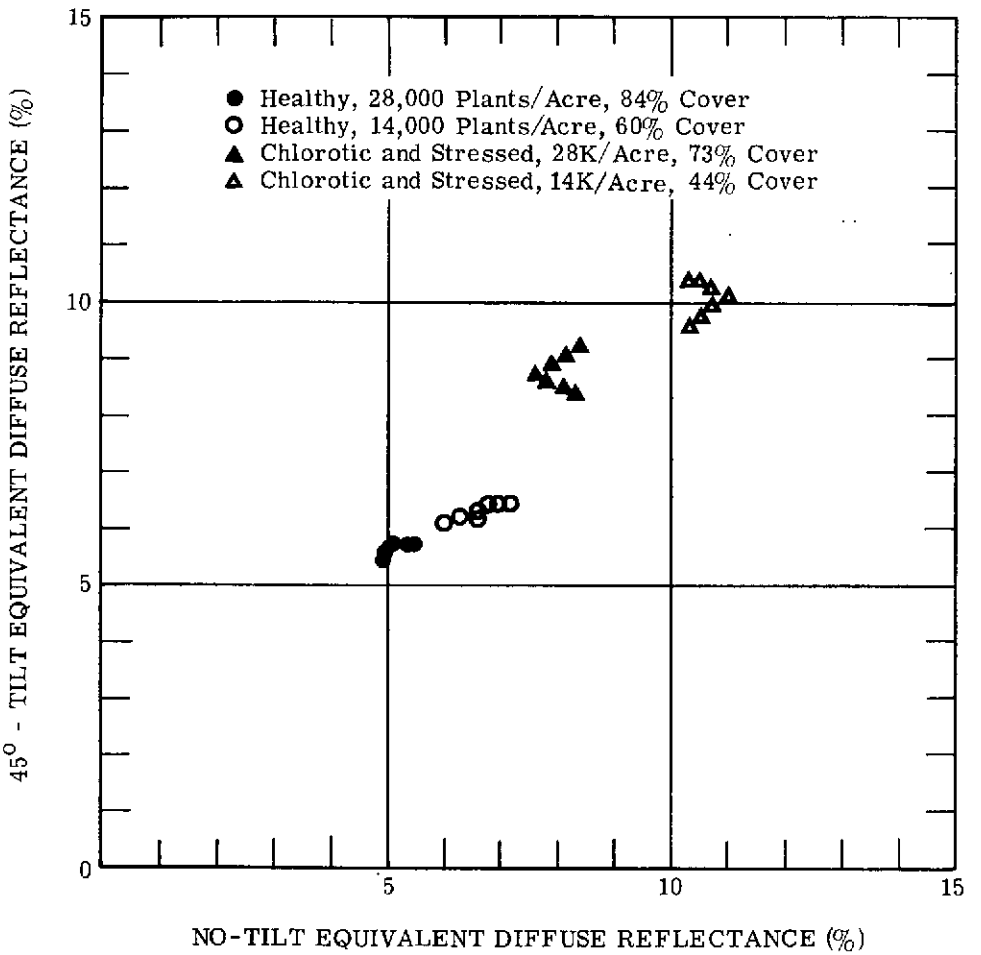

(a) 570 nm

FIGURE 18. EFFECTS OF DENSITY AND CONDITION ON MULTI-ASPECT REFLECTANCE OF CORN CANOPY, SIMULATED CORN, ±30° SCAN COVERAGE (Continued)

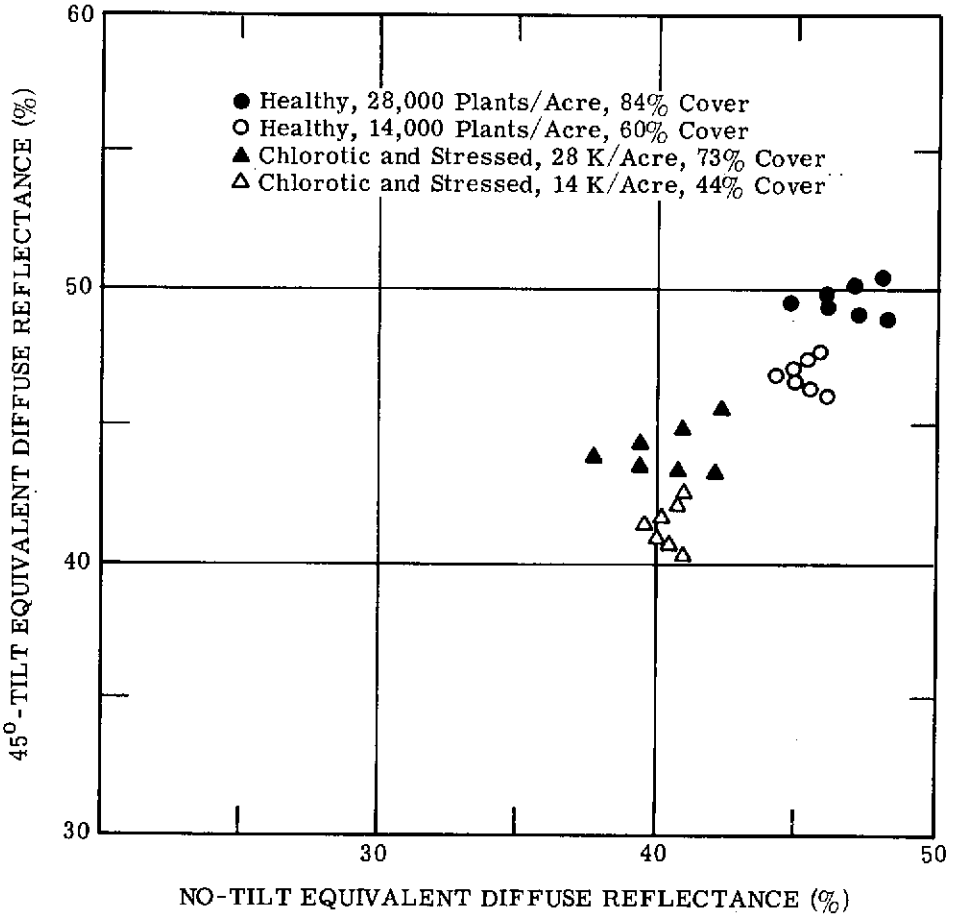

(b) 760 nm

FIGURE 18. EFFECTS OF DENSITY AND CONDITION ON MULTI-ASPECT REFLECTANCE OF CORN CANOPY, SIMULATED CORN, ±30° SCAN COVERAGE (Concluded)

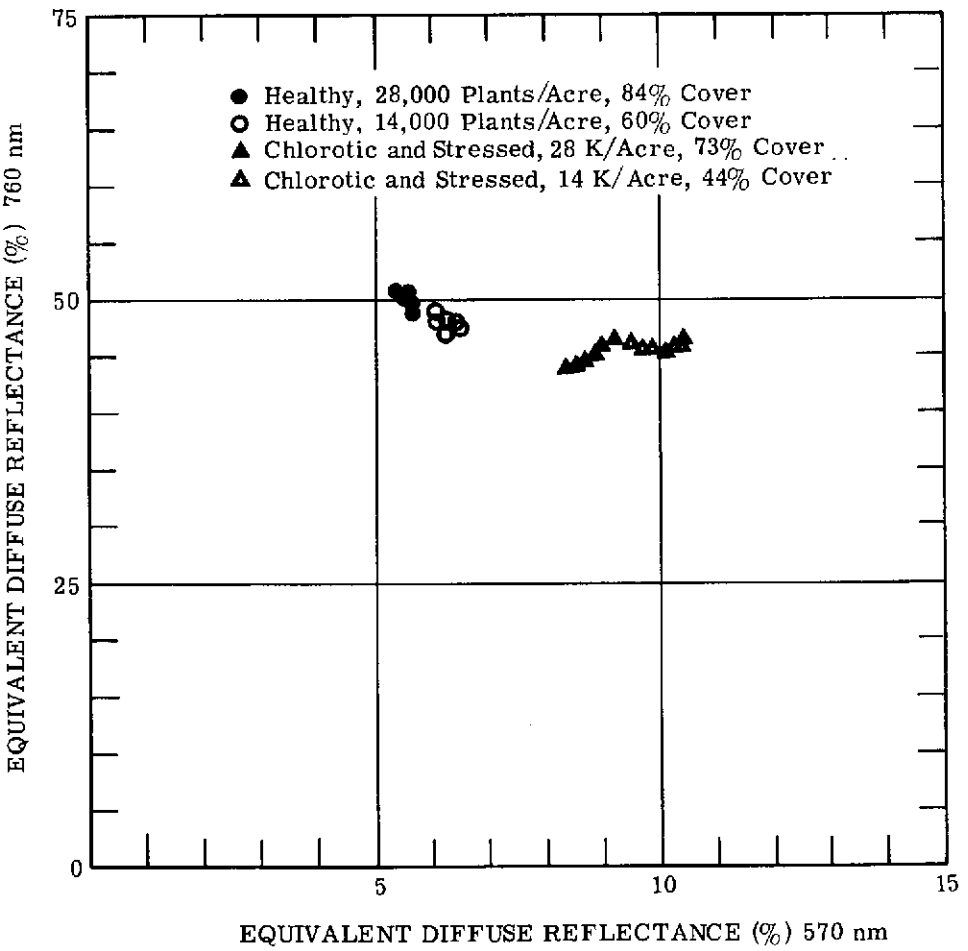

FIGURE 19. EFFECTS OF DENSITY AND CONDITION ON SINGLE-ASPECT REFLECTANCE OF CORN CANOPY, SIMULATED CORN, $\pm 30^{o}$ SCAN COVERAGE

Another factor that affects the reflectance of crops with less than 100% cover is the spectral reflectance of the underlying soil. The reflectances of a light soil were used for the calculations presented in Figs. 18 and 19. Similar calculations also were made for a dark soil. Figures 20 and 21 present scatter diagrams for the results of calculations at a 0^{o} scan angle for each of the four canopy types (two conditions, each at two densities), both with a light soil and a dark soil underneath. The multi-aspect diagram for 570 nm (see Fig. 20(a)) shows that there is little effect for a dense healthy canopy. As the density decreases, however, the soil whose reflectance differs in greater degree from that of the healthy corn (in this instance the light soil) causes a shift in canopy reflectance. Soil color has a more pronounced effect on the stressed chlorotic canopies, because of their reduced ground cover percentages.

The final effect studied was that of corn tassels on the reflectance of a mature canopy. Tassels appear in late July or early August after the corn stalks have reached their full height. Tassel colors vary somewhat from variety to variety and generally change color as they mature (e.g., light green upon emerging and reddish brown upon maturing). The color change in corn fields at the time of tasseling is striking when viewed obliquely from ground level; calculations were made to estimate the effect on airborne multi-aspect data. Calculated reflectances for healthy corn with and without tassels are presented in Figs. 22 and 23; two tassel colors, two densities, and two soil colors were used for the calculations.

There are three groupings of points on the scatter plot for 570 nm (see Fig. 22(a)). The first group includes both the high densities—irrespective of soil color, without tassels and with reddish tassels—and the low densities—with dark soil and reddish or no tassels. The second includes the light tassels on high density plots, while the third includes the low density plots on light soil for all three tassel conditions. Thus, tassels do change the multi-aspect reflectances of a corn canopy, but their effects can be overshadowed by soil-color differences on thin canopies. The same general conclusions can be drawn from Fig. 22(b) for 760 nm, although the grouping of plots is somewhat different and tassel color has more influence.

The final scatter diagram (see Fig. 23) of the corn-tassel effect is for the best channels, 570 and 760 nm (both tilted). Here, the dispersion pattern is mostly vertical in extent, as opposed to the radial dispersion of the other two figures. The highest points are for high density and for the lower density with light soil and no tassels. The middle group of points is primarily for low density with light soil and tassels, while the lowest points are for reddish tassels and low density with dark soil. A comparison with Fig. 13(b) shows a similar type of dispersion in the empirical data for corn fields. The corn fields in the test area were indeed in the process of tasseling at the time of the flight, and there were fields at all stages of development—some with mature reddish-brown tassels, others with light-green tassels, and still others without tassels. There was very little corn blight in the area that year, so most corn fields were healthy.

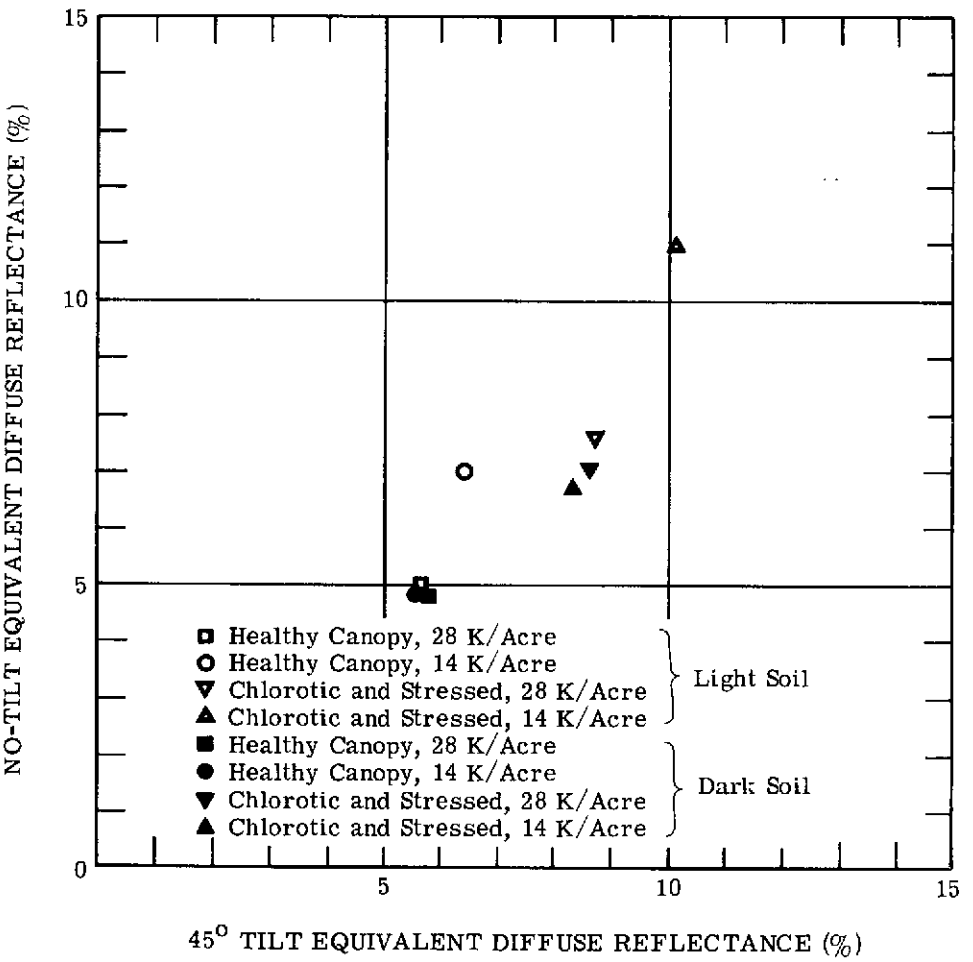

(a) 570 nm

FIGURE 20. EFFECT OF SOIL COLOR ON MULTI-ASPECT REFLECTANCE OF CORN CANOPY (Continued)

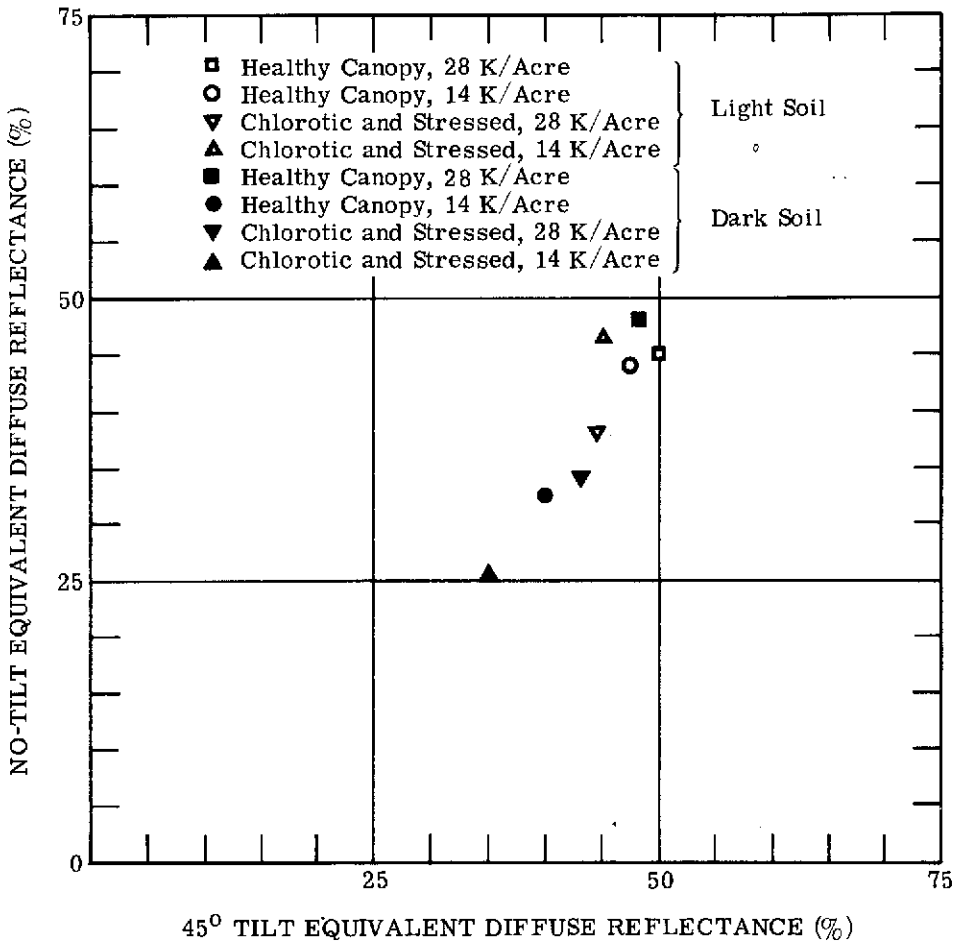

(b) 760 nm

FIGURE 20. EFFECT OF SOIL COLOR ON MULTI-ASPECT REFLECTANCE OF CORN CANOPY (Concluded)

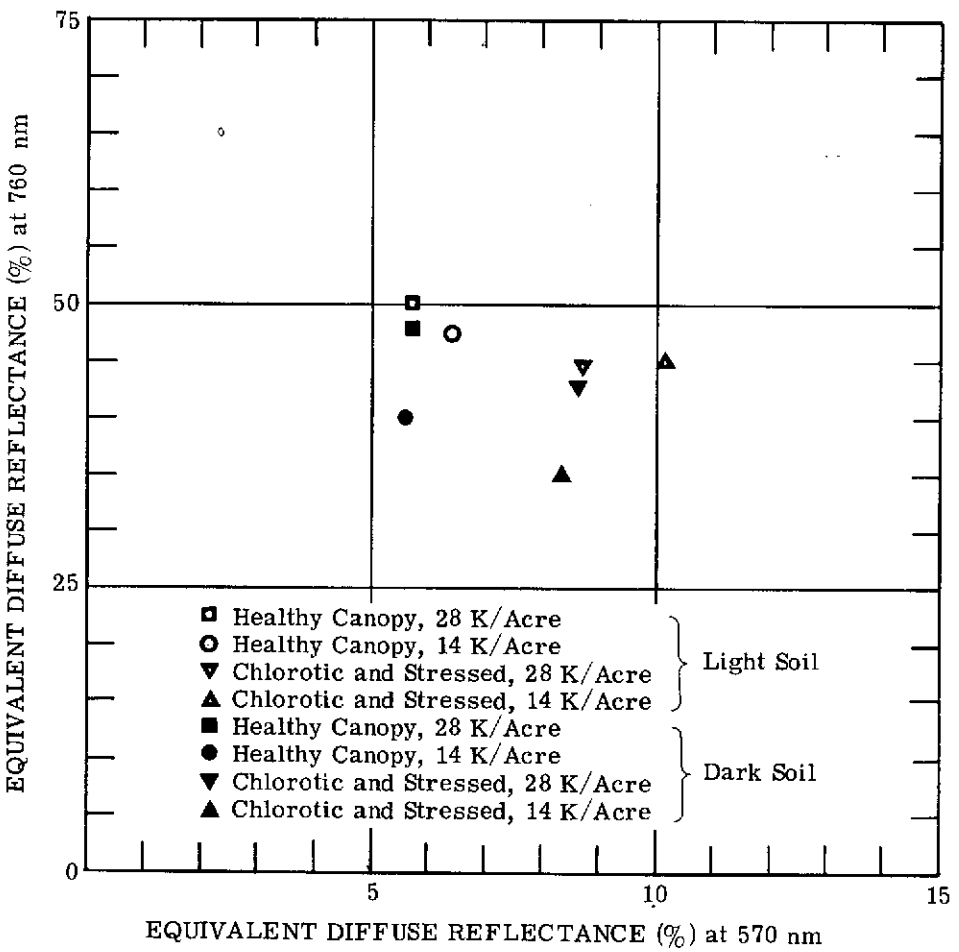

FIGURE 21. EFFECT OF SOIL COLOR ON SINGLE-ASPECT REFLECTANCE OF CORN CANOPY, 45° TILT

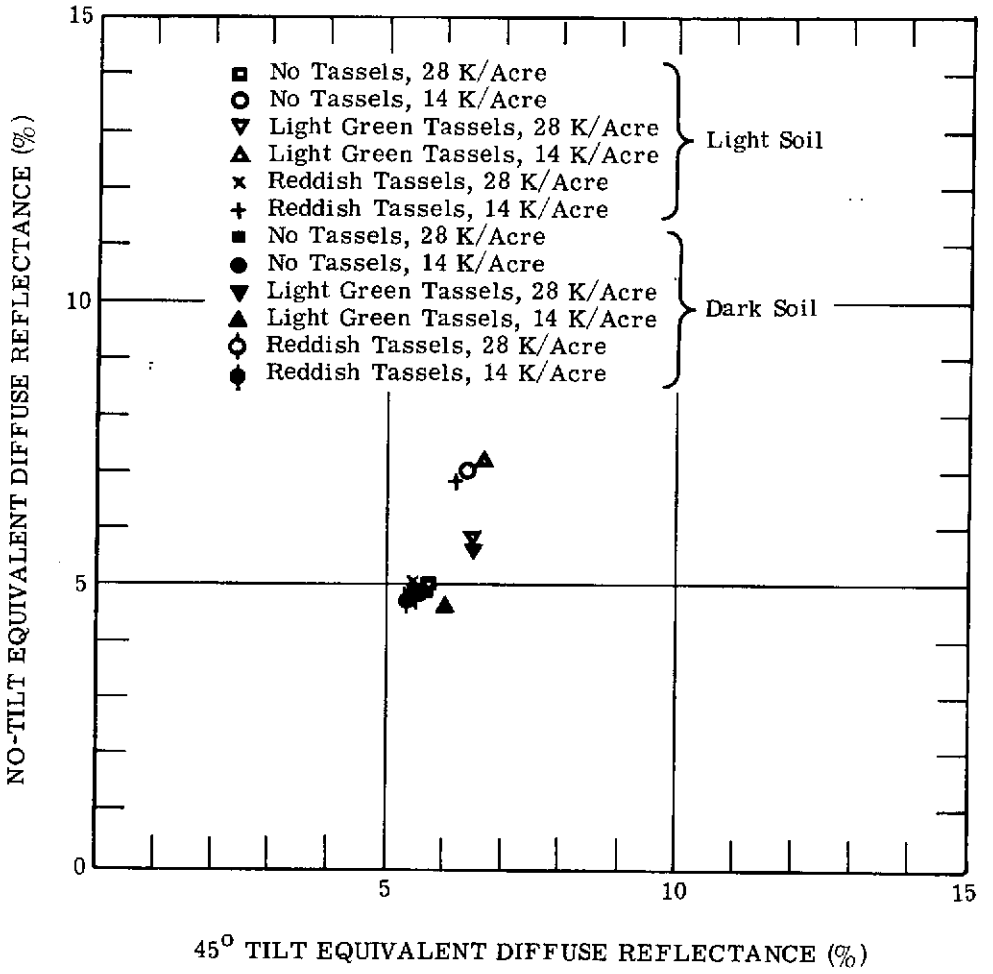

(a) 570 nm

FIGURE 22. EFFECT OF TASSEL COLOR, SOIL COLOR, AND DENSITY ON MULTI-ASPECT REFLECTANCE OF CORN CANOPY (Continued)

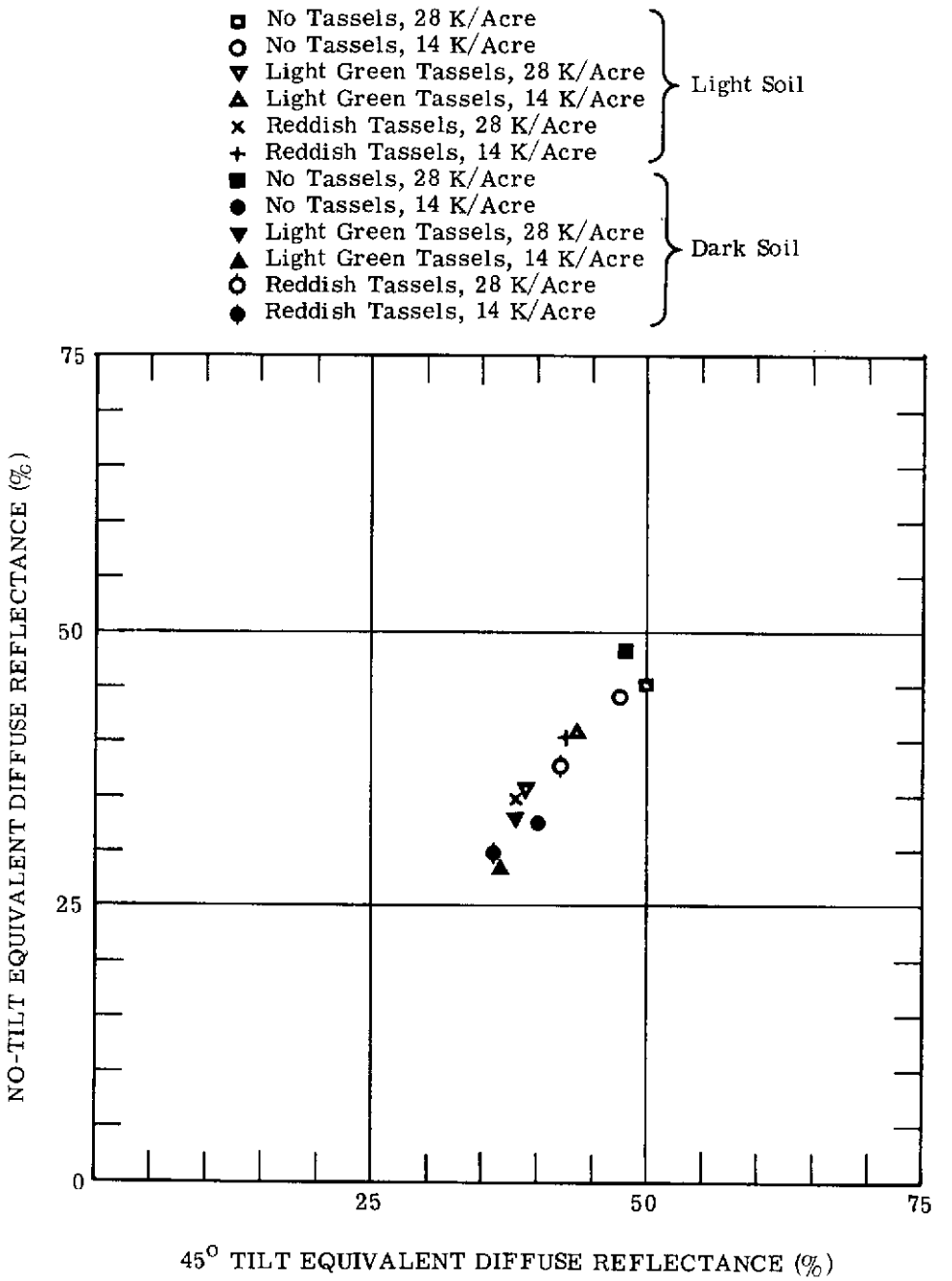

(b) 760 nm

FIGURE 22. EFFECT OF TASSEL COLOR, SOIL COLOR, AND DENSITY ON MULTI-ASPECT REFLECTANCE OF CORN CANOPY (Concluded)

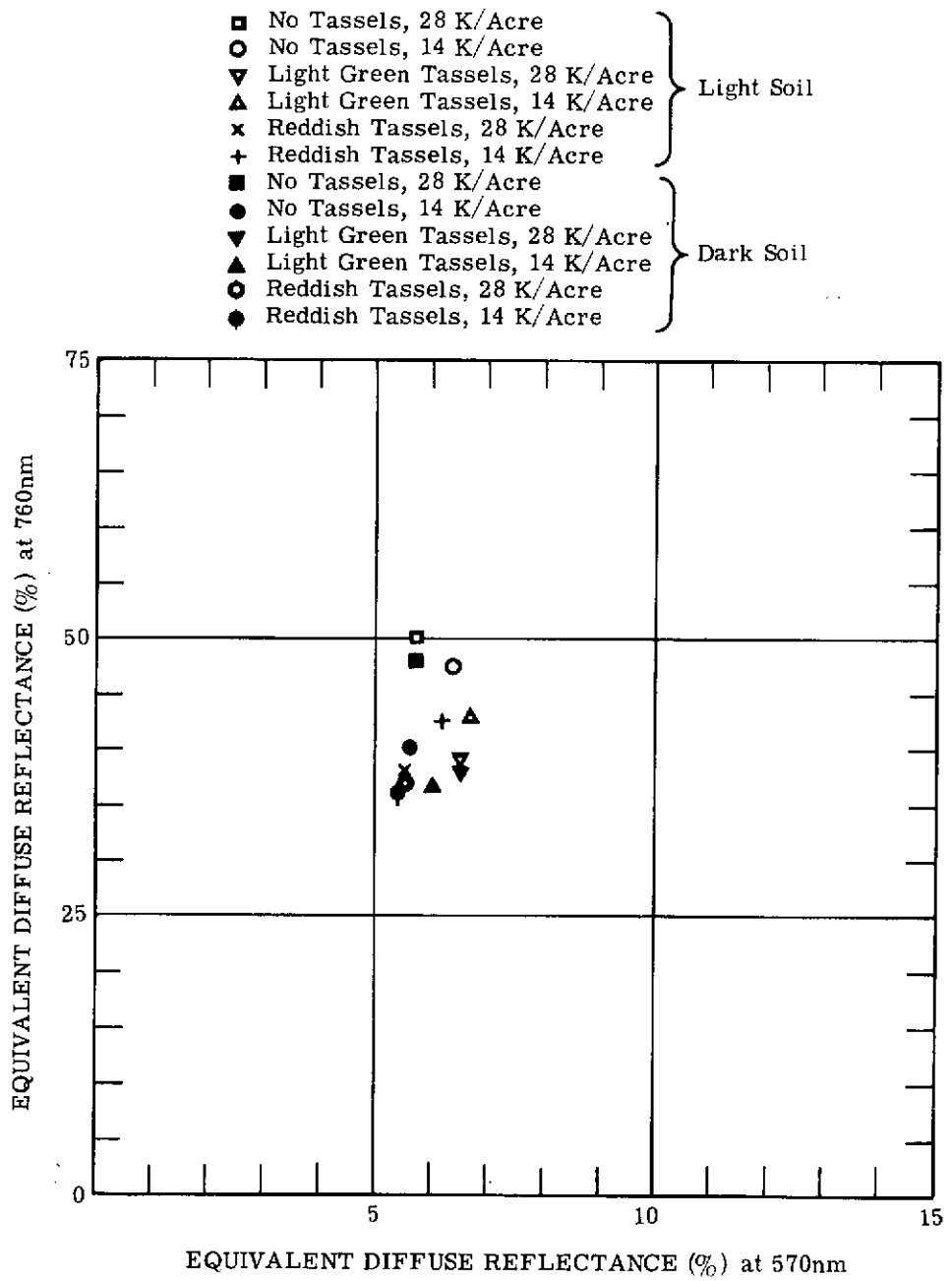

FIGURE 23. EFFECTS OF TASSEL COLOR, SOIL COLOR, AND DENSITY ON SINGLE-ASPECT REFLECTANCE OF CORN CANOPY, 45° TILT

3.3.2 FORESTRY APPLICATIONS

Multispectral scanner data have been used previously with computer classification procedures to type-map forest species. Mappings into broad categories such as deciduous versus coniferous stands generally are easiest, but there has been some success in mapping upland hardwoods versus bottom-land hardwoods [12] and in identifying specific species [13]. In addition to species identity, another very important characteristic of forest stands is their standing volume or biomass. Various ground sampling procedures are commonly used to estimate the volumes of stands.

Techniques that use aerial photography also exist. These generally depend on measurements of tree crown closure, crown diameter, and/or stand height (see Section 3.3.3.2 and Appendix B). Because reflectances observed at two or more angles depend on the structural parameters of a canopy, we have begun to investigate the feasibility of using multi-aspect scanner data to estimate important characteristics of tree stands.

When deciduous trees are in a leafless condition their stems are visible from above. As a starting place, we chose to collect multi-aspect data over leafless trees with an underlying snow cover to provide a uniform background against which to view the trees. Corresponding calculations were made with the Suits canopy-reflectance model for a range of canopy parameters that allows some interpretation of multi-aspect scanner data.

3.3.2.1 Photointerpretation Techniques for Forest Mensuration

Techniques have been developed to use aerial photography for estimating timber volume. Such techniques offer several advantages over the more traditional ground-measurement methods. These advantages include a reduction in expensive field work, more rapid surveys, and ease of surveying isolated areas. The same advantages would also apply to multi-aspect techniques with multispectral scanners—should such techniques be successfully developed. In view of this pertinence, aerial photo methods of volume estimation (described in more detail in Appendix B) are summarized below.

Ground measurements of height, age, and basal area provide one basis for determining stand volumes, while diameter at breast height (dbh) and merchantable height measurements can determine individual tree volumes. Since these variables cannot be measured directly in aerial photographs, substitute measurements are made of related quantities (i.e., total height, crown diameter, and crown closure instead of merchantable height, dbh, and basal area, respectively).

Established aerial tree volume tables permit estimates of the volumes of individual trees from measurements of total tree height and crown diameter. Trees selected according to some sampling procedure can thus be measured to provide individual tree-volume estimates which are extrapolatable to estimates for entire forests.

The use of aerial-stand-volume tables is an alternative to tree-volume tables. Here, relationships have been established previously between characteristics of whole stands of trees and the stand volume. The stand method adds crown closure as a variable in the estimation model, and redefines height and crown diameter to be average characteristics of trees in the stand.

Aerial stand methods possess advantages over individual tree methods for estimating timber volumes from aerial photography. (See Appendix B for further discussion of forest mensuration methods.)

3.3.2.2 Multi-Aspect Data Collection and Data Preparation

Data were collected in Michigan in March and April of 1973, generally under the desired conditions. The first data set, 20 March, was collected over the Saginaw Forest near Ann Arbor, an experimental forest of The University of Michigan's School of Natural Resources. The flight was made in conjunction with a test flight of the scanner system after over-winter modifications, and it posed some difficulties in processing. Data that have not yet been analyzed were collected on a second flight made on 11 April over natural stands of aspen near Cadillac in the Northwestern part of the Lower Peninsula.

The Saginaw Forest data were collected from an altitude of 0.61 km (2000 ft) with headings, tilt angles, and sun positions as listed in Table 12. As the table shows, the data were collected very shortly after solar noon with the sun azimuth 10^{o} to 20^{o} from due South.

A malfunction in the scan-motor synchronization on this first flight of the season caused straight roads and field boundaries to appear undulating along the flight line. These undulations were removed by use of manual inputs to program DESNAKE (see Appendix A). Selected areas were then manually placed in spatial registration and signatures extracted for analysis.

3.3.3.3 Theoretical Reflectance Calculations

The major portion of this forestry study involved the calculation of multi-aspect reflectances of leafless tree stands as functions of several parameters. The Suits bidirectional-reflectance model for canopies was used, and the ground surface was assumed to be snow covered.

A simplified physical model was assumed for trees. Each tree stem was assumed to have a conical shape with five (non-independent) parameters: d_s = stem basal diameter, h = stem height, a_b = stem basal area, a_p = stem vertical profile area, and v_s = stem volume. The relationships between these parameters are as follows:

TABLE 12. SAGINAW FOREST FLIGHT, 20 MARCH 1973

Time (EST)	Tilt Angle (°)	Heading (°) (CW from N)	Altitude (km)	Sun Zenith Angle (°)	Sun Azimuth Angle (°) (CW from N)
13:10	0	180	0.61	42.5	190°
13:30	45	180	0.61	43.4	197°
13:34	45	360	0.61	43.7	199°

Parameter	Typical Units
Tree Basal Area $a_b = \pi d_s^2/4$	(m^2)
Tree Profile Area $a_p = d_s h/2$	(m^2)
Tree Stem Volume $v_s = a_b h/3 = \pi d_s^2 h/12$	(m^3)

For a tree stand, which is composed of many individual trees, we must use "per unit area" designations and add N, the number of tree stems present per unit area. (For this report, stand parameters are capitalized to differentiate them from tree parameters.) Each stand was assumed to be composed of trees of equal size, so:

Parameter		Typical Units
Stand Height	$H = h$	(m)
Stand Stem Density	N	(# stems/ha)
Unit Stand Basal Area	$A_b = Na_b$	(m^2/ha)
Unit Stand Profile Area	$A_p = Na_p$	(m^2/ha)
Unit Stand Stem Volume	$V_s = Nv - N(a_b h)/3 = A_b H/3$	(m^3/ha)

Since trees have branches as well as stems, it was necessary to include branch parameters in the model. A two-layer canopy was used. The top layer contained all the branches and a portion of the stem, while the bottom layer contained only the remainder of the stem. Branches were assumed to be randomly positioned and oriented, as well as being describable by an average diameter, d_b, and a total length, l_b, or equivalently by d_b and a total per-tree branch volume, v_b. The unit stand branch volume was $V_b = Nv_b$.

The principal spectral feature that one observes in data such as that described above is the difference in reflectance between the tree bark and the snow. Bark tends to have a low reflectance (e.g., 10 to 20%) at visible wavelengths and high reflectance (e.g., up to 50 or 60%) at near-infrared wavelengths, according to spectral reflectance measurements made of Bigtooth Aspen (Populus gradidentata) bark under this project. One of several spectral reflectance measurements is presented in Fig. 24, (a) from 0.35 to 1.00 μm and (b) from 1.0 to 2.6 μm. A Beckman spectrophotometer with an integrating sphere coated with barium sulphate was used. The laboratory measurements were digitized, corrected for the non-unity reflectance of barium sulphate, and graphed on a line-printer output. The bark sample was collected at breast height (1.37 m or 4.5 ft) in May 1973 and kept refrigerated until measured five weeks later.

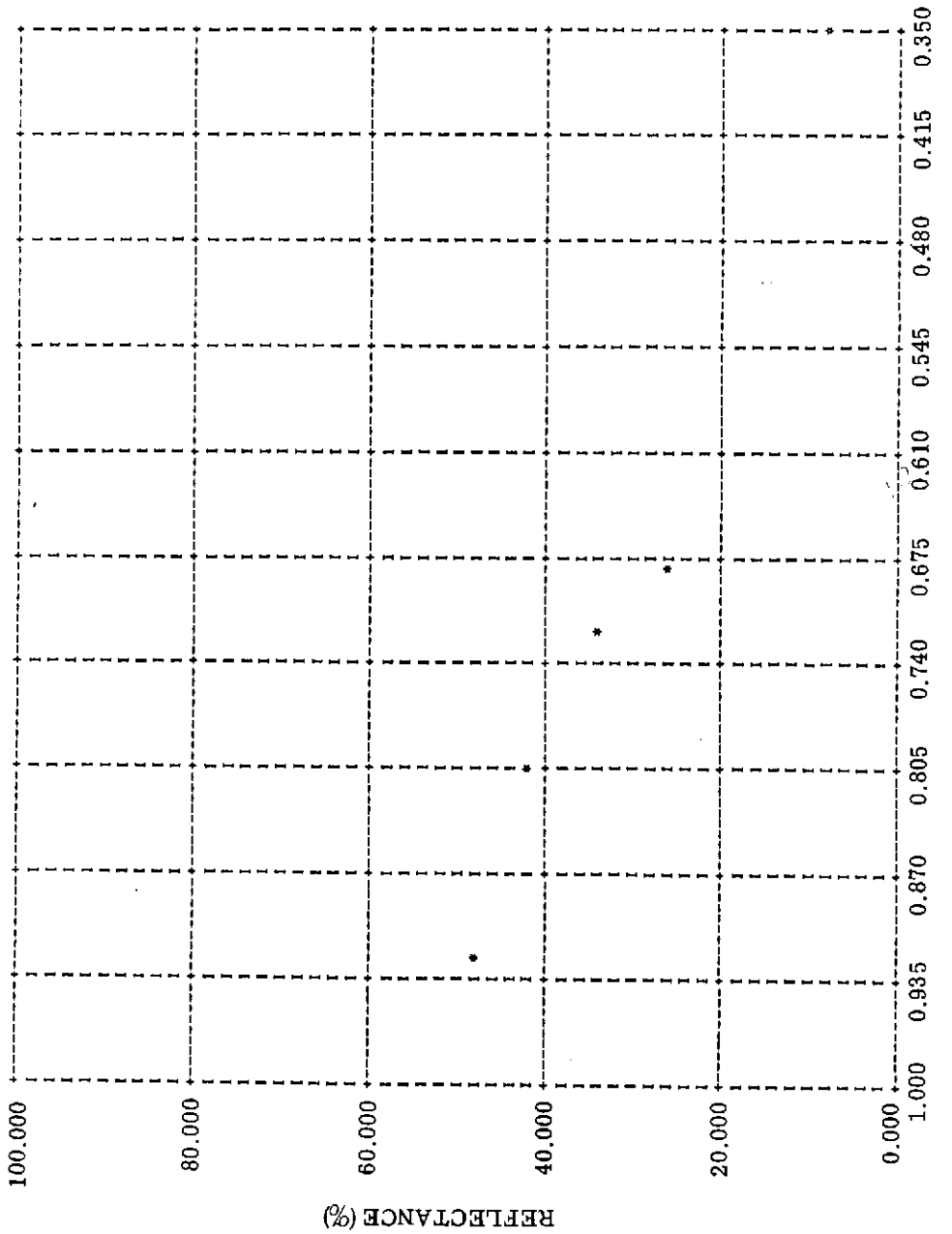

(a) 0.35-1.0 μm

FIGURE 24. SPECTRAL REFLECTANCE OF ASPEN BARK (Populus grandidentata) (Continued)

C-2

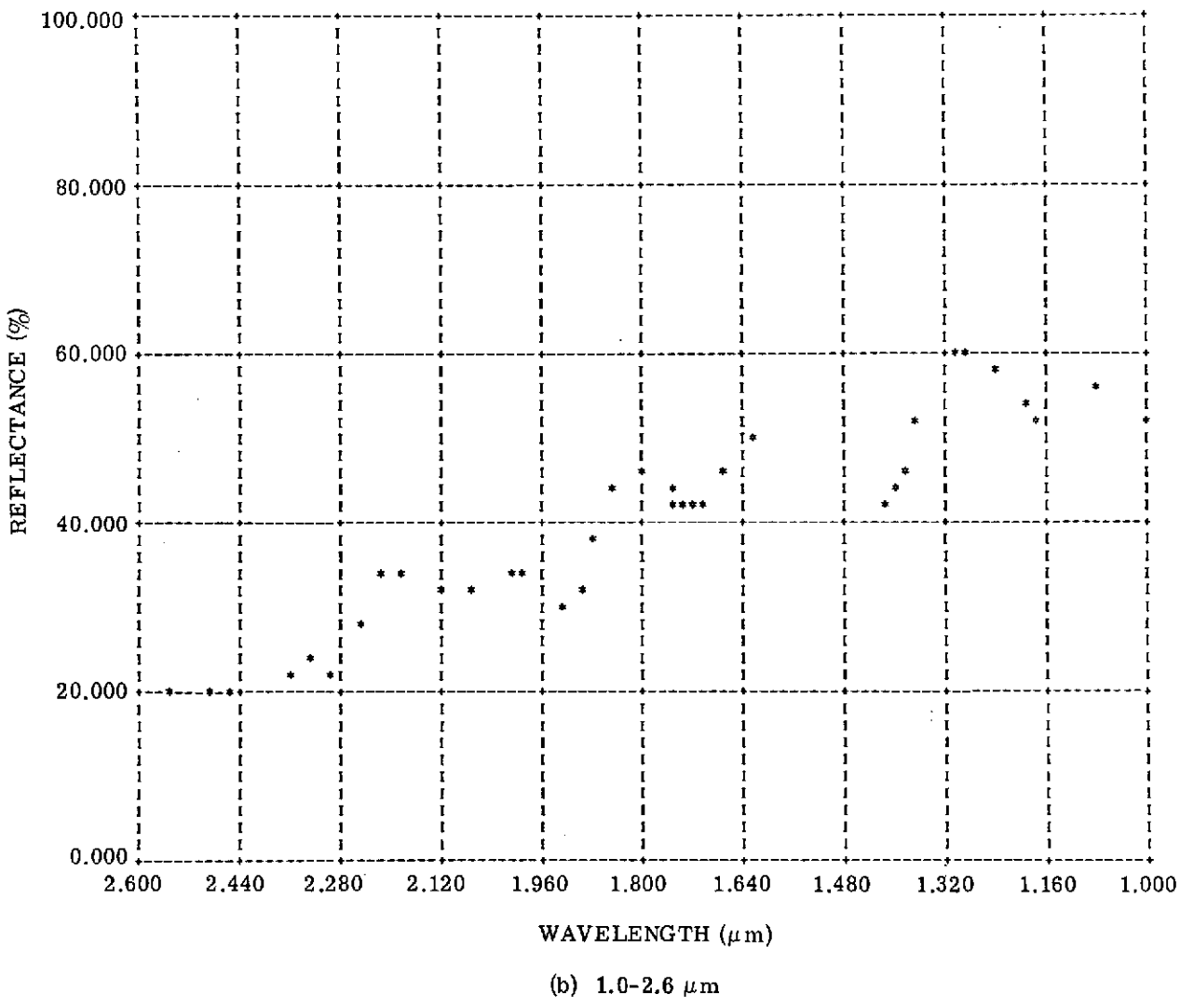

(b) 1.0-2.6 μm

FIGURE 24. SPECTRAL REFLECTANCE OF ASPEN BARK (Populus grandidentata) (Concluded)

A wide range of bark reflectance values was used in the calculations: 1, 2, 4, 8, 12, 16, 20, 24, 28, 32, 48, 64, and 83%. An 83% reflectance was used for the snow. Other parameters that were used were as follows: (a) 14.14, 20.00, and 28.28 m^2/hectare for unit stand basal area, A_b; (b) 14.14, 20.00, and 28.28 m for stand height, H; (c) 500, 700, and 1000 stems/hectare for stand stem densities, N; and (d) 5, 12.5, and 25mm average branch diameters, D_b, for different unit stand branch volumes, V_b.

3.3.3.4 Analysis of Results

Analysis of the theoretical reflectance calculations and corresponding scanner data was not completed during this reporting period. However, it is useful to present a few interim results that illustrate major effects.

The first graph (see Fig. 25) illustrates the way in which canopy reflectances at both no-tilt and 45^o-tilt aspects depend on stem volume for a stem-only canopy. Results for only the two extreme values of bark reflectance are presented.

The second graph (see Fig. 26) illustrates the large influence of branches on the reflectance of a canopy having a single-stem configuration and volume. The top pair of lines is for the stem-only case. Note that there is a cross-over between the reflectances at the two aspects as the bark reflectance approaches the value for snow. When branches are added with a volume amounting to 20% that of the stems, the overall canopy reflectance decreases markedly. When the average branch diameter is decreased from 25mm to 12.5 and then 5.0, the total length of such branches increases, such that the total cross-sectional area of branches increases and the canopy reflectance decreases even further. Note also that the cross-over point between the two aspects moves to lower bark reflectances as branch diameter decreases.

The final graph (see Fig. 27) is of empirical data extracted for a sugar-maple (Acer saccharum) stand in the Saginaw Forest. The voltage values for the sugar maple were divided by those for open snow. Reflectance values for the sugar-maple canopy were computed by assuming that the snow reflectance was 83% at all wavelengths. Although the x-axis on this figure is wavelength, we have seen earlier that bark reflectance (for aspen) increases with wavelength. Consequently, the graph approximates the canopy reflectance versus bark reflectance graph of Fig. 26. The cross-over between canopy reflectances at two aspects is clear and matches the trend shown in theoretical model predictions.

Thus far these results have not been subjected to more detailed analysis and interpretation, nor have we established a match between theoretical and empirical stand parameters. We have, however, shown that trends predicted by the model exist in empirical multi-aspect data. For an answer to the question of whether forest-stand-volume information can be

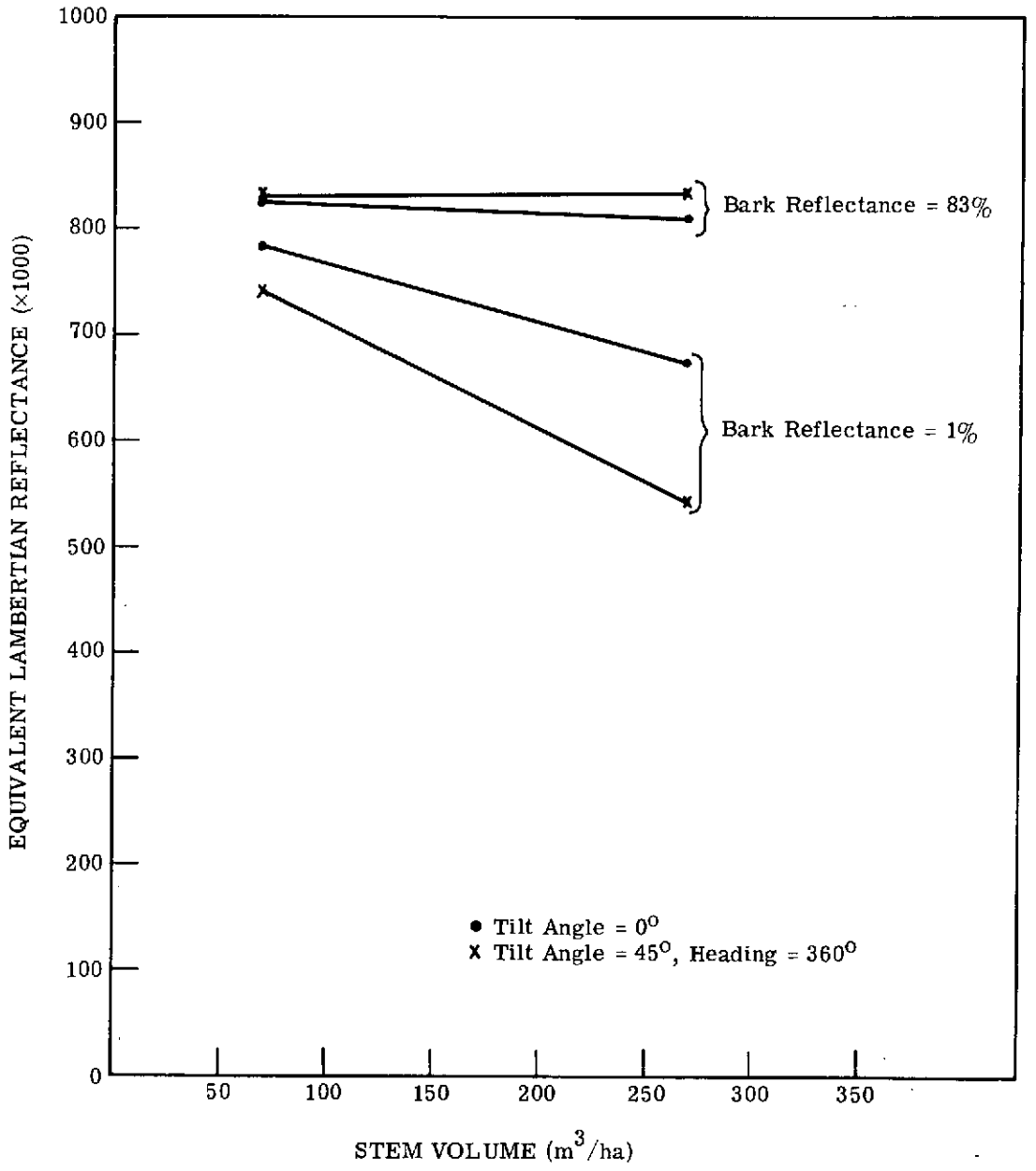

FIGURE 25. THEORETICAL STEM-ONLY FOREST CANOPY MULTI- ASPECT REFLECTANCE: BARK REFLECTANCE AND STEM VOLUME DEPENDENCE. Ground reflectance 83% (snow), scan angle 0° (nadir), sun azimuth 185°, sun zenith 53°.

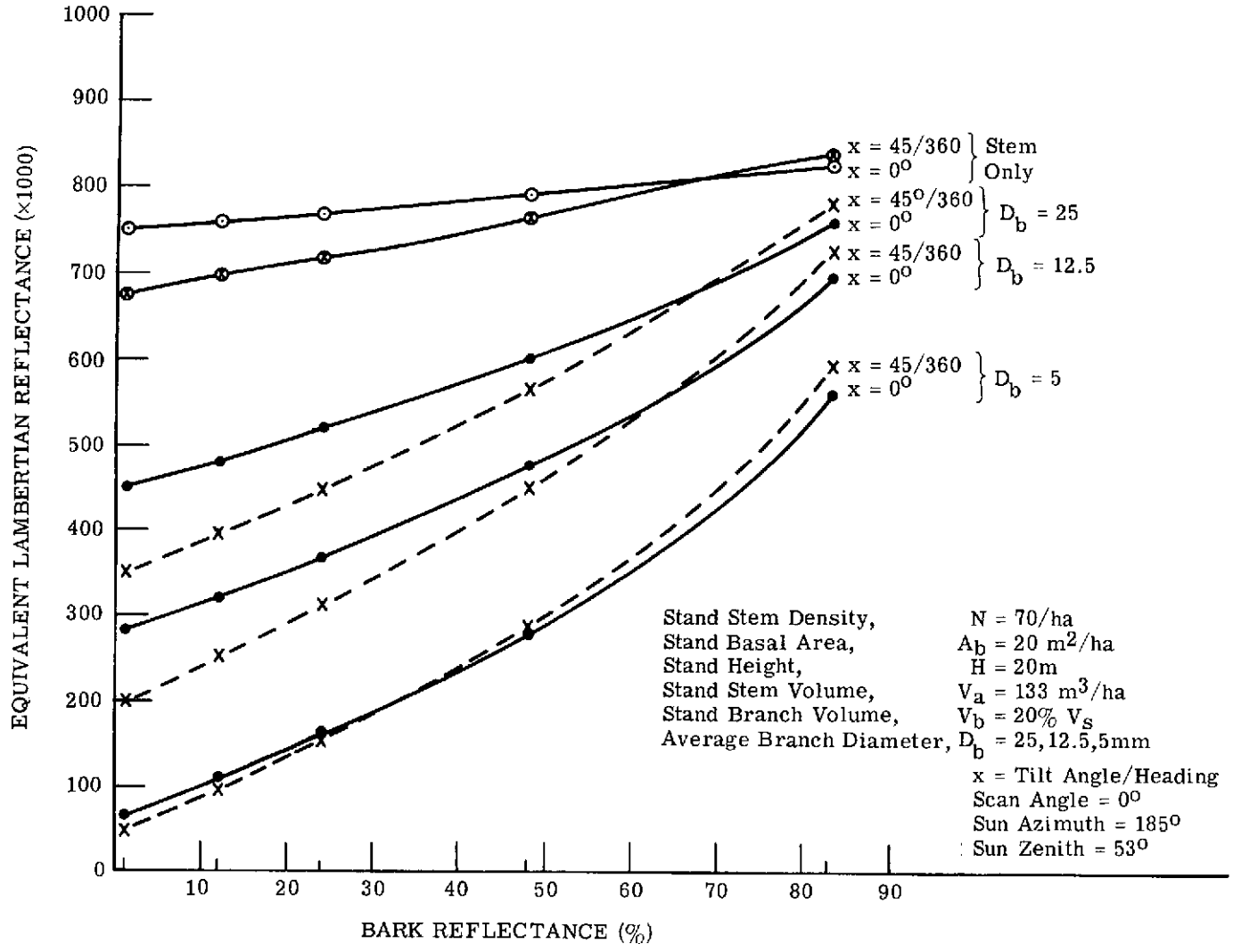

FIGURE 26. EFFECT OF BRANCHES ON THEORETICAL MULTI-ASPECT REFLECTANCE FOR LEAFLESS FOREST

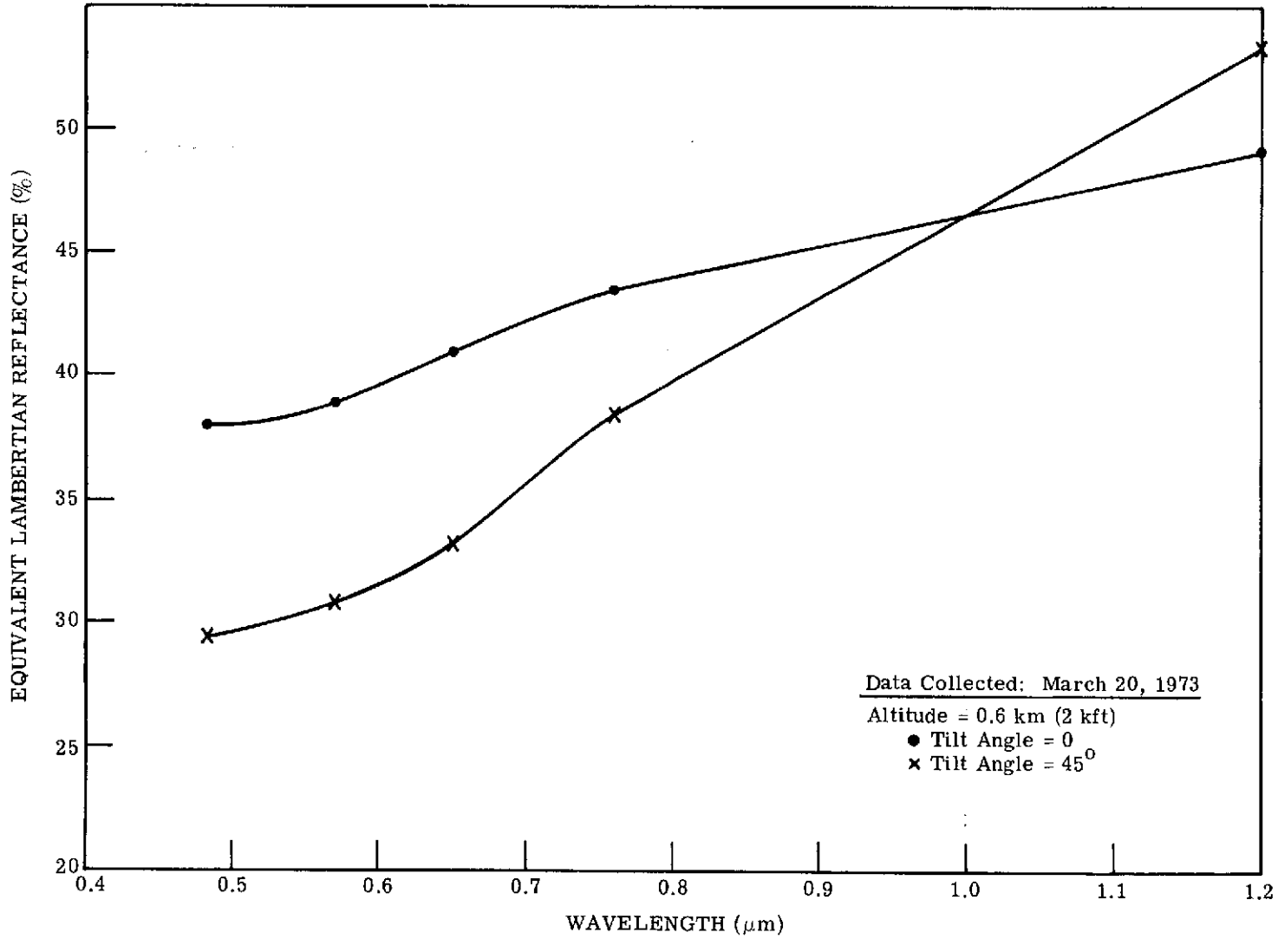

FIGURE 27. MULTI-ASPECT REFLECTANCES FOR LEAFLESS SUGAR MAPLE STAND. Snow covered background.

extracted from multi-aspect data, further analysis will be required. We conjecture that it may be possible to extract such information if one parameter such as stand height or stem density is obtained independently and/or reliable relationships are established between volumes and diameters of stems and branches for specific species of interest.

4
CONCLUSIONS AND RECOMMENDATIONS

A two-part study of remote sensing data was undertaken at ERIM. The first part of our study examined variations in multispectral signatures with time of day and with scan angle, both of which limit the accuracy of machine classification under differing conditions. In the other part of our investigation, we introduced the use of multi-aspect remote sensing and examined its potential for improving classification accuracy and extracting other information.

4.1 MULTISPECTRAL SIGNATURE ANALYSIS

Variations in multispectral signatures were examined to ascertain their magnitude, probable causes, and restriction on the accuracy of machine classification as conditions deviate from those of signatures extracted for classifier "training." This study was performed on a uniquely suitable data set which provided repeated data obtained at widely differing times of day over the same area—a predominantly agricultural site in Ingham County, Michigan. Efforts were concentrated on studying the temporal variations in the signatures, and classification tests were run to measure the degradation of results when signatures from the first time of day were used in classifying other data taken at later times during the same day. Variations in the signatures as a function of scan angle were also analyzed. Detailed comparisons were made with the predictions of a radiative transfer model developed at ERIM, and also, in lesser detail, with those of a canopy model for bidirectional reflectance also developed at ERIM.

4.1.1 CONCLUSIONS

(1) There are sizable variations in signature means as a function of both time of day and scan angle.

(2) A radiative transfer model developed at ERIM was successful in predicting the trends in the data at the shortest wavelengths, but it did not include all variations at the longer wavelengths. Two forms of deviation we found may be attributable to causes explicitly excluded from this model:

(a) Brighter than predicted signals in the afternoon at all wavelengths may be caused by higher overall illumination from high thin cirrus clouds (known to be present) which reflect additional light to the ground—the model assumes no cloud cover.

(b) Additional anti-solar peaking, especially at longer wavelengths, is apparently caused by bidirectional-reflectance properties of the surfaces which are not included in this model—the model assumes Lambertian (perfectly diffuse) surface reflectors.

(3) Comparison of empirical data at longer wavelengths with predictions of a canopy bidirectional reflectance model shows similar curve shapes, but the model predicts less variation than is observed in the data. However, model calculations were made for somewhat different conditions and should have been more closely matched to the observed conditions for a truer comparison.

(4) Time-of-day effects cannot be ignored. This is shown by the serious degradation when signatures from the first run were used in classification tests on later runs: recognition decreased from an average 84% correct on the first run at 9:33 AM LST to essentially 0% correct by 11:33.

(5) Recognition was 0% correct in the afternoon when we had expected the accuracy to rise again to approach that for morning runs having corresponding solar angles. The reasons for this are not fully understood; however, we suspect uncorrected run-to-run calibration changes for one or more channels, because χ^2 calculations indicated that use of fewer channels (in particular, four calibrated in this study) would give better results with the current data.

(6) Some means of signature extension is needed to compensate for temporal variations during large-area surveys with airborne scanner data.

(7) The behavior in the far-infrared (direct-thermal) radiance channel was analyzed separately since different physical processes are involved. The temperatures rose during the morning, then stayed roughly constant throughout the afternoon as anticipated, rather than declining as does reflected radiance at shorter wavelengths. There was a clear-cut difference between the temperatures of the various ground covers, with trees staying cooler than corn and corn cooler than pasture—this is physically reasonable and expected. Finally, the temperatures of surfaces within any one crop were not uniform, the sunlight side being slightly, but definitely, warmer.

4.1.2 RECOMMENDATIONS

(1) We should further investigate the reasons for the 0% correct recognition on the afternoon runs for which signatures from the first morning runs were used; we should also better quantify the performance degradation. The classification tests should be repeated using a selected subset of channels to determine whether there is any intrinsic improvement with fewer channels, and careful attention should be paid to checking the calibration variations.

(2) Bidirectional reflectance effects should be studied in depth and related to the deviations between the empirical data and predictions of the radiative transfer model, with calculations made under matching conditions.

(3) Various signature-extension techniques, such as those studied under other tasks on this contract, should be applied to the Ingham County data set, since it is ideally suited for the study of temporal extension.

(4) A complete set of all 12 morning runs (of which only four were used this year) should be digitized, at least for a subset of channels, and used as a basic data set for studying adaptive processing (or other temporal extension techniques), run-to-run calibration stability, etc.

4.2 MULTI-ASPECT REMOTE SENSING TECHNIQUES

Multi-aspect remote sensing techniques applicable to multispectral scanner data were introduced and their use explored for improved classification performance as well as for increasing the extractability of other information. Multi-aspect data were collected by the ERIM M-7 multispectral scanner which was tilted so that its scan plane intersected the ground at two or more different angles on successive passes over a scene. These data were placed in spatial registration and analyzed. Theoretical calculations of reflectance also were made and analyzed.

4.2.1 CONCLUSIONS

(1) The use of multi-aspect data offers some promise for improved classification performance over that obtainable with conventional multispectral scanner data. The following results were obtained with multi-aspect data collected over an agricultural area in mid-August.

(a) Results with manually registered data from 69 agricultural fields showed slightly more accurate and more consistent classification performance for multi-aspect data than both tilt-only and no-tilt data for one selection of training and test fields.

(b) Results for switched roles of training and test fields in the manually registered data were not as consistent, but the switch in roles was complicated by the use of combined, instead of multi-modal, signatures.

(c) A classification map produced from six channels of machine-registered multi-aspect data was examined and found to exhibit better overall qualities than six-channel maps from either no-tilt or tilt-only data — classification patterns were most spotty on the no-tilt map; mature trees appeared to be most accurately delineated on the multi-aspect map; and overall delineation of corn fields was best on the multi-aspect map. (Although corn fields were slightly better recognized on the multi-aspect map, the tilt-only map had more false corn detections in trees. In several no-tilt corn fields there were numerous false tree detections.)

(d) A rank-ordering of the multi-aspect channels, based on average pairwise probability of misclassification between signatures, showed a balance between the tilt and no-tilt channels: two tilt channels were assigned the highest rank while no-tilt channels placed in the next several ranks.

(2) Maps of the difference between tilt and no-tilt signals in several channels and corresponding scatter diagrams of class mean signals exhibited interesting characteristics.

(a) On the 0.55- to 0.60-μm difference map, bare soil exhibited the greatest relative signal increase in going from no-tilt to tilt geometry. The effect appears to decrease progressively as the fields contain more and more vegetation biomass (and/or green vegetation).

(b) On the 0.62- to 0.70-μm difference map, vegetation signatures have more nearly equal difference values, but bare soil has a markedly lower difference value.

(3) Theoretical multi-aspect reflectance calculations for corn canopies show that variations in canopy physical characteristics produce substantial changes in reflectances (although extraction of such information from empirical data has not yet been attempted).

(a) The greatest effect was produced by the combination of a stressed canopy with 50% chlorotic leaves.

(b) Soil-color differences became important only when coupled with low plant densities.

(c) Corn-tassel effects were discernible on multi-aspect scatter diagrams, and the dispersion pattern of different tassel, soil, and density conditions in healthy corn came closest to matching empirical scatter plots for tilt channel 9 (760 nm) versus tilt channel 5 (570 nm).

(4) The canopy reflectance model predicted trends found in empirical data for a leafless deciduous tree stand with snow-covered ground. The analysis was not completed, so the feasibility of extracting information on forest stand characteristics (such as stand volume) was neither established nor rejected; further work is recommended.

4.2.2 RECOMMENDATIONS

(1) Classification performance on the machine-registered multi-aspect data set should be analyzed more completely than was possible here—owing to the late availability of the machine-registered data. For example, the degree of misregistration in the multi-aspect data should be analyzed in comparison with typical ground-structure sizes in order to evaluate how much such misregistration might be degrading both the cross-aspect entries in the signature-correlation matrices and classification performance.

(2) Additional analyses should be performed on multi-aspect signatures to better explain observed signal patterns and dispersions, to form and enhance human intuitions useful in data interpretation, and to explore signal combinations for extracting information on scene material conditions.

(3) The feasibility study for extracting forest-stand characteristics from multi-aspect scanner data should be continued and completed.

Appendix A
SOFTWARE DEVELOPMENT

Five general computer programs were developed and used for this task. They are designed to process digital multispectral scanner data or signatures within the ERIM multispectral processing system. All except one employ the IBM-7094 computer system.

Program SMOOTH operates on data contained in a specified portion of a data file, averaging over pixels within adjacent rectangles of a specified number of scan lines and pixels (picture elements) per line. Its use reduces the quantity of data for subsequent processing; but because it does so at a later stage than our usual averaging during analog-to-digital conversion, it allows intermediate processing steps to be applied. It also can be used to coarsen spatial resolution by averaging over an area larger than a ground cover's structure or some other structure in the data (such as the skew or misregistration between channels which is possible in multi-aspect data).

Program MERGE combines scenes from two data sets by producing a composite data vector for each pixel. A one-to-one assignment is made of channel values in corresponding pixels from an equal number of scan lines and pixels per scan line in each scene. This program was used on this task to manually register data for the same fields from passes made at two different view aspects. Matching starting points and field sizes in the data for each aspect were selected by hand.

Program DESNAKE corrects for certain geometric distortions by shifting entire scan lines left or right. Such shifting was used to compensate for loss of roll stabilization in the airborne scanner data; this loss had caused straight roads under the plane's trajectory to follow snake-like paths in the data (hence the program name "de-snake"). The program performs interpolation between an arbitrary number of specified break-points along the flight path.

Program STEPLIN is a modification of the prior DIST program which calculates the pairwise probability of misclassification between all pairs of signatures in a set. It differs in using the algorithm of the "best linear" classification rule, or optionally a divergence approximation to the best linear rule, instead of DIST's quadratic rule. Hence, STEPLIN more closely approximates the results of classifying with the linear recognition rule, and takes appreciably less computer time—which for a large number of signatures represents a significant saving since the number of pairs increases as the square of the number of signatures. This program, unlike the others, operates on the ERIM CDC-1604 computer.

Program SIGCOM, used to combine signatures, employs a package of standardized signature manipulation subroutines developed for this and future signature analysis needs. Present

capabilities include the following: combining signatures with various weighting options; multiplicative scaling of signature means and, optionally, the covariance matrix with a different factor for each channel; adding a different constant to each channel mean; taking channel subsets; and calculating the χ^2 fit of a data mean vector to a signature. Since standardized subroutines have been written to perform the mechanics of reading, printing, punching, storing, and copying signatures, other programs and capabilities can be quickly added as they are needed.

Appendix B
AERIAL PHOTO METHODS OF ESTIMATING TIMBER VOLUME

B.1 INTRODUCTION

Aerial photography has proven to be a valuable tool for forest mensuration, chiefly as a result of the development of photogrammetric techniques and the availability of high-quality vertical photography. It is used both as a supplement and as a direct method for estimating timber volume and other stand characteristics.

Prior to the introduction of aerial photography, ground methods were used exclusively to collect inventory data. A great deal of money was expended in developing and refining these techniques because these data formed the basis for a multitude of decisions concerning the management of forest land. Numerous methods were developed and utilized, but basically the estimation of standing-timber volume was accomplished by measuring the characteristics of either entire forest stands (to provide a direct estimate of standing volume) or a representative sample of individual trees. These estimates then were projected to estimate the volume of large timber tracts. Each method offered specific advantages, and the use of one rather than the other depended upon the requirements of the inventory.

When the concept of using aerial photography to predict volume was introduced, it appeared to offer several distinct advantages and immediate uses: expensive field work could be substantially reduced, extensive areas or low-value timber could be inventoried economically, measurements could be obtained much more rapidly, especially in isolated areas and areas where weather conditions affected ground surveys. This saving in time either could reduce inventory costs or the sampling intensity could be increased to provide greater accuracy.

With photography, as with ground inventories, two different approaches were taken to estimate timber volumes—stand measurements and sample trees measurements. Again, each aerial method offers particular advantages over the other and is similiar to its corresponding ground method, except that the measurements used to estimate volume are obtained remotely. The remainder of this section discusses and compares these two aerial-photo approaches to timber-volume estimation.

B.2 VARIABLES USED TO ESTIMATE STANDING TIMBER VOLUME

Ground estimates of gross tree and stand volumes are based on measurements of basal area, age, diameter at breast height (dbh), and merchantable and total height. Height, age, and basal-area information provide the basis for determining stand volume, while tree volume is estimated from dbh and merchantable height. Since not all these variables can be measured directly from aerial photographs, a slightly different set of variables, capable of being measured directly from aerial photography yet still highly correlatable with gross volume, must

be used. The three most common variables used to estimate standing timber volume from aerial photography are total height, crown diameter, and crown closure. These variables can be viewed as substitutes for merchantable height, dbh, and basal area, respectively.

Height

The height of a tree or a stand can be determined by using any or all of three methods:

(1) Measurement of photographic relief displacement
(2) Measurement of parallax—the difference in relief displacement between two stereo photographs.
(3) Measurement of shadow length

The parallax method is most accurate and applicable to a greater variety of situations than the other methods because dense forest stands and irregular topography make shadow length measurements impractical, while relief displacement is difficult to measure when small scales are involved or the base of an object is obscured. A further advantage in using parallax measurements is that, on commonly available photography, trees and stands can be grouped into 10-ft height classes.

Crown Closure

Crown closure, which is a measure of stand density, is expressed as a percentage of the total ground area covered by a forest canopy. Three methods of measurement are most common: dot grid, density scale, and stereogram. An interpreter uses a dot grid to measure crown closure by counting the dots that fall on tree crowns and comparing this number to the total number in the sample area. Crown closure is estimated with a density scale and stereogram by visual comparison between the area of interest and the known standard. The density scale graphically portrays a variety of stand densities, while the stereogram method provides the interpreter with actual photographic examples of stands that exhibit a variety of known densities. The standard error of crown closure measurements is consistently less than or equal to 10% [14].

Crown Diameter

Crown diameter is measured by using either a dot scale (with graduated circles to represent a variety of tree crown sizes) or a wedge comprised of two diverging lines. The dot scale is overlaid on the tree whereas the wedge is placed tangent to the crown for measurement. Tree crowns can be classified into 5-ft diameter classes without difficulty [15].

Accuracy

The accuracy of these variables in predicting gross standing volume is dependent on their correlation with volume and their ability to be measured from aerial photography. Of the three predictor variables, total height exhibits the highest correlation coefficient with volume.

Crown closure is a close second, while crown diameter is a poor third. These variables, and transformations of them, form excellent models for estimating standing-timber volume. The standard error of estimate for aerial-stand-volume tables constructed by S. F. Gingrich and H. A. Meyer is 25% [16]. A standard error of estimate of 17% has been obtained by others.

B.3 AERIAL METHODS OF ESTIMATING GROSS STANDING TIMBER VOLUME

B.3.1 AERIAL TREE VOLUME TABLES

Aerial-tree-volume tables estimate the volume of individual trees by measuring tree height and crown diameter (crown area). Several other variables that express the effects of competition by neighboring trees are sometimes utilized, but the most useful are direct measurements of individual tree characteristics [17].

These tables are constructed by determining the volume of a representative sample of trees from ground measurements and then correlating these volumes with photo-measurements of the same trees. Once the relationship between photo-measured variables and volume is determined, the volume of unknown trees can be predicted by substituting their photo-measured variables into the previously determined regression equation and solving for the independent variable volume.

Volumes of large forested areas are estimated using aerial-tree tables by stratifying the forest, allocating sample plots, and measuring individual trees within these plots. The sample data collected are then projected to predict the volume of the entire area. Volume is usually expressed in gross cubic feet with no cull estimation.

B.3.2 AERIAL STAND VOLUME TABLES

Stand volume tables are constructed using the same procedures except that stand characteristics (crown closure, stand height, and stand crown diameter) are utilized as independent variables. Volumes of a representative sample of stands that exhibit a variety of density, height, and crown characteristics are determined from ground measurements and then correlated with their photo-measured variables by regression analysis. The stand method incorporates another variable, crown closure, into the model. The variables of height and crown diameter are still utilized, but they are redefined to describe characteristics of entire forest stands. Stand height and stand crown diameter can be viewed as an average of individual (dominant and co-dominant) trees comprising the stand (e.g., the average of the three tallest trees for stand height) [16].

B.3.3 OTHER METHODS

Several other aerial methods exist for estimating standing-timber volume. In one, stereograms that portray a variety of stand conditions of known volume are used to estimate volume of unknown stands by visual comparison. In another, existing tree and stand tables based on ground measurements are converted to aerial tables by using photo-variables to estimate the independent ground variables on which the tables are based. Since these methods, based in part on subjective decisions, are either not as accurate or not as statistically sound as those mentioned earlier, they will not be discussed further.

B.3.4 COMPARISON

Both tree and stand aerial methods provide an estimate of gross standing-timber volume solely from photographic measurements, once the initial volume tables are constructed. However, most aerial volume tables, especially those based on the earliest aerial methods, use the stand approach—not the tree concept—to estimate volume. Several valid reasons account for the preferred use of stand tables.

First, tree tables require the use of large-scale photography in their construction and application in order to accurately identify and measure all trees within a sample plot. Since large-scale photography of most areas is not available, special flights to collect such photography are necessary. When the use of aerial tables was first proposed, the availablility of high-quality large-scale stereo photography was a limiting factor in their application. Another limitation was the difficulty encountered in accurately determining the photographic scale of this photography, especially in isolated areas, because few benchmarks appear within the field of view on scales applicable to tree-volume tables. Also, the tables are limited to forest types that do not grow in dense stands—such stands inhibit identification and measurement of all trees in the sample plot. An excessive number of photo-measurements is necessary in the application of tree-volume tables, and a well designed statistical-sampling system must be utilized for accurate prediction of standing volume.

Since aerial-stand tables, on the other hand, are not affected by these limitations, their construction was more prevalent. Because it is not necessary to see or measure every tree, small-scale photography can be used as the basis for photographic measurements. Federal agencies such as ASCS, SCS, and the Forest Service procure photography applicable to the stand-table method on a regular basis; therefore, special photographic missions are not a prerequisite. While scale determination is difficult on large-scale photography, it is facilitated on smaller-scale photography by the presence of numerous cultural and geographical features. Finally, stand tables not only require fewer photo-measurements in their application, but also provide direct estimates of volume per acre.

REFERENCES

1. R. Vincent, G. Thomas, and R. Nalepka, Signature Extension Studies, Report No. 190100-26-T, Environmental Research Institute of Michigan, Ann Arbor, (In Press).

2. R. B. Crane, Adaptive Processing Using a Decision-Directed Kalman Filter and Feature Extraction of Multispectral Data, Report No. 190100-31-T, Environmental Research Institute of Michigan, Ann Arbor, (In Press).

3. R. Horvath, M. Spencer, and R. Turner, Radiative Transfer in Real Atmospheres - Atmosphere Correction and Simulation of Space-Acquired Remote Sensor Data: 0.4-to 1.0-μm Spectral Range, Report No. 10657-4-F, Environmental Research Institute of Michigan, Ann Arbor, January 1973.

4. W. A. Malila, R. H. Hieber, and A. P. McCleer, Correlation of ERTS MSS Data and Earth Coordinate Systems, Presented at the Purdue Conference on Machine Processing of Remotely Sensed Data, West Lafayette, October 1973.

5. W. A. Malila and R. F. Nalepka, Type II Progress Report, Report No. 193300-16-P, Environmental Research Institute of Michigan, Ann Arbor, July 1973.

6. G. H. Suits, The Calculation of the Directional Reflectance of a Vegetative Canopy, Remote Sensing of Environment, Vol. 2, 1972, pp. 117-125.

7. S. Stewart, D. Christenson, and L. Larsen, Systematic Monitoring and Evaluation of M7 Scanner Performance and Data Quality, Report No. 190100-23-T, Environmental Research Institute of Michigan, Ann Arbor, (In Press).

8. R. B. Crane and W. Richardson, Performance Evaluation of Multispectral Scanner Classification Methods, Proceedings of the Eighth International Symposium on Remote Sensing of Environment, Vol. II, Report No. 195600-1-X, Environmental Research Institute of Michigan, Ann Arbor, 1972, pp. 815-31.

9. R. E. Turner, Atmospheric Effects in Remote Sensing,Selected Papers from the March 26-28, 1973,Remote Sensing of Earth Resources Conference, Vol. II, ed. F. Shahrokhi, University of Tennessee Space Institute, Tullahoma, 1973.

10. R. L. Lillestrand, Techniques for Change Detection, IEEE Transactions on Computers, Vol. C-21, No. 7, July 1972, pp. 654-659; and private communications with Mr. Leon Bonrud, Control Data Corporation, Minneapolis, Minn.

11. G. H Suits and R. G. Safir, Verification of a Reflectance Model for Mature Corn with Applications to Corn Blight Detection, Remote Sensing of Environment, Vol. 2, 1972, pp. 183-192; and private communications with G. H. Suits, Environmental Research Institute of Michigan, Ann Arbor, and G. R. Safir, Michigan State University, East Lansing.

12. F. P. Weber, R. C. Aldrich, F. G. Sadowski, and F. J. Thomson, Land Use Classification in the Southeastern Forest Region by Multispectral Scanning and Computerized Mapping, Proceedings of the Eighth International Symposium on Remote Sensing of Environment, Vol. I, Report No. 195600-1-X, Environmental Research Institute of Michigan, Ann Arbor, 1972, pp. 351-73.

13. W. G. Rohde and C. E. Olson, Multispectral Sensing of Forest Tree Species, Photogrammetric Engineering, Vol. 38, No. 12, December 1972, pp. 1209-15.

14. H. A. Meyer and D. P. Worley, Volume Determinations from Aerial Stand Volume Tables and Their Accuracy, Journal of Forestry, Vol. 55, 1957, pp. 368-72.

15. J. W. Willingham, Estimation of Forest Management Inventory Data from Aerial Photographic Measurements, Forest Science, Vol. 3, 1957, pp. 270-74.

16. S. F. Gingrich and H. A. Meyer, Construction of an Aerial Stand Volume Table for Upland Oak, Forest Science, Vol. 1, 1955, pp. 140-47.

17. G. M. Bonner, A Tree Volume Table for Red Pine by Crown Width and Height, Forestry Chronicle, Vol. 40, 1964, pp. 339-46.

DISTRIBUTION LIST

NASA/Johnson Space Center
Earth Observations Division
Houston, Texas 77058

ATTN: Dr. A Potter/TF3 (4)
ATTN: Mr. Robert MacDonald (1)
ATTN: Mr. B. Baker/TF3 (8)
ATTN: Mr. R. Dean Bretton/TF53
Chief Earth Resources Research Data Facility (8)
ATTN: Mr. A. H. Watkins/HA (1)

NASA/Johnson Space Center
Facility & Laboratory Support Branch
Houston, Texas 77058

ATTN: Mr. D. Riley BB631/B4 (1)

NASA/Johnson Space Center
Computation & Flight Support
Houston, Texas 77058

ATTN: Mr. Eugene Davis/FA (1)

NASA Headquarters
Washington, D.C. 20546

ATTN: Mr. C. W. Mathews (1)

U.S. Department of Agriculture
Agricultural Research Service
Washington, D.C. 20242

ATTN: Dr. Robert Miller (1)

U.S. Department of Agriculture
Soil & Water Conservation Research Division
P.O. Box 267
Weslaco, Texas 78596

ATTN: Dr. Craig Wiegand (1)

U.S. Department of Interior
Geological Survey
Washington, D.C. 20244

ATTN: Dr. James R. Anderson (1)

Director, Remote Sensing Institute
South Dakota State University
Agriculture Engineering Building
Brookings, South Dakota 57006

ATTN: Mr. Victor I. Myers (1)

U.S. Department of Interior
Fish & Wildlife Service
Bureau of Sport Fisheries & Wildlife
Northern Prairie Wildlife Research Center
Jamestown, North Dakota 58401

ATTN: Mr. Harvey K. Nelson (1)

U.S. Department of Agriculture
Forest Service
240 W. Prospect Street
Fort Collins, Colorado 80521

ATTN: Dr. Richard Driscoll (1)

U.S. Department of Interior
Geological Survey
Water Resources Division
500 Zack Street
Tampa, Florida 33602

ATTN: Mr. A. E. Coker (1)

U.S. Department of Interior
Director, EROS Program
Washington, D.C. 20244

ATTN: Mr. J. M. Denoyer (1)

Earth Resources Laboratory, GS
Mississippi Test Facility
Bay St. Louis, Mississippi 39520

ATTN: Mr. R. O. Piland, Director (1)
ATTN: Mr. Sid Whitley (1)

U.S. Department of Interior
Geological Survey
GSA Building, Room 5213
Washington, D.C. 20242

ATTN: Mr. W. A. Fischer (1)

NASA Wallops
Wallops Station, Virginia 23337

ATTN: Mr. James Bettle (1)

Purdue University
Purdue Industrial Research Park
1200 Potter
West Lafayette, Indiana 47906

ATTN: Dr. David Landgrebe (1)
ATTN: Dr. Philip Swain (1)
ATTN: Mr. Terry Phillips (1)

U.S. Department of Interior
EROS Office
Washington, D.C. 20242

ATTN: Dr. Raymond W. Fary (1)

U.S. Department of Interior
Geological Survey
801 19th Street, N.W.
Washington, D.C. 20242

ATTN: Mr. Charles Withington (1)

U.S. Department of Interior
Geological Survey
801 19th Street, N.W.
Washington, D.C. 20242

ATTN: Mr. M. Deutsch (1)

U.S. Geological Survey
801 19th Street, N.W., Room 1030
Washington, D.C. 20242

ATTN: Dr. Jules D. Friedman (1)

U.S. Department of Interior
Geological Survey
Federal Center
Denver, Colorado 80225

ATTN: Dr. Harry W. Smedes (1)

U.S. Department of Interior
Geological Survey
Water Resources Division
901 S. Miami Ave.
Miami, Florida 33130

ATTN: Mr. Aaron L. Higer (1)

University of California
School of Forestry
Berkeley, California 94720

ATTN: Dr. Robert Colwell (1)

School of Agriculture
Range Management
Oregon State University
Corvallis, Oregon 97331

ATTN: Dr. Charles E. Poulton (1)

U.S. Department of Interior
EROS Office
Washington, D.C. 20242

ATTN: Mr. William Hemphill (1)

Chief of Technical Support
Western Environmental Research Laboratories
Environmental Protection Agency
P.O. Box 15027
Las Vegas, Nevada 89114

ATTN: Mr. Leslie Dunn (1)

NASA/Langley Research
Mail Stop 470
Hampton, Virginia 23365

ATTN: Mr. William Howle (1)

U.S. Geological Survey
Branch of Regional Geophysics
Denver Federal Center, Building 25
Denver, Colorado 80225

ATTN: Mr. Kenneth Watson (1)

NAVOCEANO, Code 7001
Naval Research Laboratory
Washington, D.C. 20390

ATTN: Mr. J. W. Sherman, III (1)

U.S. Department of Agriculture
Administrator
Agricultural Stabilization and Conservation Service
Washington, D.C.

ATTN: Mr. Kenneth Frick (1)

Pacific Southwest Forest & Range Experiment Station
U.S. Forest Service
P.O. Box 245
Berkeley, California 94701

ATTN: Mr. R. C. Heller (1)

Pacific Southwest Forest & Range Experiment Station
U.S. Forest Service
P.O. Box 245
Berkeley, California 94701

ATTN: Dr. P. Weber (1)

NASA/Johnson Space Center
Mission Planning & Analysis Division
Houston, Texas 77058

ATTN: Mr. H. G. De Vezin/FM8 (1)

University of Texas at Dallas
Box 688
Richardson, Texas 75080

ATTN: Dr. Patrick L. Odell (1)

Department of Mathematics
University of Houston
Houston, Texas 77004

ATTN: Dr. Henry Decell (1)

Institute for Computer Services and Applications
Rice University
Houston, Texas 77001

ATTN: Dr. M. Stuart Lynn (1)

U.S. National Park Service
Western Regional Office
450 Golden Gate Avenue
San Francisco, California 94102

ATTN: Mr. M. Kolipinski (1)

U.S. Department of Agriculture
Statistical Reporting Service
Washington, D.C. 20250

ATTN: D. H. VonSteen/R. Allen (2)

U.S. Department of Agriculture
Statistical Reporting Service
Washington, D.C. 20250

ATTN: Mr. H. L. Trelogan, Administrator (1)

Department of Watershed Sciences
Colorado State University
Fort Collins, Colorado 80521

ATTN: Dr. James A. Smith (1)

Lockheed Electronics Co.
16811 El Camino Real
Houston, Texas 77058

ATTN: Mr. R. Tokerud (1)

TRW System Group
Space Park Drive
Houston, Texas 77058

ATTN: Dr. David Detchmendy (1)

IBM Corporation
1322 Space Park Drive
Houston, Texas 77058

ATTN: Dr. D. Ingram (1)

S&D—DIR
Marshall Space Flight Center
Huntsville, Alabama 35812

ATTN: Mr. Cecil Messer (1)

Code 168-427
Jet Propulsion Laboratory
4800 Oak Grove Drive
Pasadena, California 91103

ATTN: Mr. Fred Billingsley (1)

NASA/Johnson Space Center
Technical Library Branch
Houston, Texas 77058

ATTN: Ms. Retha Shirkey/JM6 (4)

NASA Headquarters
Washington, D.C. 20546

ATTN: Mr. W. Stoney/ER (1)
ATTN: Mr. Leonard Jaffe/ER (1)
ATTN: Mr. M. Molloy/ERR (1)
ATTN: Mr. G. Thorley/ERR (1)

Ames Research Center
National Aeronautics and Space Administration
Moffett Field, California 94035

ATTN: Dr. I. Poppoff (1)

Goddard Space Flight Center
National Aeronautics and Space Administration
Greenbelt, Maryland 20771

ATTN: Mr. W. Nordberg, 620 (1)
ATTN: Mr. W. Alford, 563 (1)

Lewis Research Center
National Aeronautics and Space Administration
21000 Brookpark Road
Cleveland, Ohio 44135

ATTN: Dr. Herman Mark (1)

John F. Kennedy Space Center
National Aeronautics and Space Administration
Kennedy Space Center, Florida 32899

ATTN: Mr. S. Claybourne/FP (1)

NASA/Langley
Mail Stop 214
Hampton, Virginia 23665

ATTN: Mr. James L. Raper (1)